A system for the measurement and statistical analysis of accelerations experienced by a shaft vehicle

Author:
Hendy, David

Publication Date:
1987

DOI:
https://doi.org/10.26190/unsworks/8615

A SYSTEM FOR THE MEASUREMENT AND STATISTICAL ANALYSIS OF ACCELERATIONS EXPERIENCED BY A SHAFT VEHICLE

by

DAVID HENDY

A THESIS SUBMITTED TO THE UNIVERSITY OF NEW SOUTH WALES

FOR THE DEGREE OF MASTER OF ENGINEERING

JUNE 1987

ABSTRACT

This thesis reports on the design and construction of what appears to be the first digital accelerometer system for use on mine shaft vehicles. A major part of the project was concerned with developing a theoretical model of a digital radio link in a mine shaft.

It is considered that the "State of the Art" has been advanced in three key areas during the development of this system, namely:

a) Accelerometer systems for use in mine shafts.

b) Digital radio links in mines.

c) The analysis of forces experienced by shaft vehicles.

Starting from the base of work already in existence for analog radio links for mine shafts, a computer based theoretical model was developed for a digital link. The model concentrated on the effects of signal loss, and inter-symbol interference due to standing wave effects and transmitted pulse shapes.

Using the results of the model, guidelines and specifications were derived for the digital link to be used for the accelerometer. Specifications for the accelerometer were derived by considering the major limitations of existing units and the specifications for vibration analysis equipment used in other fields.

Armed with the guidelines and the specifications the digital accelerometer was designed and constructed. The test results gathered during the testing phases of the development showed very good correlation with the theoretical results.

The digital link uses a quaternary modulation method and has a speed of 36 kbits per second and an average error rate of 1 in 710,000.

The major finding of the work are:

a) Inter-Symbol interference is not considered a problem for digital links up to a speed of 30 kbaud.

b) The large system losses predicted and measured are due to inefficient signal couplers. Propagation losses and standing wave effects, in comparison, have minimal effect.

c) Higher carrier frequencies, than those often used in analog links, in the order of 300 kHz to 1 MHz offer advantages in lower system losses.

I hereby declare that this submission is my own work and that, to the best of my knowledge and belief, it contains no material previously published or written by another person nor material which to a substantial extent has been accepted for the award of any other degree or diploma of a university or other institute of higher learning, except where due acknowledgement is made in the text.

D. Hendy

June 1987

CONTENTS PAGE

CONTENTS - CONTINUED PAGE

CONTENTS - CONTINUED PAGE

APPENDICES

LIST OF FIGURES

LIST OF TABLES PAGE

LIST OF PRINCIPAL SYMBOLS

α	Attenuation Coefficient
β	Phase-Change Coefficient
ε_e	Permittivity of rock surrounding the shaft
ε_o	Permittivity of air
ε_w	Permittivity of the wire rope
Φ	Magnetic flux
ϕ	Phase of transmitted signal
Γ	Propagation coefficient ($\alpha + j\beta$)
λ	Wave length
μ_e	Permeability of shaft rock
μ_o	Permeability of air
μ_w	Permeability of the wire rope
ρ_o	Wire rope offset from the centre of the shaft
ρ_r	Transmission line reflection coefficient for receiver end
ρ_t	Transmission line reflection coefficient for transmitter end
σ_e	Conductivity of shaft rock
ω	Radian frequency ($2\pi \times$ frequency)
a_o	Radius of the shaft
B	Magnetic field
c	Radius of the wire rope
g	Acceleration due to gravity (9.8 metres per second^2)
I_n	Modified Bessel functions of the first kind
i_o	Current flowing in the transmitter coupler
i_r	Current flowing in the wire rope at the receiver end
i_t	Current flowing in the wire rope at the transmitter end
j	$\sqrt{-1}$
K_n	Modified Bessel functions of the second kind

L_t	Self inductance of the transmitter coupler
M	Mutual inductance
M_r	Mutual inductance for the receiver coupler
M_t	Mutual inductance for the transmitter coupler
N_r	Number of turns for receiver coupler
N_t	Number of turns for transmitter coupler
V_o	Voltage across transmitter coupler
V_1	Induced voltage across rectangular coupler
V_r	Received voltage at input to receiver
V_{ri}	Received voltage at receiver coupler
Z	Shaft vehicle position down the shaft
Z_o	Characteristic impedance of shaft
Z_r	Shaft termination impedance at receiver end
Z_t	Shaft termination impedance at transmitter end
Z_w	Series impedance of the wire rope

CHAPTER 1

INTRODUCTION AND BACKGROUND

1.1 INTRODUCTION

This thesis documents the development of a system to measure and analyse the accelerations experienced by a shaft vehicle. It was developed for ZC Mines Ltd., Broken Hill, for the testing of shaft conditions. The system is unique in the way it measures and records the accelerations.

It is considered that the "State of the Art" has been advanced in three key areas during the development of this system, namely:

a) Accelerometer systems for use in mine shafts.

b) Digital radio links in mines.

c) The analysis of forces experienced by shaft vehicles.

The thesis follows the development from the initial identification of the need for such a system through to the first test results.

The system developed during the course of this project is operational and has been used for a number of trial shaft accelerometer tests. The data collected shows considerably more detail than the previously used accelerometer. The new accelerometer will allow for more informative shaft testing and analysis.

As the topics discussed in this thesis are diverse, the literature is reviewed in the relevant sections of text, rather than in one chapter.

1.2 BACKGROUND AND HISTORY

1.2.1 THE SHAFT

The ZC Mines shaft at Broken Hill was sunk in the years 1936 to 1939 during a major building and expansion programme. The programme included office facilities, concentration mill, winding and haulage facilities and engineering workshops [1]. The shaft is 947 metres deep, of rectangular cross section with a timber supporting structure. The shaft had a designed life of 30 years at a haulage rate of 0.8 million tonnes per year, but has been in continuous service for some 46 years with a current haulage rate of 1.0 million tonnes per year.

Over its 46 year life the shaft has developed a curvature of approximately 1.5 metres over its length. This has resulted from the mining of the ore body which lies in close proximity to the shaft. Hence there has been a steady increase in the maintenance requirements of the shaft along with a desire for greater reliability and haulage capacity.

Over the years a number of significant shaft problems have resulted in loss of haulage time and considerable repair cost. There has always been a difficulty in detecting areas requiring maintenance at the early stages of deterioration and there by minimising:

a) the amount of damage done as a result, and

b) the maintenance work required to rectify the fault.

Hence reliable methods for early detection of shaft problems have been sought by ZC Mines for some time.

1.2.2 PREVIOUS TESTING PROCEDURES

The two main methods used by ZC Mines for a number of years, to evaluate shaft conditions and maintenance requirements have been:

a) regular shaft inspections (qualitative),

b) accelerometer tests (quantitative).

1.2.2.1 Shaft Inspections

These are a visual method of checking the shaft conditions. A team of men (usually 2-3) ride on a platform, on the top of the skip. The skip is lowered down the shaft at a slow speed of 1-2 metres per second. As they travel down, the men look for signs of wear or damage that indicate maintenance is required in a particular area. The method is qualitative, as no measurements to indicate the effects of wear or damage on shaft performance can be taken. Comparisons with past shaft inspections are also qualitative by nature. It is time consuming and expensive as a full shaft inspection can take up to four hours of shaft time and 16 to 20 man hours. It is however, reliable and is currently one of the most widely used methods of checking shaft conditions [2].

1.2.2.2 Accelerometer Tests

These tests are an instrument based method of checking shaft conditions. Accelerometer tests have been used widely [2,3,4] in South Africa, Canada and Australia (at ZC Mines). Common use started in the 1950's and 60's and initially accelerometer tests were used to measure the effectiveness of braking systems. Later this expanded into the area of shaft alignment. Now the tests are mainly used to indicate the state of the shaft guidance system.

Blaauw [2] used accelerometer tests to compare the results of a mathematical model of shaft and vehicle behaviour with actual behaviour. Galloway and Tiley [3] considered accelerometer testing to be the best tool for measuring shaft and vehicle performance during actual haulage. Jones and Albert [4] found that an accelerometer when properly used was a very useful tool for testing shaft guides for alignment and emergency braking systems. Prior to January, 1984 the only device used at the ZC Mines was a Cambridge Accelerometer which is capable of recording accelerations in two directions verses time and distance.

The Cambridge unit is entirely mechanical using two sprung masses as the transducers; these are attached to needle pens marking a 20 millimetre wide cellophane tape see Figure 2.

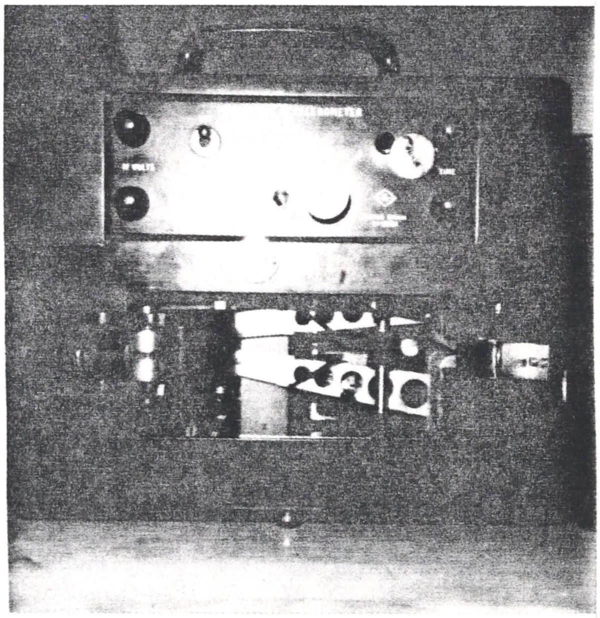

Figure 1

The Cambridge Accelerometer Unit

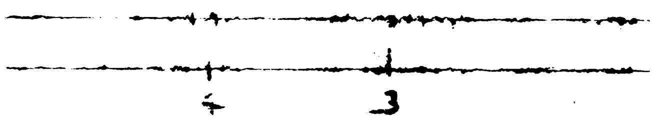

Figure 2

Example trace from the Cambridge Accelerometer

The middle trace, in Figure 2, is the distance recording pulse produced by a "fifth wheel" attached to the skip. This wheel is in contact with the shaft guides and gives one pulse for every 4.5 metres travelled. The basic specifications of the Cambridge unit are:

TABLE 1

Cambridge Accelerometer Specifications

Frequency response	:	0 - 30 Hz
Resolution	:	0.13 g
Range	:	± 4 g
Distance recording range	:	unlimited
Distance resolution	:	4.5 m
Distance repeatability	:	± 10 m

The main limitations with this device are:

a) The unreliability of the distance recording mechanism due to slippage of the fifth wheel in the high acceleration environment.

b) The time taken to analyse the results from a run.

c) Limited frequency response.

d) Difficulty in comparing the results from a number of runs.

Summarising these, the Cambridge unit is limited by it not having a quantitative analysis system {(b) and (d) above}; and its poor specifications {(a) and (c)}. The first is true with the other units commonly available on the market.

1.2.3 LIMITATIONS OF AVAILABLE ACCELEROMETER SYSTEMS

The science of vibration analysis has progressed tremendously over the last twenty years with the advent of cheap computing hardware, the Fast Fourier Transform (FFT) and other analysis tools [5]. The market offers a large range of highly sophisticated vibration analysis equipment for gear boxes, motor bearings etc., but not skips travelling in mine shafts.

There are available a number of accelerometer instruments which record on paper charts the forces experienced by shaft vehicles [2,3,4]. These instruments generally use piezo-electric transducers and an analog radio link [2,4] to transmit the transducer signals to the surface recording equipment. These instruments have the following advantages over the Cambridge unit:

a) Increased accuracy through the use of piezo-electric transducers.
b) Greater range of mounting options for the transducers.
c) Wider frequency response, generally up to a few hundred hertz.
d) Plots of velocity and jerk are sometimes available as well as acceleration.

The limiting factor with these types of instruments is still the lack of any quantitative analysis system. As they still rely upon the human interpretation of the raw plots of acceleration, velocity etc., which is still laborious and qualitative.

1.2.4 REQUIRED IMPROVEMENTS

To advance shaft accelerometer testing, to a similar level achieved in other areas, major developments in the instrumentation system were required. The most significant was to feed the measurements directly into a computer. This would enable the use of advanced statistical analysis, of the type discussed in [5]. Secondly, a more accurate and reliable distance recording method was required to enable pin-pointing the locations of disturbances.

A significant improvement in frequency response was required to enable worthwhile frequency analysis to be performed on the recorded data. At the same time it was considered necessary to improve the resolution and accuracy of the measurements.

1.3 SPECIFICATIONS OF THE DIGITAL ACCELEROMETER SYSTEM

As mentioned in (1.2.4) two major advancements in the technology of measuring the forces experienced by shaft vehicles were required:

a) The direct input of the measurements into a computer.

b) An accurate distance recording mechanism.

Also required was:

c) a wide frequency response, and

d) improved resolution and accuracy.

To achieve a) and d) it was decided to digitise the transducer outputs directly and transmit the measurements to the surface via a digital radio link. It appears that this is the first time a medium speed digital radio link has been developed for use in mine shafts.

As in any measurement system compromises were necessary between:

a) frequency response,

b) resolution,

c) the speed of the data link.

The speed of the data link was one of the major determining factors. It was believed that a data link of approximately 40 kbits per second would be feasible (see chapter 2) giving two data channels at 20 kbits per second each.

A frequency response of 500 Hz was considered necessary to capture all important frequency components. The frequency response and the data link speed determine the resolution, currently eight bits which is four times that of the Cambridge unit. The resolution could be further improved, with a little more effort and no increase in link speed, to nine or ten bits.

The repeatability and accuracy of the distance measuring system were major limitations with the existing instrument. Hence, the specifications for the new instrument called for significant improvements in these areas. It was decided that the distance resolution and repeatability of the system should be a maximum of ± 1 metre. In summary the specifications of the system were:

TABLE 2

Digital Accelerometer System Specifications

Frequency Response	:	5 - 500 Hz (-3 dB)
Range	:	± 5 g Nominal; adjustable from ± 0.25 g to ± 50 g
Resolution	:	±0.03 g Nominal (1 part in 128 of range)
Distance Resolution and Repeatability	:	± 1 metre
Data Storage Method	:	In real time onto computer disc
Data Link Speed	:	40 kbits per second

CHAPTER 2

DIGITAL RADIO COMMUNICATIONS IN MINE SHAFTS

For radio frequencies, mine shafts behave as lossy coaxial transmission lines [6,7,8]. In general the losses due to the shaft are not significant. For the shaft at ZC Mines they are less than 16 dB/km for frequencies less than 1 MHz.

The areas that cause significant signal degradation are the termination impedances [8,9] and signal couplers. Firstly, the headframe is generally a low impedance to earth, while, the shaft vehicle has a high impedance. This results in a great amount of signal reflection due to poor impedance matching. Secondly, the physical constraints on the design of the signal couplers result in low efficiency couplers. The use of ferrite cored toroids would have been the most desirable, ensuring maximum signal transfer. However, this was not practical as the required core sizes ruled out any ready supply. Instead rectangular wooden cored coils were used, resulting in much poorer signal coupling and greater system losses.

To better understand and quantify the above effects, a theoretical model of the transmission and reception of a Pulse Code Modulated (PCM) carrier was developed. The model calculates the theoretical:

a) Received signal strength verses shaft position for the transmitter.

b) Received pulse shape and Inter-Symbol Interference (ISI) effects for given system parameters.

2.1 TRANSMISSION LINE MODEL AND PARAMETERS

The block diagram for a shaft radio link is shown in Figure 3 below. The transmitter and coupler are mounted on the shaft vehicle located Z metres below the surface. The transmitter output voltage (V_o) appears across the coupler inducing, via the mutual inductance M_t, a current i_t in the hoist rope.

The shaft acts as a lossy transmission line with a propagation coefficient Γ and a characteristic impedance Z_o. The impedance Z_t, between the shaft wall and the vehicle, terminates the line at the vehicle end. The impedance Z_r, between the wire rope and ground, terminates the line at the receiver end. As the termination impedances differ from Z_o, standing waves result and the reflection coefficients ρ_r and ρ_t are non zero.

The net current flowing at the receiver end, taking into account losses and standing waves, is i_r. The current i_r induces, via the mutual inductance M_r, a voltage V_{ri} across the receiver coupler. The receiver and coupler, located some distance apart, are connected by a lossy cable reducing the signal by a factor CF to a level V_r.

The voltages V_o, V_{ri} and V_r are functions of time and distance (except for V_o) and the excitation factor $e^{-j\omega t}$ is assumed throughout. The relative phase difference between V_o and V_r is unimportant and is not considered in the equations that follow. Appendices One and Two provide more detailed derivations of the equations and model parameters used below.

The received voltage (V_r) for steady state conditions ie., for continuous wave transmission is given by:

$$V_r = \frac{V_r}{V_{ri}} \cdot \frac{V_{ri}}{i_r} \cdot \frac{i_r}{i_t} \cdot \frac{i_t}{V_o} \cdot V_o \tag{2.1}$$

When the various elements of (2.1) are put in the terms of the components of Figure 3, (2.1) becomes:

$$\frac{V_r}{V_o} = \frac{M_t\ M_r\ \omega\ e^{-\Gamma z}}{CF\ L_t\ |Z_o + Z_t|} \cdot \frac{[\ 1 - \rho_r\ ]}{[\ 1 - \rho_t \rho_r e^{-2\Gamma z}\ ]} \tag{2.2}$$

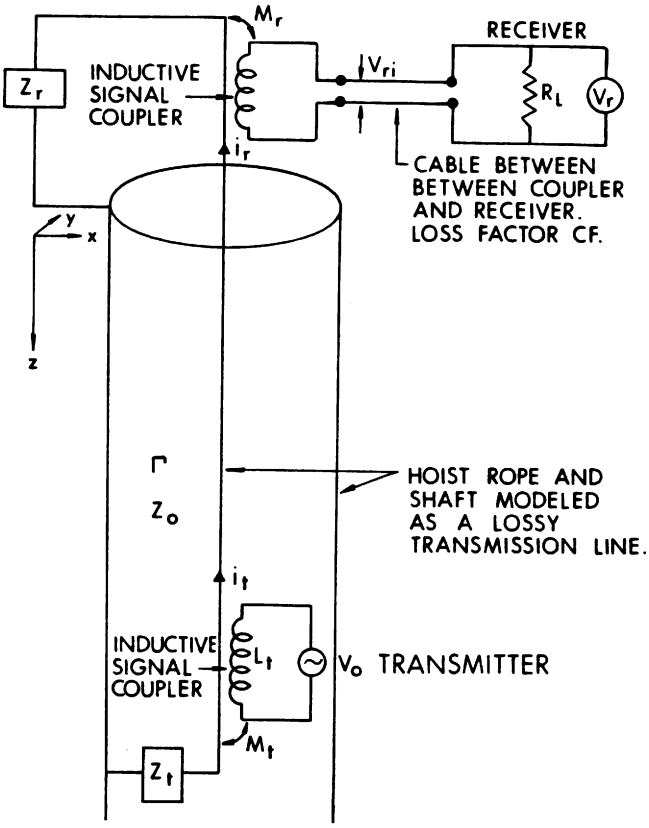

Figure 3

Block Diagram of a Mine Shaft Radio Link

Steady state principles no longer apply when pulse shapes and ISI affects are considered and a discrete series equation must be used:

$$\frac{V_r}{V_o} = \frac{M_t\ M_r\ \omega\ e^{-\Gamma z}[1 - \rho_r]}{CF\ L_t\ |Z_o + Z_t|} \cdot \sum_{n=0}^{\infty} (\rho_t \rho_r e^{-2\Gamma z})^n \tag{2.3}$$

To calculate V_r the following parameters had to be determined:

a) Propagation coefficient Γ.

b) Characteristic impedance Z_o.

c) Mutual and self inductances for the signal couplers.

d) Termination impedances of the headframe and shaft vehicle.

e) The cable loss factor CF.

2.1.1 PROPAGATION COEFFICIENT FOR A MINE SHAFT

It has been found that on the whole the propagation coefficient for a mine shaft or tunnel with an axial conductor has the following characteristics:

a) The attenuation (α) increases up to a frequency in the order of 100 MHz and then starts to decrease again [10,11,12].

b) For frequencies below the order of 30 MHz a TEM like mode, often referred to as the coax or transmission line mode, is the only one that will propagate [12,13].

c) The phase-change coefficient (β ie., $2\pi/\lambda$) decreases as the axial conductor approaches the shaft wall and is greater than the free air value [14,15].

d) The attenuation (α) increases as the axial conductor is moved closer to the shaft wall [15,16,17].

The ZC Mines shaft is rectangular in cross section and Mahmoud and Wait [15,18] have derived a modal equation for this type of cross-section. To keep the mathematics manageable they have made a simplifying assumption that the short walls are either perfectly electrical or magnetic (ie., infinite conductivity and permeability). Loss factors calculated from the modal equation were up to a factor of five smaller than those calculated for a circular shaft (see Appendix One).

With the propagation coefficient for low frequencies being independent of cross sectional shape [19,20], the modal equation in [15,18,21] is considered unsuitable for real shafts at low frequencies. Therefore the modal equation, derived by Wait and Hill [14,22,23], for shafts of a circular cross section with an offset axial conductor was used.

The modal equation relates to a uniform circular shaft of radius a_o. The shaft is bounded by a homogeneous lossy dielectric with permittivity ε_e, conductivity σ_e and permeability μ_e. The shaft is assumed to contain air with the normal free space parameter values of ε_o, μ_o and zero conductivity.

Located in the shaft and parallel to the axis (offset = ρ_o) is a thin conductor of radius c. The conductor has a conductivity σ_w, permeability μ_w and permittivity ε_w. Figure 4 shows the geometry of the shaft and conductor.

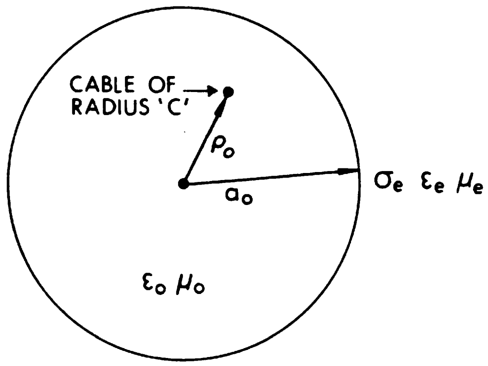

Figure 4

Geometric Arrangement of a Circular Shaft with an Offset Conductor

In the quasi-static limit the modal equation for the propagation coefficient Γ can be put in the form [12,14,23]:

$$\Gamma^2 = \gamma_o^2 \left[1 + \frac{-1}{P\gamma_o} \frac{\partial P}{\partial z} \right] \tag{2.4}$$

Where P is the propagation power loss due to the wire rope and tunnel wall losses, and γ_o^2 is the free air propagation coefficient.

The component due to the wire rope is given by:

$$\frac{-1}{P\gamma_o} \left(\frac{\partial P}{\partial z}\right)_{wire} = \frac{2\pi\, Zw}{j\omega\mu o\Lambda} \tag{2.5}$$

The component due to the tunnel wall is given by:

$$\frac{-1}{P\gamma_o} \left(\frac{\partial P}{\partial z}\right)_{wall} = \frac{\Omega}{\Lambda} \tag{2.6}$$

Substituting equations (2.5) and (2.6) into (2.4) gives:

$$\Gamma^2 = \gamma_o^2 \left[1 + \frac{\Omega}{\Lambda} + \frac{2\pi\, Z_w}{j\mu_o \omega\Lambda} \right] \tag{2.7}$$

Where:

$$\Omega = \frac{1}{\gamma_e a_o} \left[\frac{K_o(\gamma_e a_o)}{K_1(\gamma_e a_o)} + 2\sum_{m=1}^{\infty} \left(\frac{\rho_o}{a_o}\right)^{2m} \left(\frac{K_m(\gamma_e a_o)}{K_{m+1}(\gamma_e a_o)} - \frac{\gamma_e a_o}{2m} \right) \right] + \ln \frac{a_o^2}{a_o^2 - \rho_o^2}$$

Where Z_w is the series impedance of the wire rope:

$$Z_w = \frac{(j\mu_w \omega)^{1/2}}{2\pi(\sigma_w + j\varepsilon_w \omega)^{1/2} c} \cdot \frac{I_o(\gamma_w c)}{I_1(\gamma_w c)}$$

Λ accounts for the geometry of the shaft:

$$\Lambda = \ln \frac{a_o}{c} - \ln \frac{a_o^2}{a_o^2 - \rho_o^2}$$

γ_o, γ_w, γ_e are the propagation coefficients for air, the wire rope material and the surrounding medium respectively and are given by:

$$\gamma_o = j(\varepsilon_o \mu_o)^{1/2}\omega \qquad \gamma_w^{\ 2} = j\mu_w \omega(\sigma_w + j\varepsilon_w \omega)$$
$$\gamma_e^{\ 2} = j\mu_e \omega(\sigma_e + j\varepsilon_e \omega)$$

I_n and K_n are modified Bessel functions of the first and second kinds [44]. For the frequencies of interest (100 kHz < f < 3 MHz) and the rock and conductor types found in mine shafts the following assumptions can be made [8,17]:

a) $\mu_e = \mu_o$,

b) $\sigma_e >> \varepsilon_w \omega$,

c) $\mu_w = \mu_o$.

Figures 5 and 6 below show the calculated attenuation and phase-change coefficients verses frequency for the ZC Mines shaft.

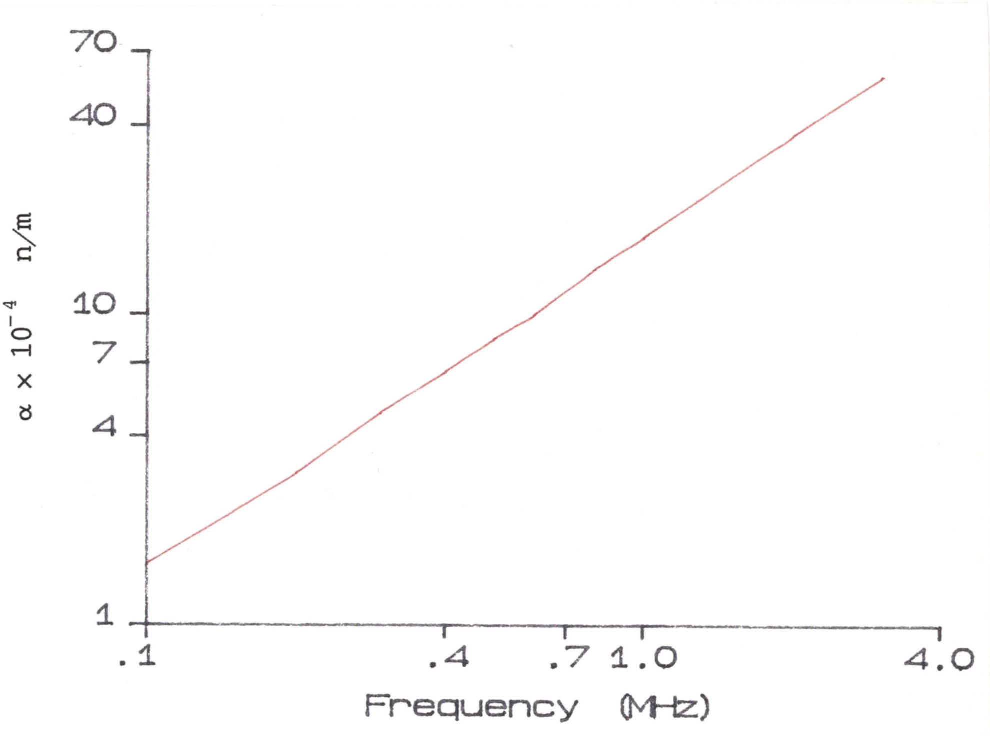

Figure 5

Shaft Attenuation (α) vs Frequency for ZC Shaft

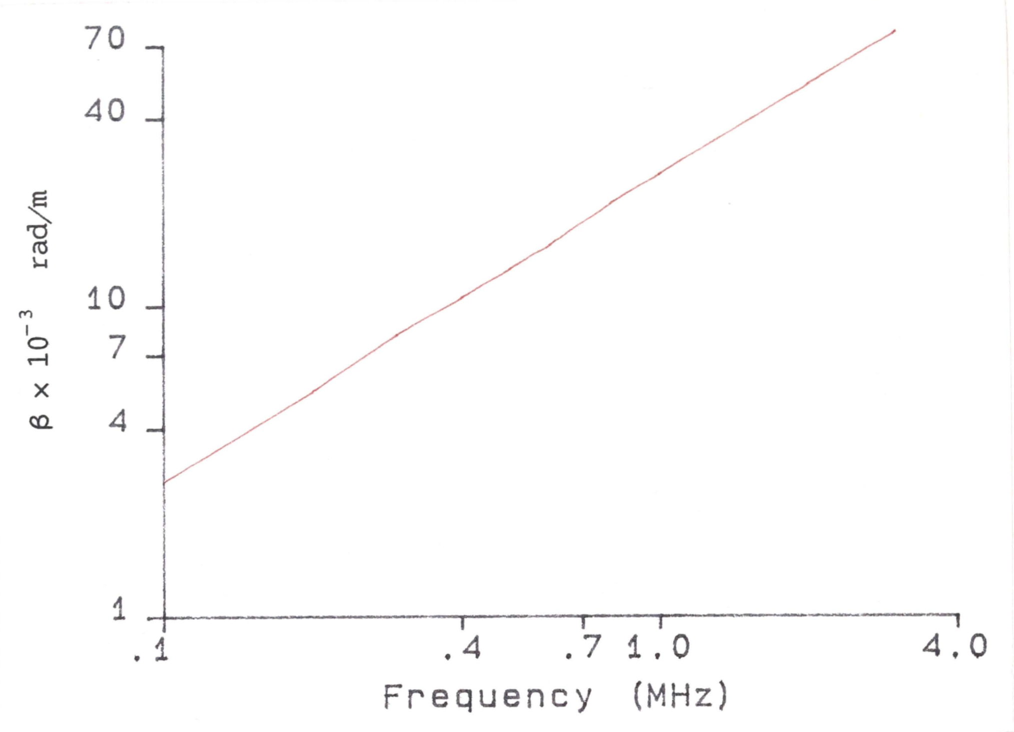

Figure 6

Phase-Change (β) vs Frequency for ZC Shaft

The geometric and electrical parameters used to calculate the above results were:

Equivalent shaft radius - 3.8 metres

Axial conductor offset from centre - 2.1 metres

Conductivity of surrounding rock - 0.001 siemens per metre

While the conductor location does effect the propagation coefficient, significant changes only occur when the conductor approaches the shaft wall. For the ZC shaft, the attenuation is effected much more by the rock conductivity than by the rope offset. The reader is referred to Appendix One for a detailed analysis of results for equation (2.7) for various parameters.

2.1.2 CHARACTERISTIC IMPEDANCE OF A MINE SHAFT

A transmission line's characteristic impedance is given by [24]:

$$Z_o = \sqrt{Z_1 Z_2} \tag{2.8}$$

Where Z_1 and Z_2 are the series and shunt impedances of the line. From Wait [23]:

$$\Gamma^2 = \hat{Z}\hat{Y}$$ $\hat{Z}$ Is the series impedance and $\hat{Y}$ Is the shunt impedance

Where $$\hat{Z} = \frac{j\mu_o \omega}{2\pi}\left(\Lambda + \Omega \right) + Z_w \quad \text{and} \quad \hat{Y} = \frac{2\pi j \varepsilon_o \omega}{\Lambda}$$

Substituting the above into (2.8) and rearranging gives:

$$Z_o = \sqrt{\frac{\mu_o \Lambda}{\varepsilon_o 4\pi^2}\left(\Lambda + \Omega + \frac{2\pi Z_w}{j\mu_o \omega}\right)} \tag{2.9}$$

Solving (2.9) for the geometric and electrical parameters above gives the following graph.

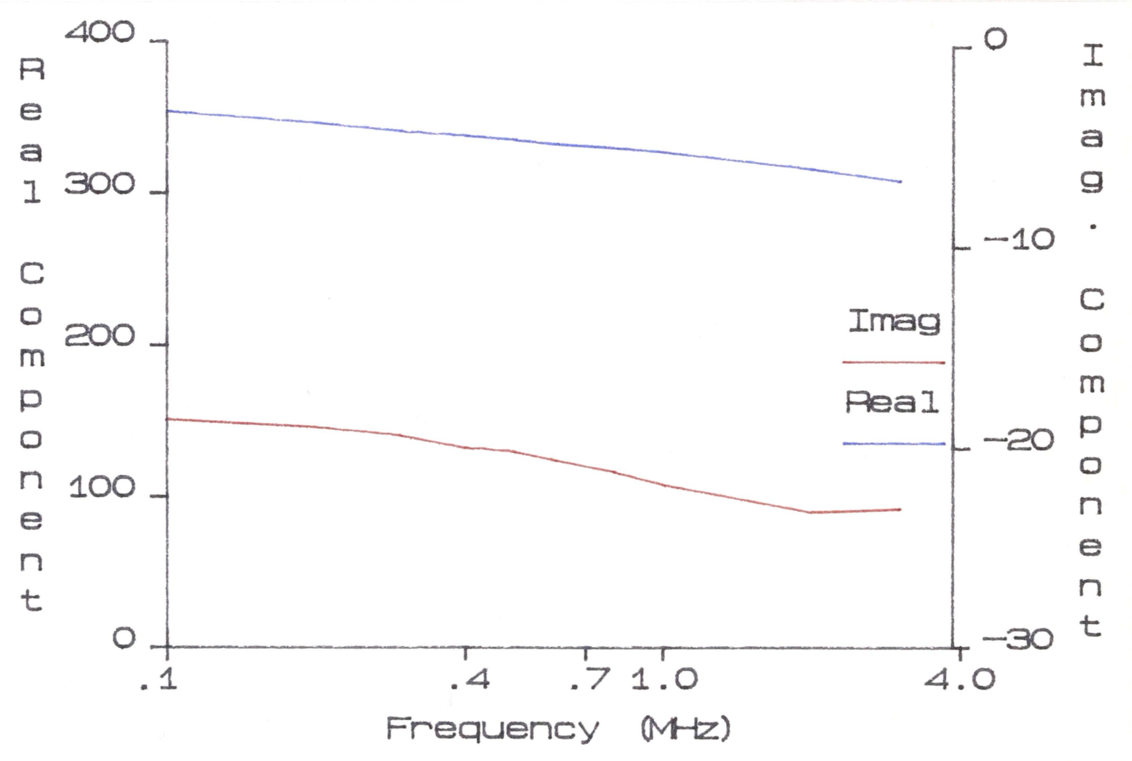

Figure 7

Characteristic Impedance Z_o vs Frequency for ZC Shaft

2.1.3 MUTUAL INDUCTANCE OF A SIGNAL COUPLER

From basic physics it is desirable, as previously mentioned, to have ferrite cored toroids as signal couplers thus assuring maximum signal transfer. Suitable ferrite cores of the necessary size (50 and 300 millimetres inside diameter for the skip and the headframe ends respectively) were not readily available in Australia. Hence the use of alternative shapes and coil formers were necessary. For the ease of manufacture and mounting, coils wound on rectangular wooden frames were used.

Lagace et al [8] provided the only detailed analysis found on the design of signal couplers. The couplers analysed in [8] were ferrite and laminated iron cored coils with carrier frequencies in the range of 30 - 50 kHz. This meant that the information regarding the design of couplers, provided by Lagace et al. [8], could not be readily used for this project.

For the basic signal coupler and wire rope configuration shown in Figure 8 the induced voltage V_1 due to the current i_2 is given by:

$$V_1 = \frac{M\,di_2}{dt} \qquad (2.10)$$

$$\text{Where } M = \frac{N_1 \Phi_{12}}{i_2}$$

$$\Phi_{12} = \int B \cdot ds$$

$$= \frac{h\mu_o i_2}{2\pi} \ln\left(\frac{b + c}{b}\right)$$

$$\therefore M = \frac{N_1 h\mu_o}{2\pi} \ln\left(\frac{b + c}{b}\right) \qquad (2.11)$$

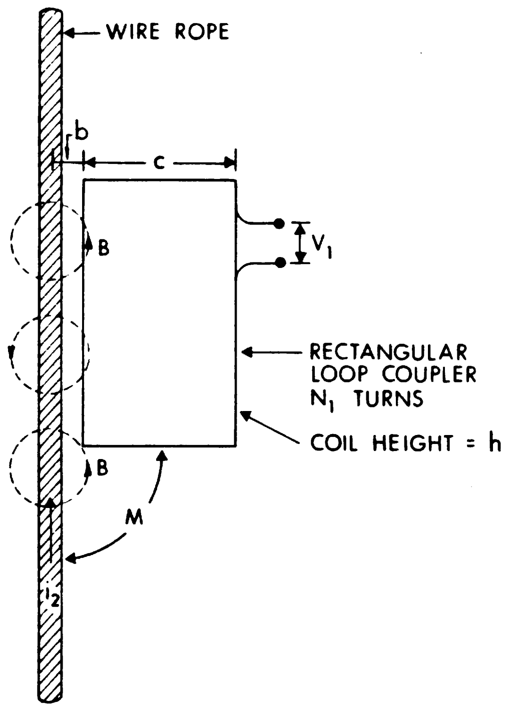

Figure 8

Rectangular Signal Coupler Configuration

In Figure 8 above, N_1 is the number of turns for the signal coupler, b, b+c and h are the radii and height respectively measured in metres. It is easily seen from equation (2.11) that the mutual inductance increases linearly with the number of turns and height; and logarithmicly with an increase in the ratio of the radii.

The aim of any coupler design is to maximise the signal transfer however, in selecting suitable sizes for the receiver coupler the following had to be taken into account:

a) The minimum distance between the coupler and the hoist rope to avoid damaging the coupler was approximately 130 millimetres.

b) The maximum coupler height to fit comfortably in the mounting frame was approximately 380 millimetres.

c) The maximum coupler width to fit in the mounting frame, while still maintaining (a), was 200 millimetres.

Given the above limits it was decided to set the outer dimensions at h = 380 and b = 180 millimetres. To give added protection the windings were recessed by 10 millimetres giving effective dimensions of h = 360 mm, c = 160 mm and b = 150 mm.

For the transmitter coupler the considerations were:

a) With accelerations in the order of 5 g being experienced at the top of the shaft vehicle, the overall size and weight should be kept low.

b) As the coupler is mounted directly on the rope the radius (b) is minimised and is equal to the rope's radius (24 millimetres). This will maximise the mutual inductance for a given height.

Dimensions of 260 millimetres high by 50 millimetres wide were selected because:

a) The coupler was small, easy to handle and mount.

b) These dimensions were similar to those used in other successful shaft communication systems at ZC Mines.

c) Realistic values for the mutual and self inductances did not require an unreasonable number of turns.

For the above dimensions the mutual inductances of the signal couplers were:

a) Receiver $M_r = 0.052\ N_r\ \mu H$

b) Transmitter $M_t = 0.059\ N_t\ \mu H$

Where N_r and N_t are the number of turns for the receiver and transmitter couplers respectively.

2.1.4 SELF INDUCTANCE OF A RECTANGULAR COIL

The self inductance of the rectangular coil geometry shown in Figure 9 is given by [25]:

$$L(\mu H) = 4.0 \times 10^{-1} \pi N^2 \frac{hc}{w} F' \qquad (2.12)$$

$$\text{Where } F' = \beta_1 \gamma + \beta_1{}' \gamma \ln(1/\gamma) + \beta_2 \gamma^2 + \beta_3 \gamma^3 + \ldots$$

$\gamma = \dfrac{w}{h}$ $\quad K = \dfrac{c}{h}$ $\quad \beta_n(k)$ is determined from Table II in [25] and all dimensions are in metres.

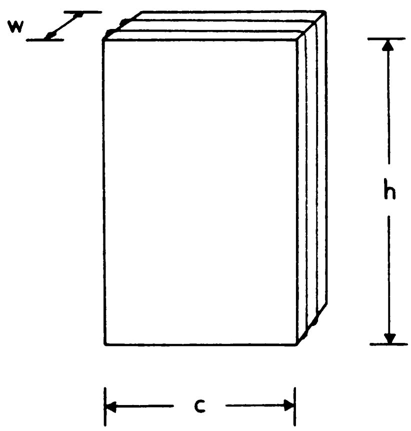

Figure 9

Geometry of a Rectangular Coil

For the selected dimensions the self inductance of the signal couplers are:

a) Receiver coupler $L_r = 0.67 N_r{}^2\ \mu H$

b) Transmitter coupler $L_t = 0.29 N_t{}^2\ \mu H$

The number of turns for each coupler was decided before the detailed analysis of Appendix One was completed. The number of turns was selected to give a self inductance of approximately 1 mH ie., $N_t = 63$, $N_r = 40$. On reflection a lower N_t would have been better as the induced hoist rope signal is inversely proportional to N_t (Appendix One).

Although this would have increased the power drain which is inversely proportional to N_t^4. The values of N_t and N_r gave the following calculated values for M_t, L_t, M_r and L_r shown below. The self inductances of the couplers were measured and showed good correlation ($\Delta < 13\%$) with the calculated values.

TABLE 3

Calculated and Measured Inductances for Signal Couplers

CALCULATED	MEASURED
$M_t = 3.72\ \mu H$	-
$M_r = 2.08\ \mu H$	-
$L_t = 1.15$ mH	1.32 mH
$L_r = 1.07$ mH	1.16 mH

2.1.5 SHAFT TERMINATION IMPEDANCES

There appears to be little quantitative work on the analysis of shaft termination impedances especially for headframes. Lagace [7] and Lagace et al. [8] indicate that:

a) For headframes, a well grounded installation in rock of high conductivity ($\sigma_e > 0.01$ S/m) will have an impedance of the order of 10 Ω. While for a poorly grounded installation in low conductivity rock ($\sigma_e > 0.001$ S/m) an impedance of 100 Ω or greater is likely.

b) The impedance between the vehicle and the shaft wall generally consists only of the capacitance between the two. Though sometimes a conductive path may exist due to moisture and dirt on the runners. The capacitance value is generally calculated by considering the shaft and vehicle as a coaxial capacitor.

Modelling the ZC Mines shaft vehicles shaft as coaxial capacitors is considered inadequate due to the geometry, see Figure 10.

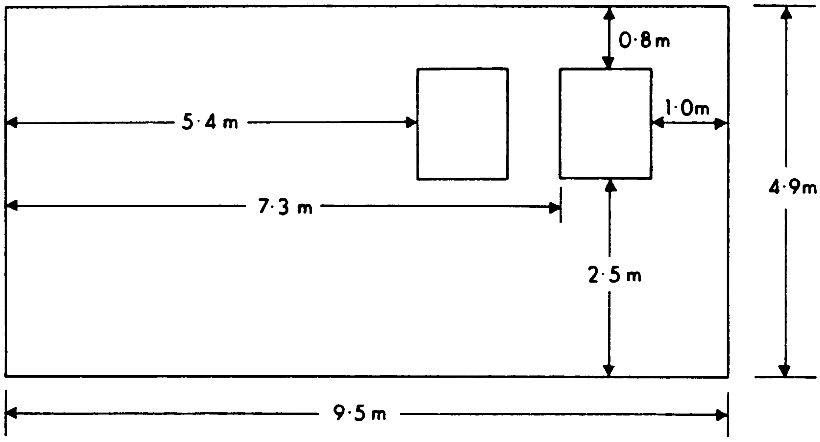

Figure 10

ZC Shaft Geometry

Instead the vehicles and shaft are modelled as offset cylinders. Smythe [26] gives the following equation for the capacitance per unit length for offset cylinders, all dimensions are in metres. The geometry for equation (2.13) is shown in Figure 11.

$$C(pF/m) = \frac{2\pi\varepsilon_o \times 1 \times 10^{12}}{\text{Cosh}^{-1}\left[-\dfrac{D_2 - R_1^{\,2} - R_2^{\,2}}{2R_1 R_2}\right]} \tag{2.13}$$

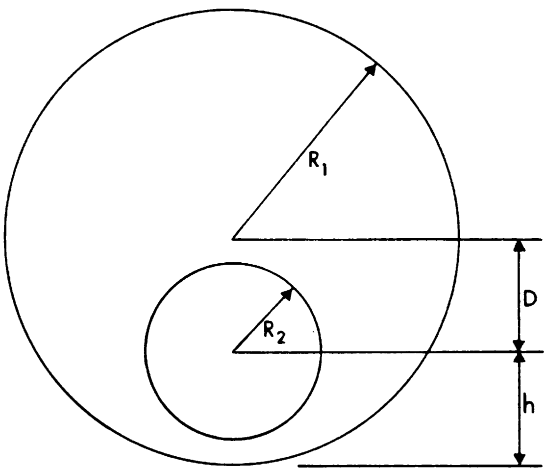

Figure 11

Geometry of Offset Cylinders

Using graphical techniques (see Figure 12) to estimate D, R_1, and R_2 for the East and West shaft vehicles the following values were obtained.

TABLE 4

Parameters and Calculated Shaft Vehicle Capacitance

East	West
D_e = 0.7 m	D_w = 2.1 m
R_{1e} = 2.3 m	R_{1w} = 3.9 m
R_{2e} = 0.9 m	R_{2w} = 0.9 m
L = 2.5 m	L = 2.5 m
C_e = 169 pF	C_w = 131 pF

These compare with a capacitance value of 82 pF if the shaft and vehicle are modelled as a coaxial capacitor.

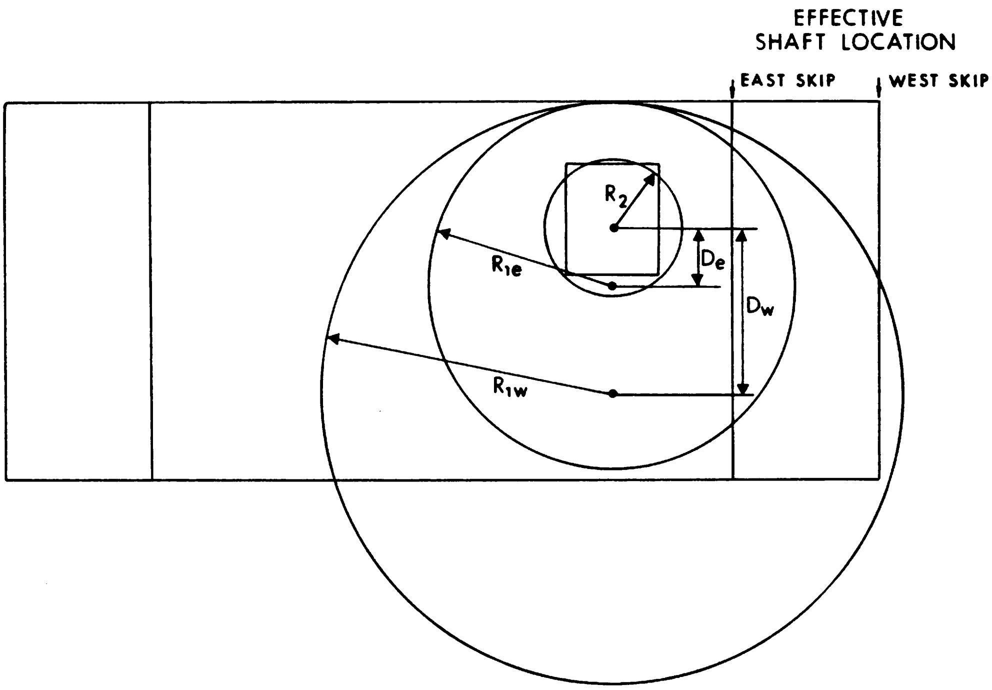

Figure 12

Determination of Measurements for an Offset Cylinder Capacitor

2.2 CARRIER FREQUENCY SELECTION

A number of factors influenced the selection of the carrier frequency, they were:

a) Transmitter power drain and efficiency.

b) Received signal strength and circuit design.

c) Standing wave patterns.

d) Transmitter modulation techniques and circuit design.

e) Signal to noise ratio.

As shown in Appendix One the signal strength induced into the hoist rope is independent of frequency. However the power required by the transmitter output amplifier is inversely proportional to frequency. As efficiency is important with a battery powered transmitter, a high carrier frequency is preferable.

The received signal strength is proportional to ω^2 for $|Z_t| > |Z_o|$ which is generally the case for frequencies up to 1 MHz. While this will have no bearing on the received signal to noise ratio [8,27], it does on the receiver circuit design. A higher frequency means a higher input level, hence a less sensitive, and easier to design, receiver front-end is required.

On the other hand as the carrier frequency is raised the effects of standing waves become more pronounced [8]. Anderson and Vanous [9] consider the effects detrimental enough to use two carrier frequencies (ratio 1.36:1) to avoid the effects of standing waves. For the ZC Mines shaft and the accelerometer system, standing waves were present but were not a significant problem (see section 2.3.1) and so a single carrier frequency was used.

The direct phase modulation technique used, sets an upper carrier frequency limit, corresponding to 1/8 of the maximum TTL clock rate (see section 3.3). It is desirable to keep the carrier frequency below 0.5 MHz to allow the use of conventional analog ICs and design techniques.

Considering the above, the most suitable carrier frequency was the highest available below 0.5 MHz. The carrier frequencies available were determined by:

a) The transmitter clock source frequency (10.25 MHz).

b) The practical frequency dividers (ie., ÷2, ÷4 etc.) available to produce the required 8 times carrier frequency.

The highest frequency below 0.5 MHz available from the transmitter clock was 321 kHz and this was used for the shaft accelerometer system.

2.3 TRANSMISSION LINE PROGRAMS AND RESULTS

In the proceeding sections, equations and/or values have been obtained for:

a) Propagation coefficient Γ.

b) Characteristic impedance Z_o.

c) Mutual and self inductance of the signal couplers.

d) Termination impedances for the shaft.

Hence, all the necessary information is available to calculate the received signal level and pulse shape using equations (2.2) and (2.3) respectively.

Two separate computer programs were developed to solve these equations. The steady state equation deals with only one frequency and is simple to evaluate.

The program used to evaluate equation (2.3) must take into account:

a) The frequency spectrum of the transmitted pulse and the different parameter values across the spectrum.

b) The discrete time nature of the series.

c) The generation of the predicted demodulated output pulse.

2.3.1 STEADY STATE SIGNAL LEVELS THEORETICAL AND PRACTICAL

When the values of M_t, M_r, CF, L_t and ω for the East shaft vehicle are substituted into (2.3) the resulting equation is:

$$\left|\frac{V_r}{V_o}\right| (\mathrm{dB}) = 20 \text{ Log} \left[\frac{8.37 \times 10^{-4} \; e^{-\Gamma z}[1 - \rho_r]}{|Z_o + Z_t|[1 - \rho_t \rho_r e^{-2\Gamma z}]} \right]$$

The program SigLev was developed to calculate this equation for a range of distances, between the transmitter and the receiver, of 0 to 1000 metres; given:

a) The propagation coefficient Γ.

b) The characteristic impedance Z_o.

c) The termination impedances Z_t and Z_r.

Figure 13 compares plots of the theoretical ratio of received to transmitted signal strength, against the measured values. The various curves represent:

Curve 1 - Measured results for East shaft vehicle.

Curve 2 - Theoretical Parameters as in Table 5
(left hand column).

Curve 3 - Theoretical Parameters as in Table 5
(right hand column).

The major item to note regarding the plots is the very large overall system loss in the order of 110 dB to 135 dB.

The loss is mostly due to the inefficient signal couplers. The consequences of losses of this magnitude on the design parameters are discussed in section 2.4.

When the receiver termination impedance is modelled as purely resistive, the theoretical ratio maxima occur considerably further from the receiver than the measured maxima. If an inductive component is added to the termination impedance then the theoretical predictions are far more accurate.

TABLE 5

Parameters for Modelled Signal Strength

Curve 2	Curve 3
σ_e = 0.001 S/m	σ_e = 0.001 S/m
Z_t = −j2934	Z_t = −j2934 (169 pF)
Z_r = 30 Ω	Z_r = 30 + j300 Ω (30 Ω + 150 μH)
Z_o = 343 − j 19 Ω	Z_o = 343 − j 19 Ω
α = 4.7×10^{-4} n/m	α = 4.7×10^{-4} n/m
β = 7.7×10^{-3} rad/m	β = 7.7×10^{-3} rad/m

When the inductive component is set to 150 μH (curve 3) the theoretical maxima and minima shift to the left to coincide with the measured results. For a large metal structure like the ZC Mines headframe one could expect an inductive component of this magnitude.

A similar difference between theoretical and measured locations of the first maxima was recorded without comment by Lagace et al. [8] for a carrier frequency of 50 kHz.

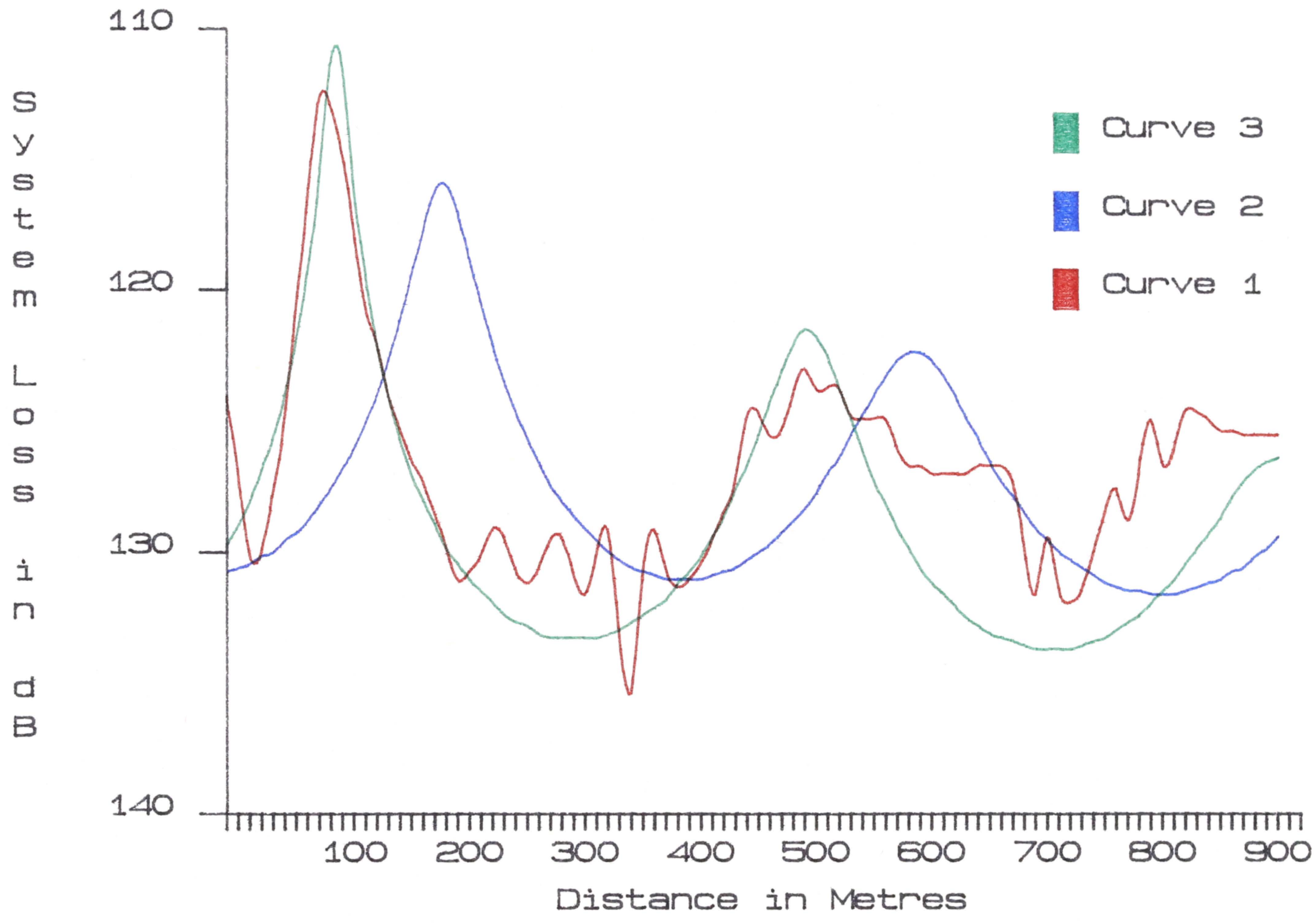

Figure 13

Measured and Theoretical System Loss for ZC Shaft

Curve 3 matches the overall shape and magnitude of the measured signal strength ratio very well. The frequent dips in Curve 1 correspond to the shaft vehicle passing plat developments down the shaft. At a plat the broad sides of the shaft open up into the tunnel for that mine level. The height of the opening is some three to four metres. Hence as the shaft vehicle passes there is a significant decrease in the capacitance between it and the shaft. As a result the received signal level is reduced proportionally.

2.3.2 RECEIVED PULSE SHAPE AND ISI - COMPUTER MODEL

In the early stages of the project a computer model of the digital radio link was developed. The main concern at the time was the effect of Inter-Symbol Interference (ISI). With the large mismatch between the termination and characteristic impedances, standing wave effects become pronounced inducing ISI. With other digital links often it is the narrow bandwidth that causes ISI. It was decided to opt for a Quaternary Modulation system to reduce the symbol rate and hence the effect of ISI see section 2.4.2 for more details. Using the work in previous sections of this chapter a program was developed to model all aspects of the digital radio link.

The basic model specifications were:

> Given an input signal the model is to work out the received signal taking into account the physical characteristics of the transmission and reception system. The input signal is to be specified mathematically and the received signal is to be displayed graphically, either in modulated or demodulated forms.

The program models the link in the frequency domain taking into account reflections from both the transmitter and receiver. The received pulse is displayed in the time domain.

The equivalent circuit that the program is based around has been previously detailed in Figure 3 in section 2.1. The flow of the model can be represented by Figure 14 below.

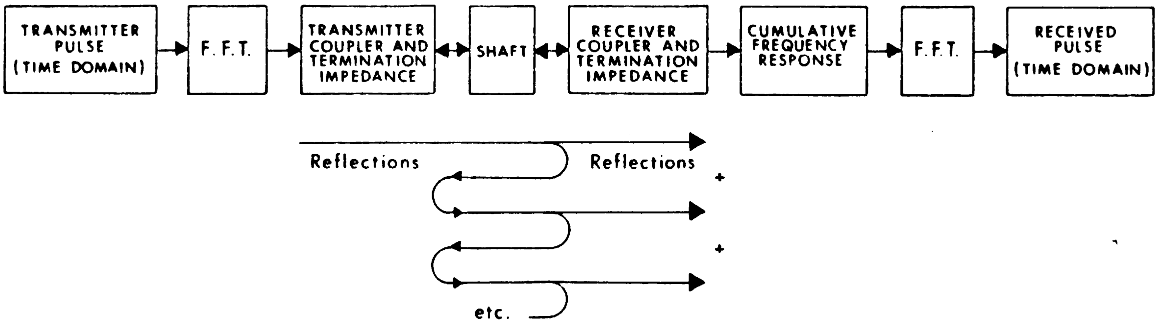

Figure 14

Model Program Flow

The program is designed to be run from an interactive graphics screen. All of the characteristics, physical and electrical as noted below, can be altered by the user before asking for the signal to be sent up the shaft.

Characteristics of the system that the user can change are:

Shaft:

Radius of shaft

Radius of wire rope

Rope offset from centre of the shaft

Conductivity of rock

Conductivity of rope

Depth of shaft (position of shaft vehicle)

Receiver:

Mutual inductance of coupler

Headframe resistance to ground

Headframe inductance to ground

Cable factor

Demodulation filter cutoff frequency

Demodulation filter order

Transmitter:

Capacitance of shaft vehicle to ground

Resistance of shaft vehicle to ground

Transmitter output voltage across coupler

Mutual inductance of coupler

Self inductance of coupler

Signal:

Frequency

Length of pulse

Start time

Number of pulses

In the model a 4096 point discrete Fourier transform (DFT) is used, which is implemented by using a fast Fourier transform algorithm with 32 bit floating point precision. The sampling rate used is two megahertz giving a time window of 2.05 milliseconds and a frequency resolution of 488 Hz. For a detailed account of the modelling approach see Appendix Two. Equation (2.3) is used to model the shaft.

$$V_r = \frac{M_r \; M_t \;\; \omega \, e^{-\Gamma z} \;\; [1 - \rho_r]}{CF \; L_t \;\; |Z_o + Z_t|} \cdot \sum_{n=0}^{\infty} (\rho_r \rho_t e^{-2\Gamma z})^n \cdot V_o$$

Where Z = Distance down the shaft

The reflection coefficients for the transmitter and receiver are calculated in the model from the user supplied characteristics.

The program is designed to be easily used by non-computer and computer people alike. Help is available at every question the user gets asked and the program validates all answers.

Users can easily model a range of signals, shafts, transmitters and receivers by having the program independently store away their characteristics.

At each question the user has the ability to back track, to previous questions, to check or change answers if they desire. The program is designed to be forgiving and flexible to user error and change of mind.

To achieve the above, a number of software tools have been used. Firstly, the FORTRAN pre-processor RatFor developed by Kernignan and Plauger [28] has been used. This gives "C" and Pascal flow control constructs to the FORTRAN language. Secondly, a pre-processor developed by D.J. Fitzgerald and Associates [29] 'VIA' has been used to give the back tracking facility in the program. Thirdly, a relational type data base was used for the entry and storage of characteristics associated with the model. The data base was developed by D.J. Fitzgerald and Associates [30]. The use of these tools has helped to ensure that:

a) the number of lines of code are kept to a minimum, and

b) the program is robust, easy to maintain and understand.

A more detailed description of the program appears in Appendix Two.

2.3.3 RECEIVED PULSE SHAPE AND ISI - THEORY AND MEASURED

Using the parameters for curve 3 in section 2.3.1 the model was run for a range of depths from 90 metres to 500 metres. A sequence of five symbols representing the dibits 00, 11, 00 and 00 were used as the transmitted signal. Each symbol was 55.5 microseconds long (symbol rate of 18 kbaud) with an output voltage of 700 volts peak to peak (see Section 2.4). These values correspond to the actual values used for the digital link. The symbols were initially modelled having a rectangular envelope but as discussed below this was later changed to reduce the effects of ISI.

The demodulation filter, selected in the model, was a third order Butterworth type with a cut off frequency of 40 kHz. The filter is applied in the frequency domain by weighting the various components by a factor appropriate for the filter and the frequency. The demodulated output from the model corresponds to the first bit of the dibit (ie., bit n). Therefore the expected output is 0,1,0,0 (ie., a high, low, high, high sequence).

From these initial runs the effects of ISI on the received demodulated output was quite evident. Figure 15 shows the ideal demodulated output. When this is compared to Figure 16 and 17 (distance = 300 and 490 metres respectively) the effects of ISI are clear. The output pulse width in Figure 17 has increased to the right by approximately 10 microseconds or 20% of a symbol. As well, significant ringing is evident at the symbol transitions. To reduce these effects, shaping of the transmitted pulse was investigated. It was also considered desirable to reduce the bandwidth of the transmitted pulse as this would allow:

a) The narrowing of the receiver input bandwidth with a resulting improvement in the signal to noise ratio.

b) Higher tuning of the transmitter and receiver signal couplers, hence reducing power requirements and boosting received voltages respectively.

The window selected was a four term Blackman Harris window [31], the reasons for its choice and its method of application are described in section 3.3.2.

Figure 18 shows the windowed transmitted pulses as generated by the model. Figure 19 shows the ideal demodulated output while Figures 20 and 21 show the output for distances of 300 and 490 metres respectively. Comparing these Figures it is evident that ISI has had a negligible effect on the pulse shape, height and position. Figure 23 shows the actual receiver eye pattern of the final digital link while transmitting a pseudo-random sequence. The overall level is quite low but greater than that predicted by the model. The use of a 20 kHz cutoff frequency in the receiver will have contributed to the higher measured ISI.

Figure 22 shows the received pulse train before demodulation for a distance of 490 metres (corresponding to the second signal strength maximum). This is the worst case of received pulse shape predicted by the model and compares well with the actual worst case at a distance of 580 metres shown in Figure 24.

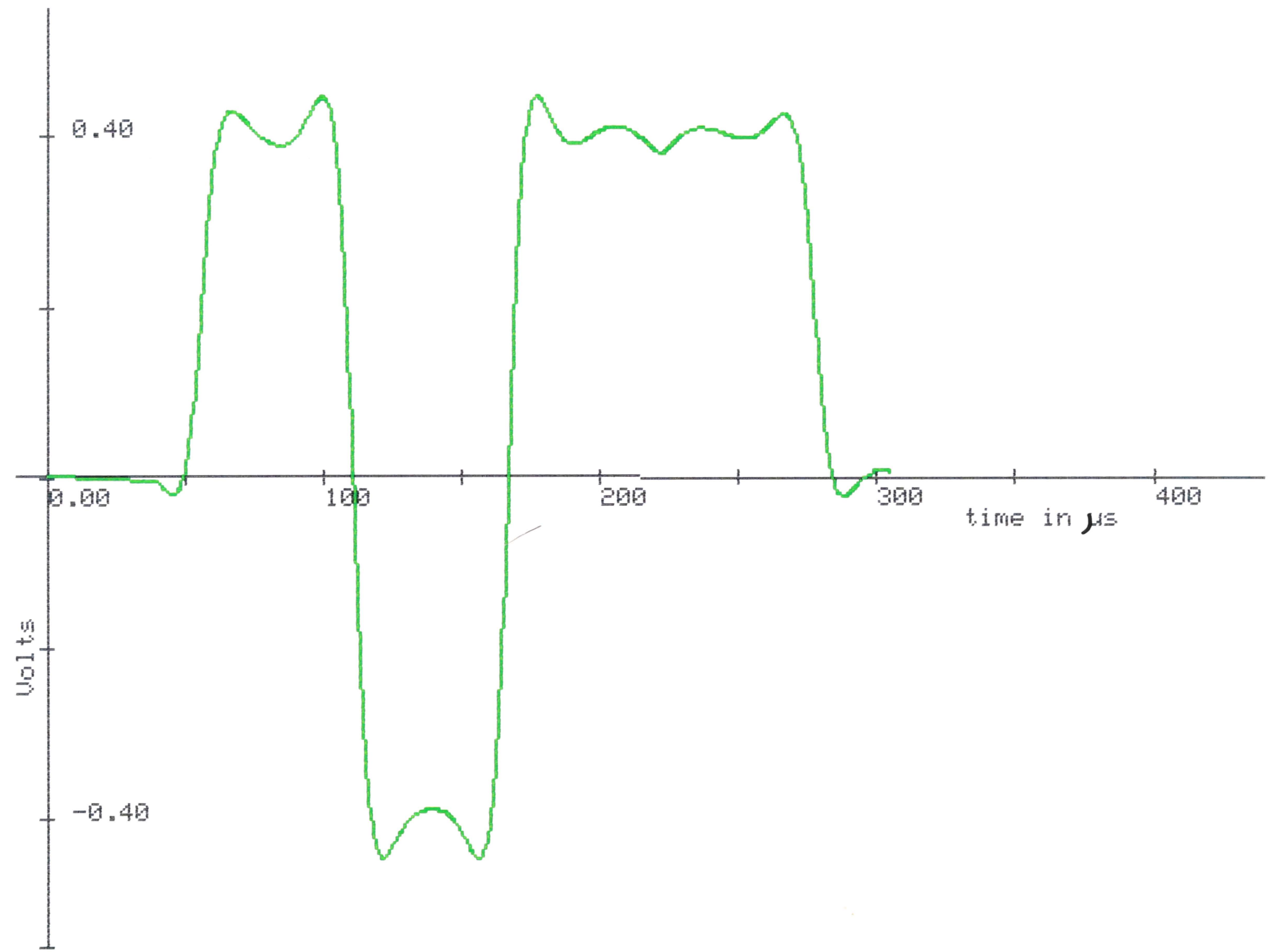

Figure 15

Demodulated Transmitted Pulse Train (Rectangular Pulses)

Figure 16

Demodulated Received Pulse Train (Rectangular Pulses) - 1

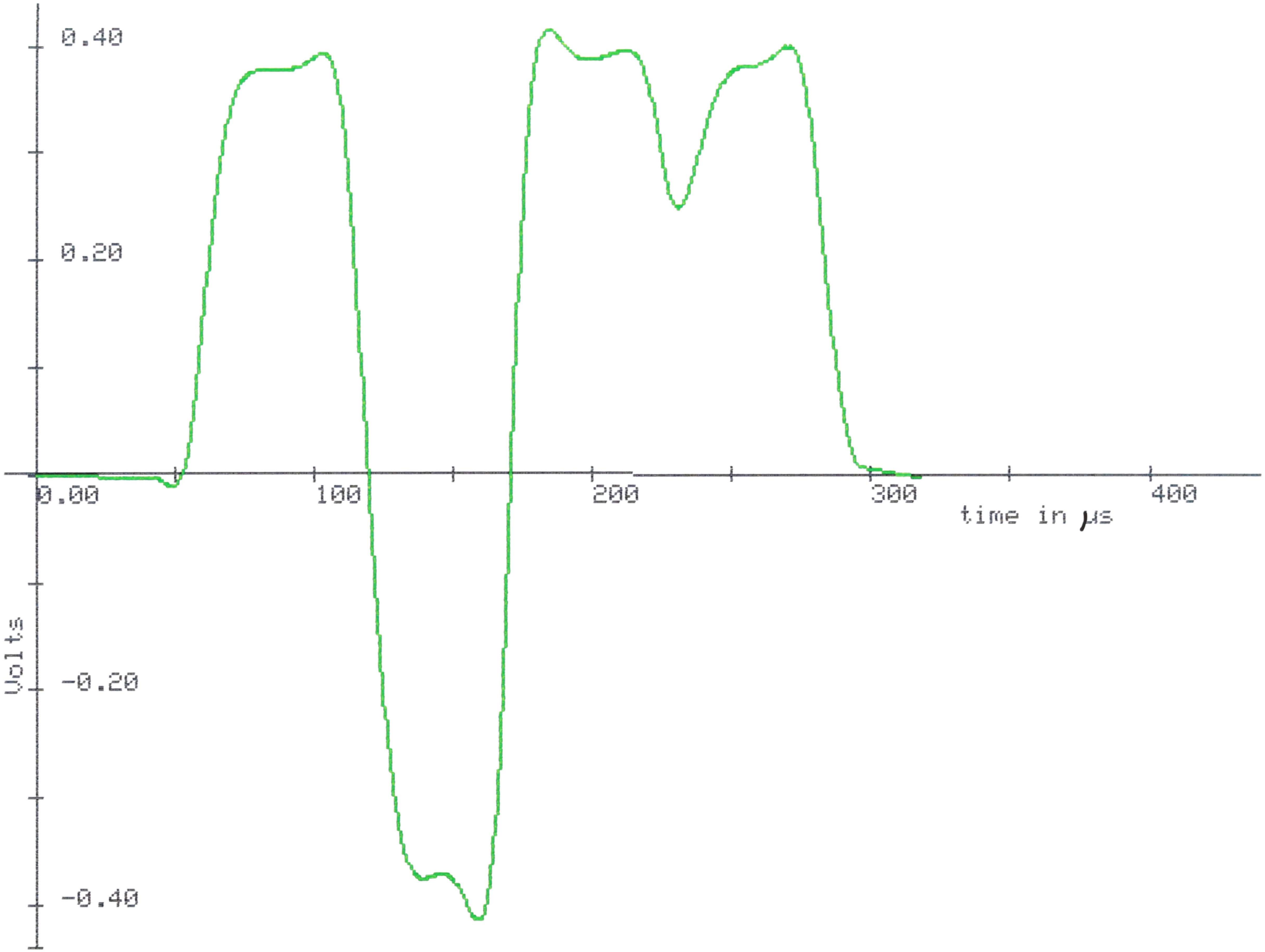

Figure 17

Demodulated Received Pulse Train (Rectangular Pulses) - 2

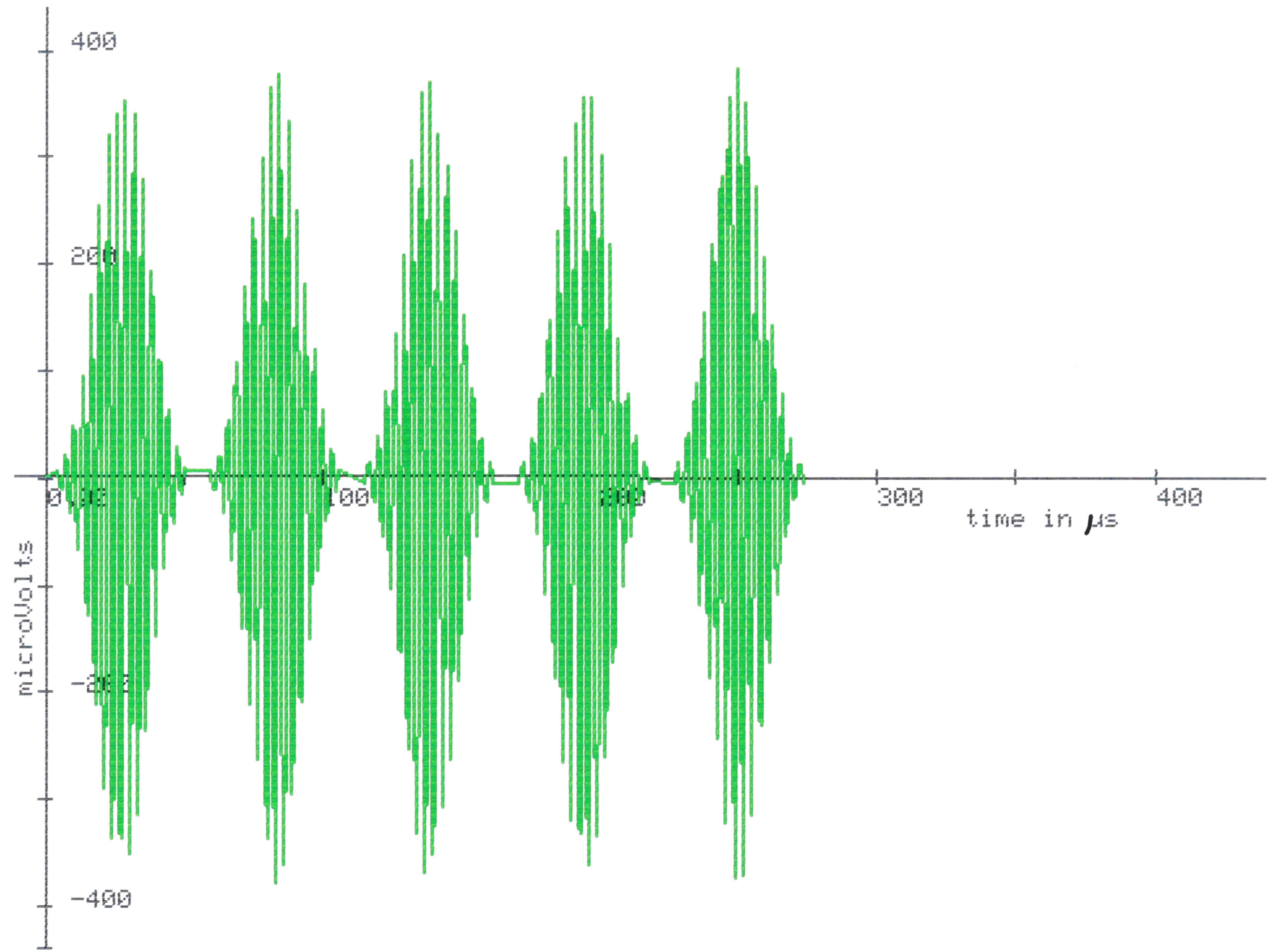

Figure 18

Modelled Transmitted Pulse Train after Pulse Shaping

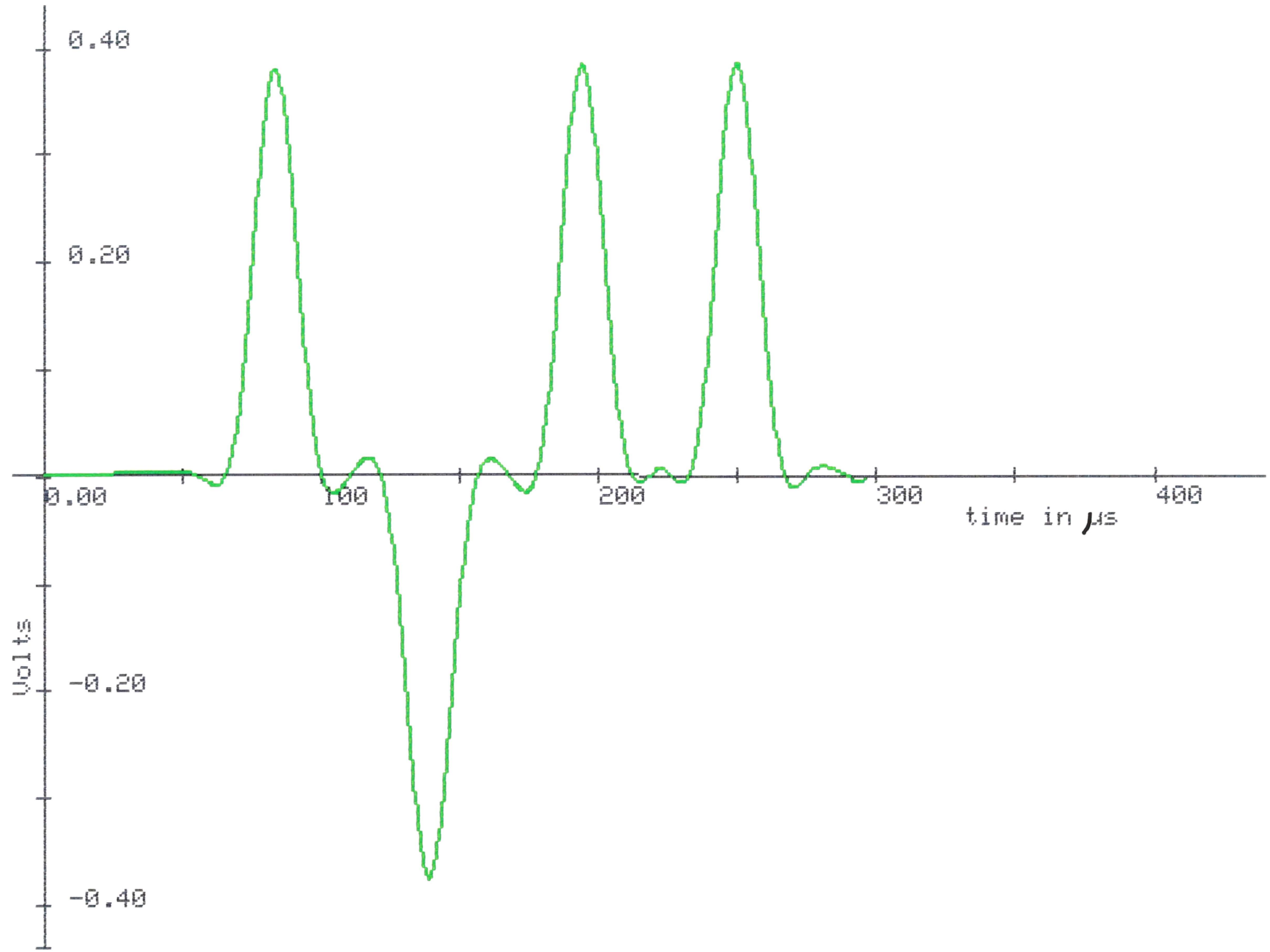

Figure 19

Demodulated Transmitted Pulse Train (Shaped Pulses)

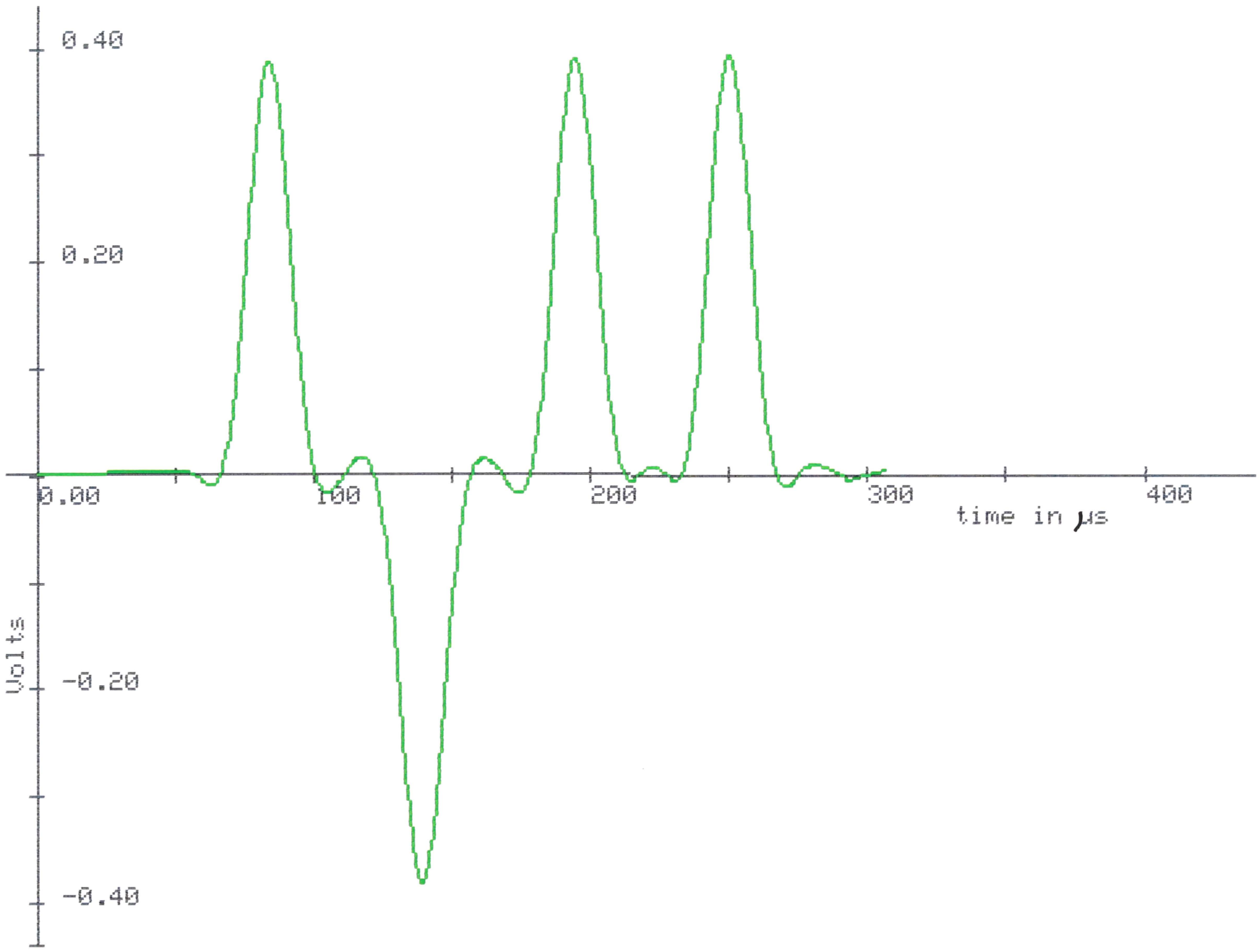

Figure 20

Demodulated Received Pulse Train (Shaped Pulses) - 1

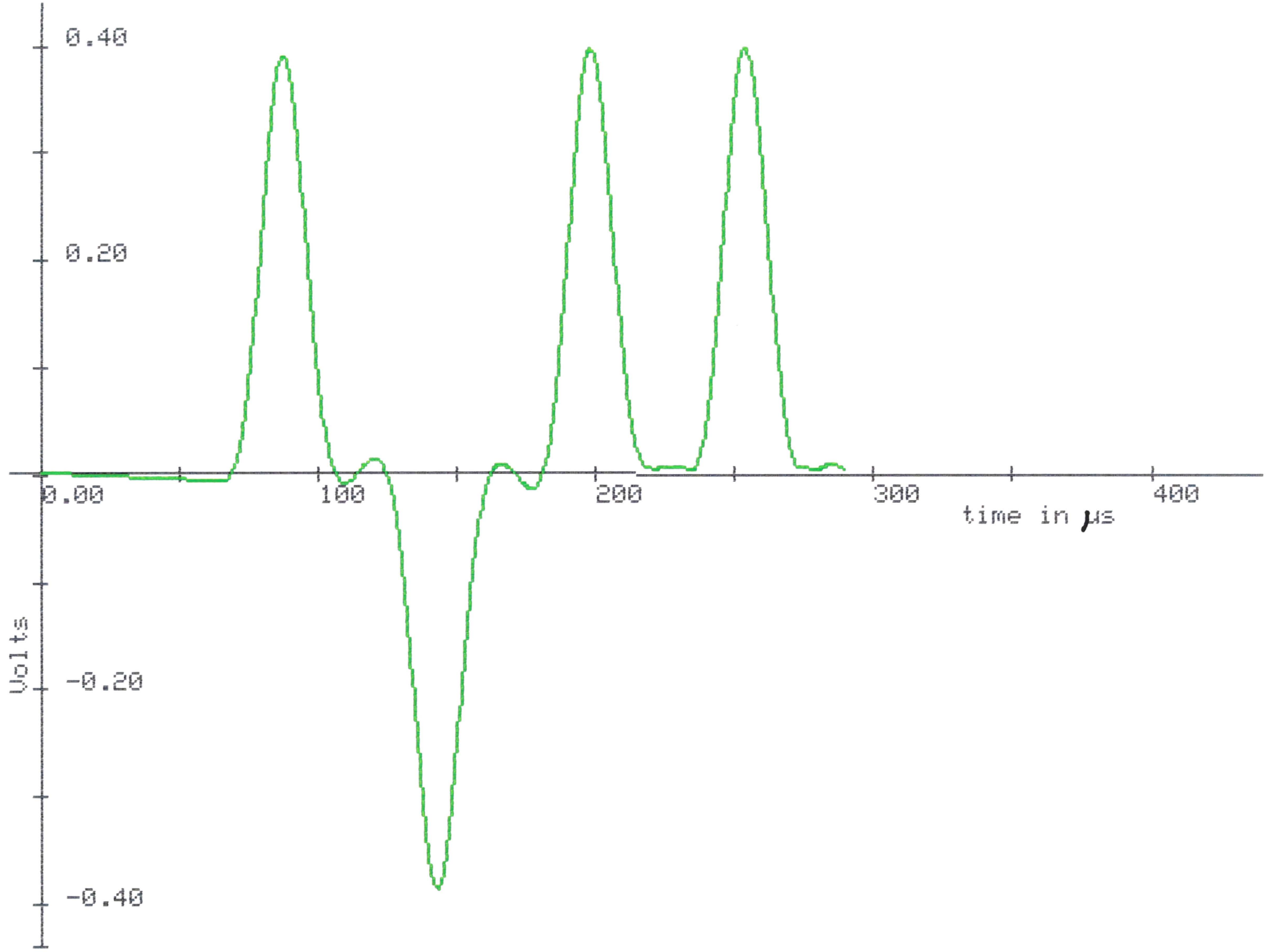

Figure 21

Demodulated Received Pulse Train (Shaped Pulses) - 2

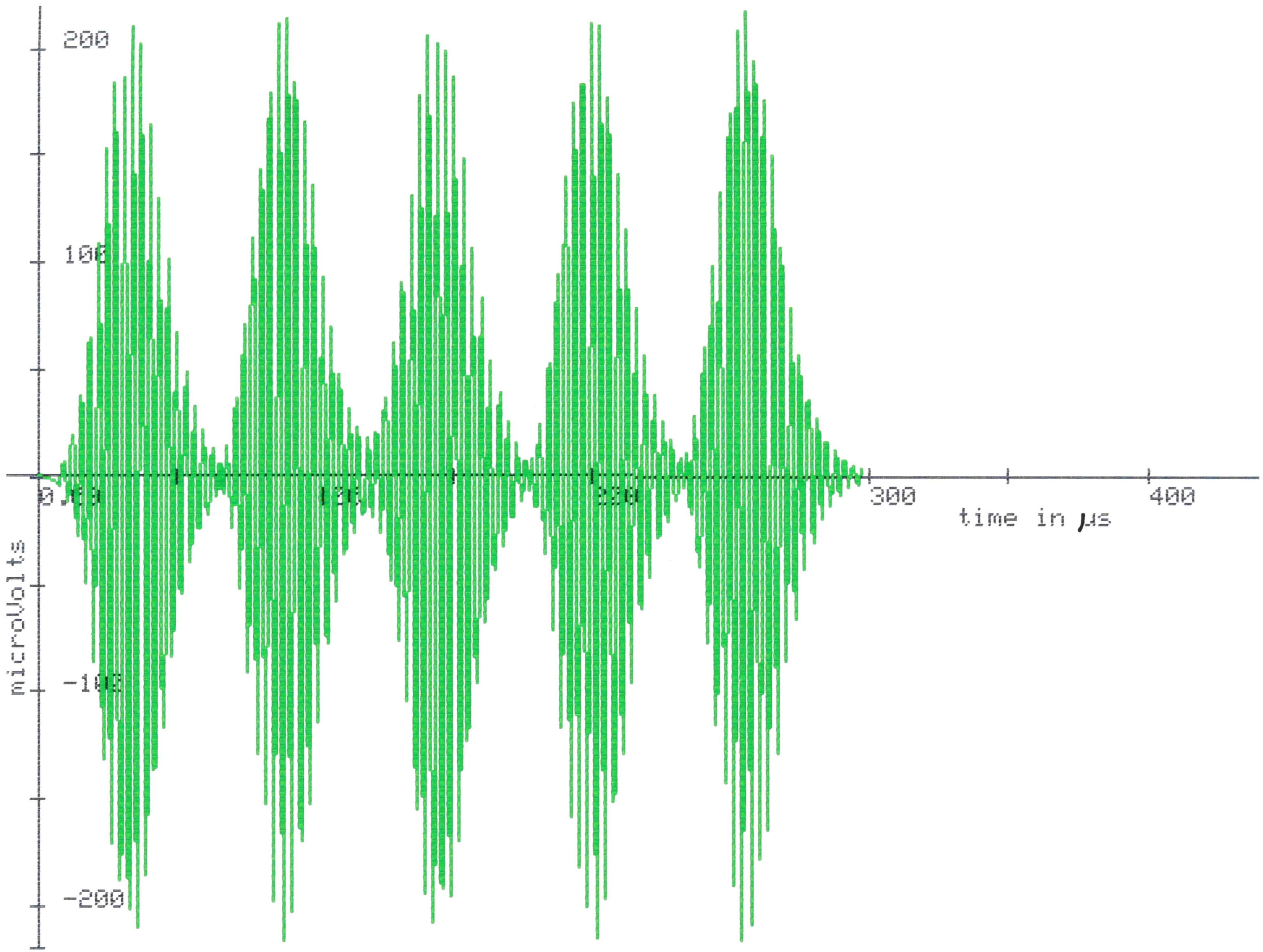

Figure 22

Modelled Received Pulse Train after Pulse Shaping

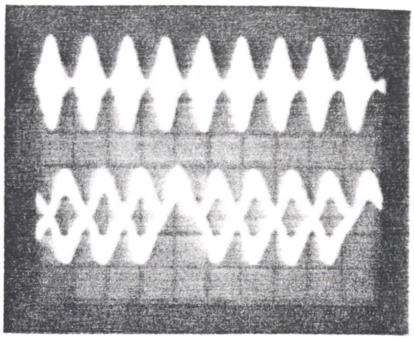

Figure 23

Actual Demodulated Received Pulse Train (Shaped Pulses)

Top trace - output of RF filter - 2 V/div

Bottom trace - output of demodulation filter - 5 V/div

Time base - 50 μs/div

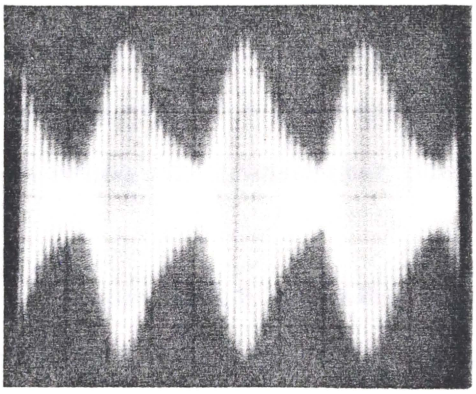

Figure 24

Actual Received Pulse Train after Pulse Shaping

Top trace - output of RF filter - 2 V/div

Time base - 20 μs/div

2.4 SYSTEM DESIGN PARAMETERS

From the theoretical model detailed in the previous section the following conclusions can be drawn:

a) The major obstacle to be overcome is the large system loss (maximum of 135 dB).

b) As long as a quaternary level modulation technique is used with narrow bandwidth pulse shaping then ISI is unlikely to be a concern.

c) A data link symbol rate of 20 kbaud is practical.

2.4.1 TRANSMITTER OUTPUT LEVEL AND RECEIVER SENSITIVITY

With a maximum system loss of 135 dB both a high transmitter output level and a sensitive receiver are required. The readily available integrated circuits for the receiver front-end determine the sensitivity and hence the transmitter output level.

The LM 733 differential video amplifier and the LM 370 AGC amplifier were selected for the first two stages of the receiver. The LM 733 has an input noise voltage of 12 μV RMS when used with a low impedance source. It was considered practical to achieve a 20 μV RMS wide-band sensitivity for the receiver. With a 135 dB system loss this required a minimum transmitter output voltage of 112 V RMS.

The receiver design incorporated four stages of band-pass filtering to reduce the effects of noise (see Section 4.1). The filters reduced the effective input noise voltage by 16 dB (relative to 20 μV) to 3 μV RMS.

The transmitter output level was set at 250 V RMS which was a practical maximum considering:

a) the power consumption of the transmitter; and

b) the current capacity of the output amplifier.

The sensitivity and output levels gave a theoretical system noise margin of 23 dB. The mine generated noise induced on to the hoist rope largely determined the practical signal to noise ratio. This was also the experience of Lagace et al. [8] and Kanda [27].

2.4.2 MODULATION TECHNIQUE

A direct Differential Quaternary Phase Shift Keying QDPSK modulation technique was selected for the following reasons:

a) The modulator is relatively easy to realise (see section 3.3) and allows direct synchronous modulation.

b) Demodulation is again easy and does not require a coherent local oscillator locked into the transmitter.

c) It offers at least a 4 dB better noise performance than other quaternary methods except for QDFSK [32,33].

2.4.3 SUMMARY OF DESIGN PARAMETERS.

The digital radio link for the accelerometer had the following design parameters:

TABLE 6

Digital Link Design Parameters

Symbol rate	:	18 kbaud
Transmitter output voltage	:	250 V RMS
Receiver input sensitivity	:	5 μV RMS
Modulation technique	:	QDPSK
Carrier frequency	:	321 kHz
Maximum system loss	:	$\simeq$ 135 dB

CHAPTER 3

THE TRANSMITTER

This chapter deals with the design aspects and circuitry of the transmitter. The transmitter's functions are to:

a) Measure the acceleration in a plane via two piezo electric transducers.

b) Transmit these measurements to a surface receiver via a 36 kbit per second digital link.

There are four major sections to the transmitter:

a) The transducers which convert the acceleration into an electrical signal.

b) Analog to digital conversion which takes the analog signals from the transducers and produces a digital symbol stream.

c) The modulator section which modulates a carrier frequency in accordance with the digital symbol stream.

d) The power amplifier which provides the feed signal to the transmitter coupler, inducing the signal onto the wire rope of the shaft vehicle.

The four sections mentioned above are shown in the block diagram of the transmitter in Figure 25.

3.1 TRANSDUCERS

For measuring the acceleration of a skip (shaft vehicle) operating in a mine shaft four factors are important:

a) the environment is very harsh,

b) electrical noise can be a problem at low output signal levels (ie., microvolt levels),

c) low frequency accelerations (< 10 Hz) are important,

d) high frequency accelerations (up to 500 Hz) are important.

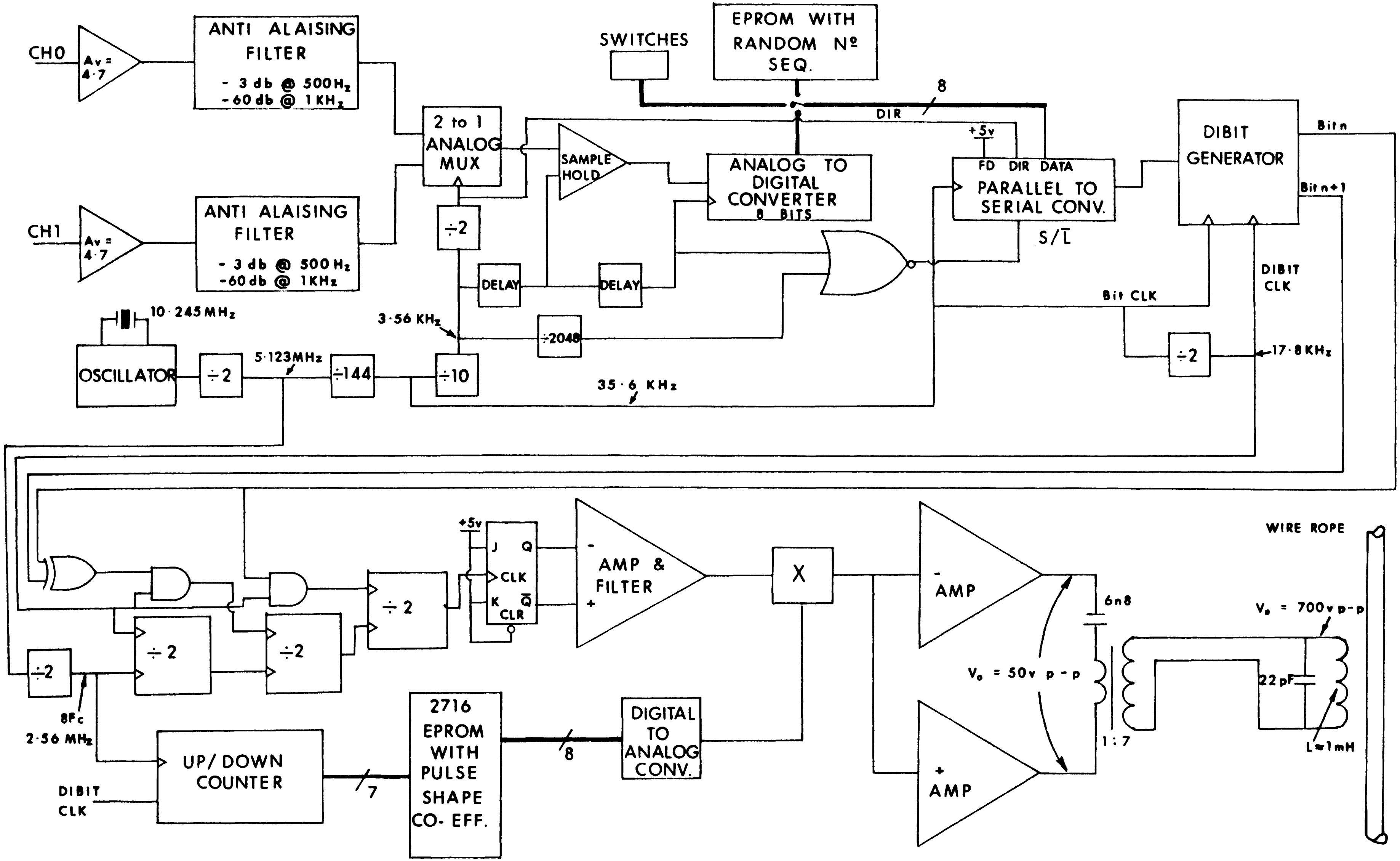

Figure 25

Transmitter Block Diagram

Today the piezo electric type of accelerometer transducer is the most popular form of accelerometer. This type of instrument has a number of characteristics which influenced the final selection of the brand and model of transducer. The conventional piezo electric accelerometer (ie., without in built amplifier) has a very low output voltage and a very high output impedance. They are often referred to as charge output devices because of these characteristics. The need for complex and sensitive preamplifiers for piezo electric transducers generally rules them out for use in a mine shaft.

One exception to this is where a preamplifier is incorporated into the transducer. This has the advantages that:

a) the preamplifier is protected from the environment,

b) the transducers output impedance and output signal level are relatively low and high respectively.

A suitable piezo electric transducer with an inbuilt preamplifier was located and used for the accelerometer.

The brief specifications are:

Make and type	:	Environmental Equipments Ltd, CV100
Frequency Response	:	5 Hz - 7 kHz ($\pm$ 3 dB)
Output Sensitivity	:	100 mv/g pk $\pm$ 4%
Dynamic Range	:	$\pm$ 50 g

A full specification sheet appears in Appendix Four.

3.2 THE ANALOG TO DIGITAL CONVERSION SECTION

This section forms the heart of the transmitter and consists of:

a) Anti aliasing filters.

b) Sample and hold circuitry and analog to digital converter.

c) Parallel to serial converter and synchronisation word generator.

d) Dibit generation.

3.2.1 ANTI ALIASING FILTERS

With digital measurement systems the need for anti aliasing filters is well known [34]. Their function is to stop frequency components above the Nyquist frequency being seen by the analog to digital converter and hence manifesting themselves as false low frequency signals [32]. The specifications for an anti aliasing filter are easily derived and depend on three factors:

a) half the sampling frequency (fs/2),

b) the resolution (or SQNR) of the analog to digital converter,

c) the required corner frequency (fc).

This may be best explained by Figure 26 below.

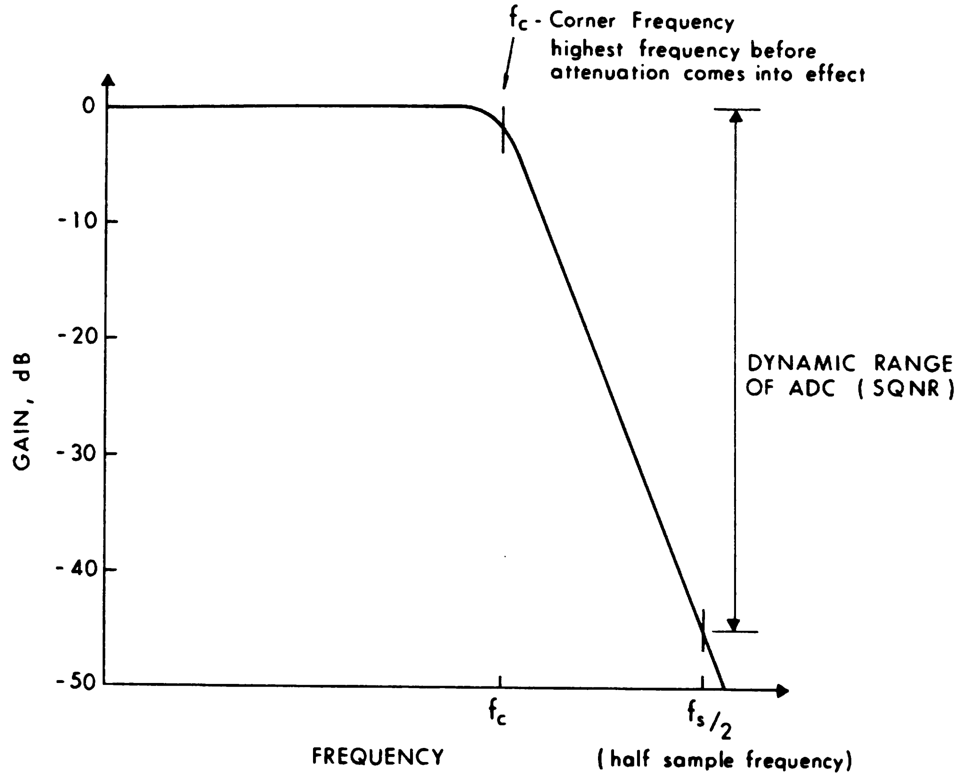

Figure 26

Important Specifications for Anti Aliasing Filters

For the accelerometer the three factors were:

a) sampling frequency/2 (fs/2) = 890 Hz,

b) resolution of ADC = 8 bits (SQNR = 48 dB),

c) corner frequency (fc) = 500 Hz.

The filter design selected to meet the above specifications was a fourth order elliptical filter. The filter is constructed using 2 x LM 348 Quad Op Amplifiers per filter [35]. The measured frequency response is shown in Figure 27. The corner frequency (-3 dB) is 473 Hz and at 500 Hz the response is -5 dB which is 2 dB below specifications. This is considered insignificant as it represents only 5.4% of the bandwidth having up to 20% greater loss.

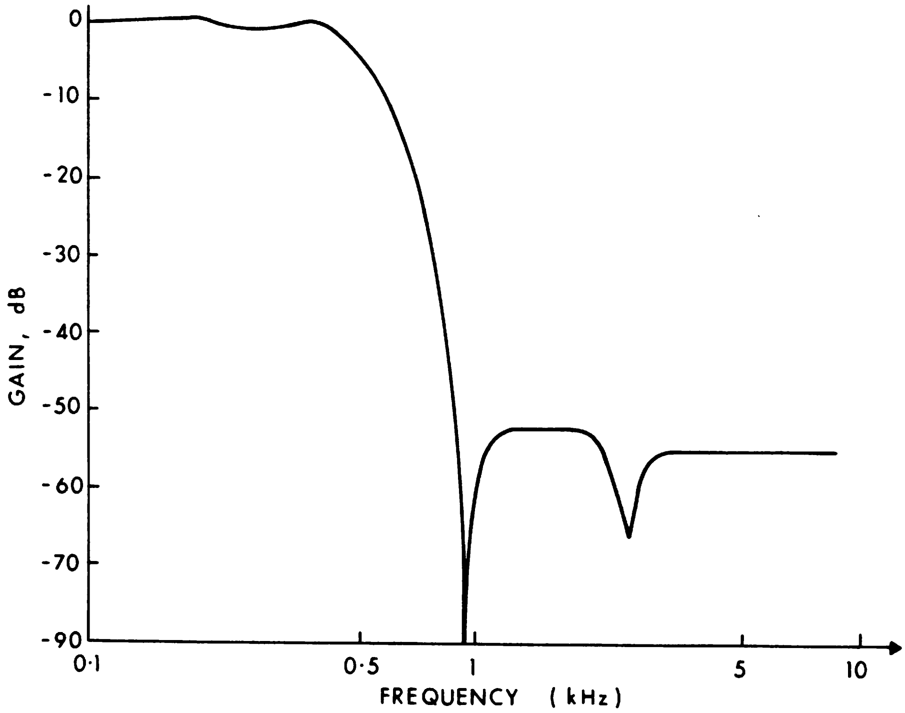

Figure 27

Frequency Response of Anti Aliasing Filters

The anti aliasing filters are preceded by a buffer using a spare Op-Amp. This amplifier has the role of adjusting the range and resolution (sensitivity) of the accelerometer.

The present gain setting gives a nominal range and resolution of ± 5.0 g and ± 0.04 g respectively. Halving the gain will double the range and halve the resolution. This amplifier also removes the DC voltage present on the output of the transducer.

3.2.2 SAMPLING AND ANALOG TO DIGITAL CONVERSION

The outputs of the anti aliasing filters are fed via a multiplexor and a sample and hold circuit to an Analog to Digital Converter (ADC). The multiplexor uses two of the four analog switches, on a 4066 analog CMOS IC, which function as a two to one time division multiplexor.

The sample and hold circuit, consisting of a LF 398, is used to ensure the ADC's input signal does not change during the conversion. The output of the sample and hold circuit is passed directly to the ADC. A hybrid 8 bit converter, DATEL Systems Model 89A, is used. A detailed specification sheet appears in Appendix Four.

3.2.3 PARALLEL TO SERIAL CONVERTER AND DIBIT ENCODER

The parallel outputs of the ADC are converted to a serial stream, by a parallel to serial converter, using 74165 shift registers. The converter also allows other information bits, as discussed below, to be inserted into the stream. As the data link employs Quaternary Differential Phase Shift Keying (QDPSK) a dibit (two bit symbol) encoder is used. The encoder consists of a two-stage shift register and buffer.

3.2.4 BIT ALLOCATION

In the early days of the project, it was thought necessary to have the following designated bits:

Data 1 ———— Data 8 MSB ———— LSB	DIRECTION BIT	FLAG BIT

The eight data bits are the output of the ADC. The direction bit identifies the transducer (or channel) the measurement was taken from. When channel one is measured the direction bit is set to one otherwise it is zero. The flag bit is always high except during a synchronising word (see section 3.2.5).

As a result of further design and prototype development, the direction and flag bits are no longer necessary. Currently they are only used for synchronisation checking within the computer. Therefore, these two bits could be better utilised by:

a) increasing the resolution of the system to 10 bits, or
b) incorporating an error detection and correction system.

Note that if (a) was adopted, the anti aliasing filter would have to be modified to produce a higher cutoff rate, as the ADC's SQNR would have increased from 48 dB to 60 dB.

3.2.5 SYNCHRONISING WORD

In a data communications link, such as the one developed here, synchronisation of the transmitter and receiver is important. For this link, synchronisation is achieved by transmitting a special "key" or synchronising word every 2048 measurements. This corresponds approximately to one every half a second. The synchronising word is unique having all bits set to zero.

The receiver is continually searching for this word and when it is detected, the receiver:

a) adjusts, if necessary, all its timing to ensure synchronisation with the transmitter,

b) reads and transfers, to the computer, the distance measurement.

In addition, the synchronising word also has the functions of:

a) providing for the computer an easy check, on whether all incoming data has been captured,

b) ensuring that if the data link is hit by impulsive noise, causing a loss of synchronising, then the maximum down time will be half a second.

3.3 THE MODULATION SECTION

The first part of the modulation section is the phase encoder which produces a wide bandwidth phase encoded carrier. The bandwidth of the signal is reduced by pulse shaping each symbol. These two areas are discussed in 3.3.1 and 3.3.2 respectively.

3.3.1 THE PHASE ENCODER

As mentioned in Section 2.4.2 a QDPSK mode of encoding is used for the radio link. For this four level method of encoding, relative (or differential) shifts in phase between symbols represent the value. The shifts and their values are given in Table 7.

TABLE 7

Phase Shifts for a QDPSK Modulator

Dibit Value	$\Delta\ \phi\ (\phi n - \phi n\text{-}1)$
00	+ 45°
01	+ 135°
10	- 45° (+315°)
11	- 135° (+225°)

To produce the QDPSK coded carrier a method described by Baker [36] is used. Figure 28 shows a block diagram of the system.

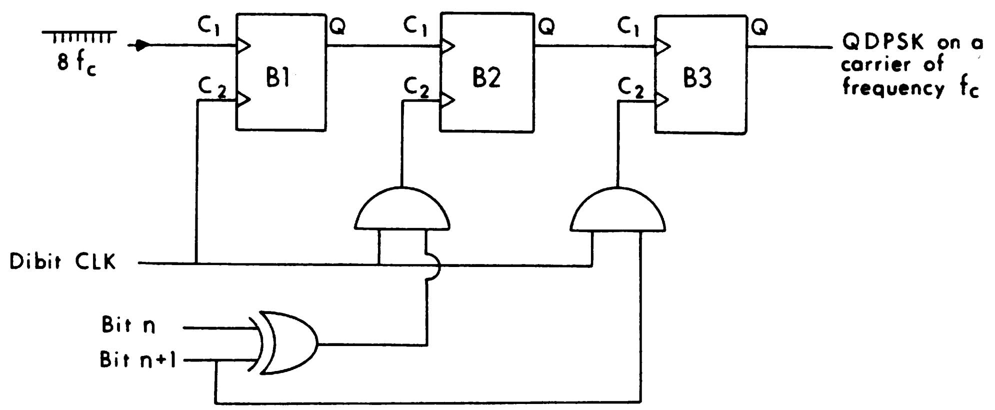

Figure 28

Block Diagram of a QDPSK Encoder

The above circuit assumes that there are an integral number of cycles of carrier frequency (f_c) for each symbol period. The three stage binary divider divides the 8 x f_c down to f_c but at each stage a phase shift of n x 45° (n = 1,2,4 respectively) can be injected at the start of each symbol.

Consider B_2, a pulse on C_2 will change its output by 180° but when this is divided down by B_3 its effect will be 90°. For a pulse on C_2 of B_1 the effect will be a shift of 45° as its original 180° shift is divided by both B_2 and B_3.

For B_3 a pulse on C_2 will produce a shift of 180° in f_c. Hence, there is the mechanism for providing the required phase shifts for QDPSK modulation by controlling when the C_2 inputs are pulsed.

It will be noticed from Table 7 that there is a common +45° shift for each valve of the dibit, then there is an extra shift of +90° for 01, +270° for 10 and +180° for 11. The small amount of logic at the bottom of Figure 28 provides this decoding.

Implementing the encoder in practice is somewhat more complicated as dual edge triggered flip flops were not readily available. Also a small amount of delay in applying the dibit clock in succession to the AND gates is required to avoid interference. The full circuit for the encoder is shown in Appendix Three. For proper operation of the circuit an integral number of carrier cycles in each symbol period is required. To achieve this all timing for the transmitter needs to be derived from the one central clock. A 10.25 MHz crystal oscillator is used as the central clock source.

3.3.2 WINDOWING AND FILTERING

As previously mentioned one of the design aims for the link was a narrow bandwidth. It is well known, through Fourier analysis, that a rapid change of phase, frequency or amplitude requires a wide bandwidth [33]. The circuit described in section 3.3.1 applies the phase changes abruptly at the transition from one symbol to another. This has two consequences, firstly a wide bandwidth (see Figure 29) is required to transmit the signal and secondly, ISI will affect up to 20% of the symbol (see Section 2.3.3). Glance [37] has shown that the frequency spectrum of a QDPSK signal is the same as a rectangular pulse of sine wave carrier with a duration of one QDPSK symbol.

The spectrum measured at the output of the phase encoder is shown in Figure 29. The envelope is a |sinc| function, as expected, with slowly decreasing side lobes.

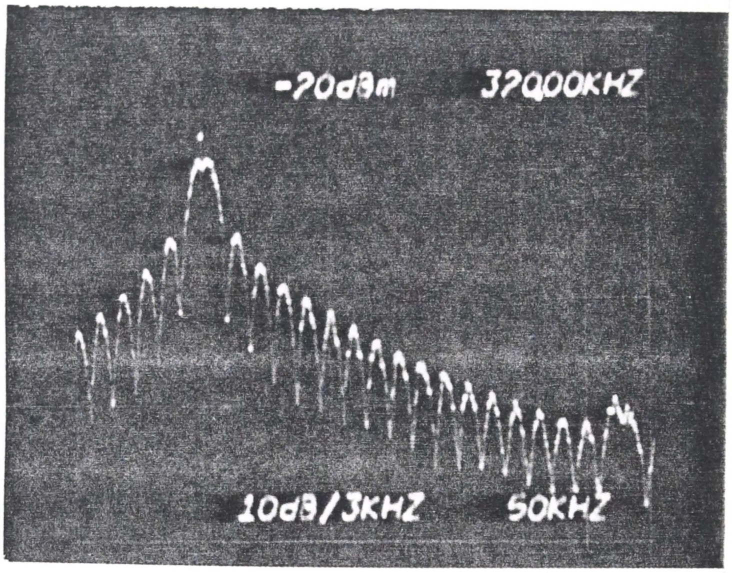

Figure 29

Frequency Spectrum of a QDPSK Signal

Obviously all the frequency components cannot be transmitted by a narrow bandwidth link. Applying a sharp filter to reject the components outside the allowable bandwidth would cause significant ringing and further ISI. A method of applying pulse shaping to reduce the bandwidth is used. Harris [31] explains in detail the importance of pulse shaping and windowing on bandwidth considerations.

Although this paper deals with the use of windows in Fourier analysis, the results apply equally to pulse transmission systems. From the work done in [31] it was decided that windowing the output of the phase encoder would be an effective way of limiting the bandwidth without inducing ISI. As well it would reduce the ISI due to the rectangular pulse shape (see section 2.3.3).

A four term Blackman Harris window [31] was selected as it is easy to compute and gives one of the narrowest overall bandwidths. Figure 30 shows the measured bandwidth of the windowed pulses.

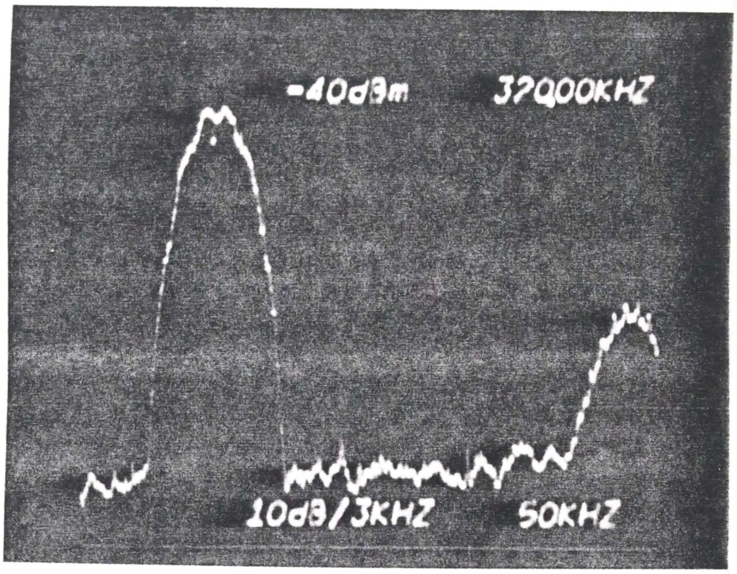

Figure 30

Frequency Spectrum of Pulse Shaped QDPSK Signal

The second hump to the right of the main lobe is the second harmonic of the carrier due to limited carrier filtering. Note that where the non-windowed signal had a spectrum consisting of many narrow lobes the shaped signal has only one wider lobe. In effect, windowing the pulse is making more effective use of a given bandwidth.

The method of applying the window is somewhat novel. The shape is stored numerically in an EPROM. As the window is symmetrical only one half of the shape is stored as 72 numbers ranging in size from 0 through to 255. The stored shape and the corresponding EPROM addresses and data are shown in Figure 31.

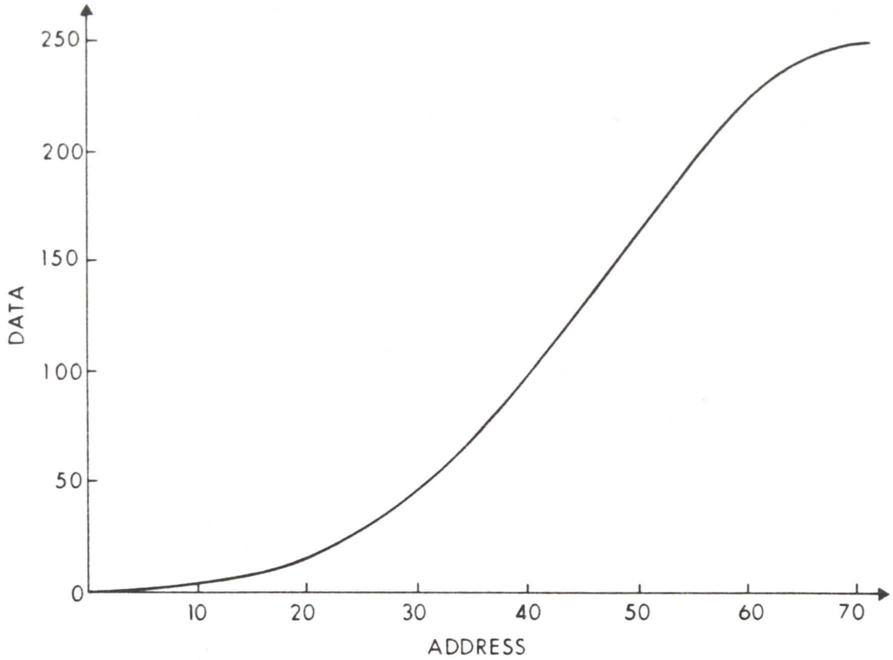

Figure 31

Pulse Shaping Window

A block diagram of the pulse shaping circuit is shown in Figure 32. A major advantage of this circuit is the ease of changing the pulse shape, achieved by re-programing the EPROM.

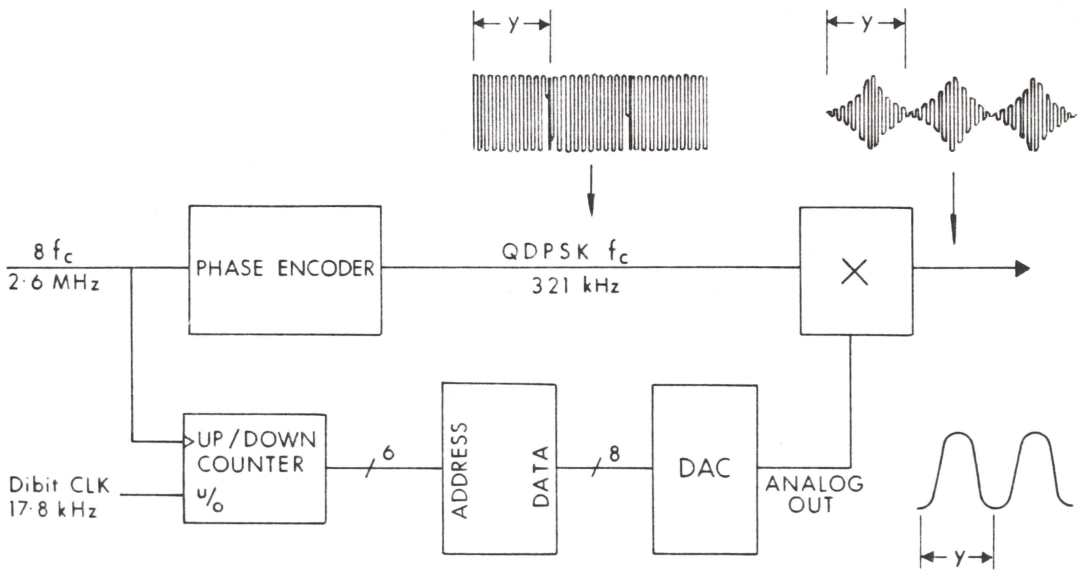

Figure 32

Block Diagram of Pulse Shaping Circuit

The window values are clocked out, at eight times the carrier frequency, to a Digital to Analog Converter (DAC). The output of the DAC is multiplied with the rectangular shaped QDPSK signal producing the pulse shaped signal ready for transmission.

3.3.3 POWER AMPLIFIER

The function of the power amplifier is to amplify the pulse shaped QDPSK signal to a suitable level for the signal coupler. A number of techniques are used to overcome output level restrictions normally imposed by limited power supply rails. They are:

a) A bridge amplifier configuration.

b) An output step up transformer.

c) Resonance tuning of both the primary and secondary transformer circuits.

These techniques combine to produce a signal level of some 250 V RMS across the signal coupler. The amplifier uses conventional Op-Amps with separate output transistors. The step up transformer has a turns ratio of 1:7.

3.3.4 TEST DATA SECTION

To help in the development of the link test data sections were included in the transmitter and receiver. In the transmitter the section was able to transmit either a known pseudo-random sequence, or a fixed data pattern. Its main functions were to enable :

a) Quantitative error rate tests to be conducted.

b) Quantitative eye pattern inspections.

c) Transmission of a fixed known data stream.

Using the quantitative methods of error rate and eye pattern tests made the design and debugging of the system considerably easier.

The section has two switches to select the inputs into the parallel to serial converter. The switches select between the outputs of:

a) the ADC,

b) an EPROM containing the pseudo-random sequence,

c) a dip switch determining the fixed data pattern.

In the receiver there is an error detection and counting circuit for use in association with (b). Figure 33 shows the block diagram for the transmitter test data section.

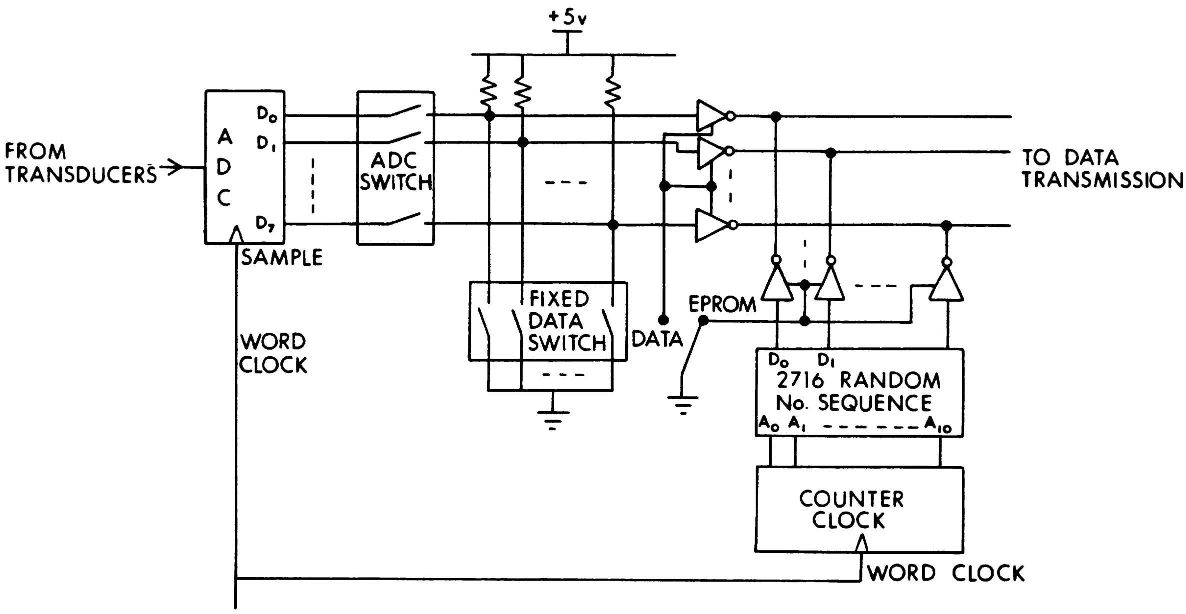

Figure 33

Block Diagram of Test Data Section

Only the eight data bits are derived from the three alternative sources. The direction and flag bits always come from the control circuitry.

If the data section is selected then the words transmitted will depend on the state of the ADC and fixed data switches. To select the fixed data switches the ADC switches must be open and visa versa.

The pseudo-random sequence has a uniform distribution with a range between zero and 255 and has 2048 numbers. The sequence is clocked out at the ADC sampling rate. Therefore the whole sequence will be transmitted once between successive synchronising words. The algorithm used [38] to generate the sequence is :

$$U_o = 1$$

$$U_{i+1} = 7^9 (U_i \div 10^{10})(\text{MOD } 10^{10})$$

3.4 MOUNTING AND CONSTRUCTION DETAILS

This section describes the methods used to construct and mount the instrument. There were two main considerations in deciding on the methods:

a) The instrument was a prototype and would require modifications.

b) The instrument would be subject to consistent shock and a poor environment.

These requirements can tend towards mutual exclusion as methods available for protecting electronic circuits usually mean that easy modification is out of the question.

For mounting the accelerometer the existing mechanical accelerometer mounting methods, mentioned in Chapter 1, were used.

Wire wrapping and chip sockets were used to construct the circuit boards. While layers of foam were placed between the boards to protect against vibration. These mounting and construction methods were decided upon because they offered:

a) The use of existing equipment (in the case of mounting arrangements).

b) Ease of circuit modification (wire wrapping).

3.4.1 MOUNTING DETAILS

The physical environment in a mine shaft is generally destructive to electronic circuitry [39,40]. The ZC Mines shaft is no exception. The main destructive elements are:

a) vibration,

b) water and corrosion.

3.4.1.1 Transmitter

By using the mounting arrangement for the mechanical accelerometer comparisons could be made between the results collected by the two accelerometers. It also gave good protection against water and corrosion but none against vibration. The mounting arrangement consisted of a metal bin which was bolted under the bottom of the skip.

It has previously been found that the bottom of the skip gave more reliable readings of acceleration for the mechanical accelerometer. A metal enclosure which fitted tightly into the bin was used to house the transmitter circuitry.

To protect the circuitry from the effects of vibration the circuit boards lie on layers of foam. The foam layers are specially contoured to follow the shape of the larger components on the circuit boards. This ensures that pressure is applied evenly to all components to keep them in place when the lid is closed. The layers are built up from the bottom of the enclosure in the following order:

a) A layer of foam with cut outs for wire wrap pins and sockets.

b) Digital transmitter board (wire wrap).

c) A layer of foam with cut outs for wire wrap board.

d) Analog transmitter board (PCB).

e) A layer of foam with cut outs for analog board.

f) Extra layer of foam to apply pressure to all components to keep them in place.

The enclosure was held in place by two brackets attached to the bin. The transducers were screwed into two of the sides of the bin to match as closely as possible the mechanical accelerometer. The arrangement of the transmitter enclosure in the metal bin and the transducers is shown in Figure 68 in Appendix Three.

The metal bin is securely fastened to the bottom of the skip, by four bolts, as shown in Figure 34 below. Note the two transducers at right angles to each other on the right hand side.

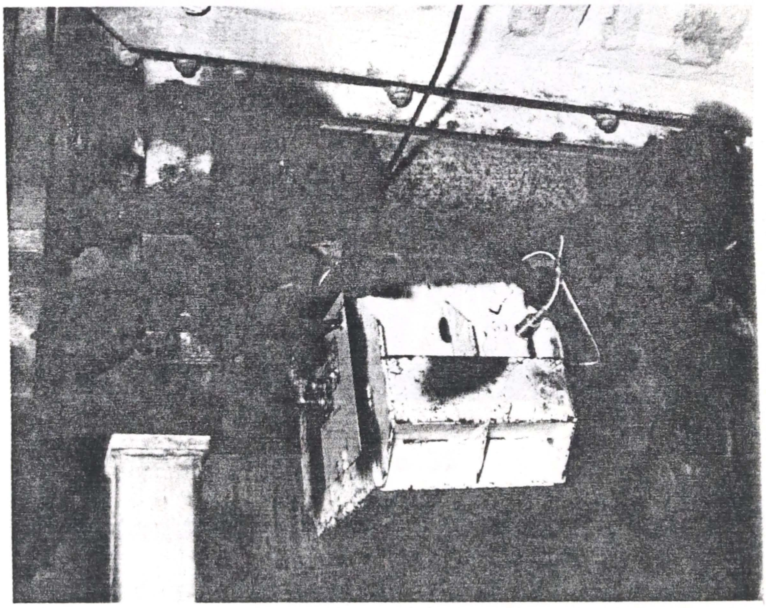

Figure 34

Mounting Arrangement of the Metal Bin to the Skip.

3.4.1.2 Signal Coupler

The transmitter coupler is held firmly onto the wire rope by two webbed belts and adhesive tape. The coupler is located approximately one metre above the end of the capel which connects the wire rope to the skip. The arrangement is shown in Figure 35.

The cable between the transmitter and coupler is passed up the side of the skip and wrapped around a tipping wheel to keep it taut. It is then taped to the capel and rope at convenient points.

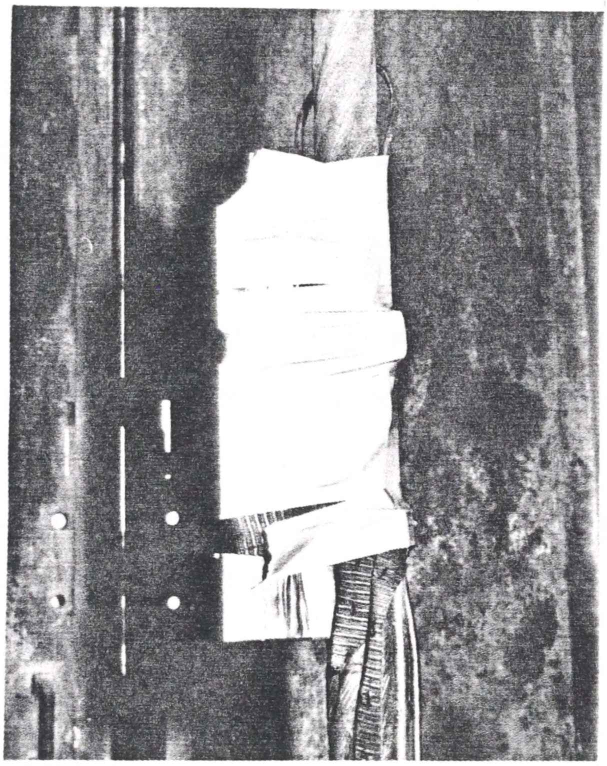

Figure 35

Mounting Arrangement for the Transmitter Coupler

3.4.2 CONSTRUCTION DETAILS

The instrument was built as a prototype with the design, construction and testing proceeding together. That is, as the design for one stage was completed it was then built and tested.

The next stage would then be designed, and so on. This required a construction technique that allowed easy changing and addition of circuitry. One further and important requirement for the transmitter was the ability to withstand vibration.

Of the two main requirements, construction flexibility was considered the most important. It would be impractical to develop the instrument using a construction technique with a high tolerance to vibration and an inability to make circuit changes.

For these reasons wire wrapping and chip sockets were selected. Wire wrapping done correctly is as reliable, if not more so, than normal printed circuit boards. But it is questionable whether socketed chips will remain in place under high vibration conditions.

For inter-connecting circuit boards multi-wire ribbon cables and connectors were used. These offered greater flexibility in the mounting arrangements of the circuit boards within the transmitter box. As well, the boards could be worked on easily by laying them out on the bench. See Appendix Three for details of the circuit and wire wrap boards.

3.4.3 POWER SUPPLY

The transmitter supply is sourced from a pair of six volt 12 amp hour sealed lead acid batteries paralleled to give a 24 amp hour supply. The transmitter circuitry requires ± 5 V, ± 15 V and ± 12 V. All except the +5 V are supplied by series regulators fed from via a ± 15 V DC - DC converter. The output voltage of the batteries (nominally 6.5 volts) is reduced by a series diode to 5.6 volts.

This is within the safe operating limits for TLL and the DC - DC converter. The DC - DC converter is an Analog Devices 951 rated at 1 amp output.

The charging of the batteries is carried out with the batteries in the transmitter box. A switch mode power supply is connected to the batteries via a Cannon socket in the side of the transmitter enclosure. The voltage is set on the power supply to provide a maximum charging current of six amps. The above mix of power supplies gives good reliability and efficiency without having to resort to great lengths.

3.4.4 PROBLEMS AND SUGGESTED IMPROVEMENTS

In the trials conducted so far the enclosures and circuitry have stood up well. The two concerns regarding the long term suitability of the transmitter enclosure and circuit construction are:

a) heat dissipation,

b) fragility of socketed components.

At the moment, because all the components are surrounded by foam heat dissipation is poor and some components reach unacceptable operating temperatures. Surface temperatures as high as 75 °C for the ADC and 63 °C for the DC - DC converter have been measured. Generally surface temperatures of 40 - 50 °C have been measured for the remaining components.

The operating temperatures for the ADC and the DC - DC converter could be significantly reduced by mounting them directly onto the transmitter enclosure.

It is also suggested that a low power CMOS ADC be used. This would probably negate the need for heat sinking the ADC. Use of CMOS technology throughout the transmitter would have two main and obvious advantages:

a) reduced power consumption, and

b) reduced heat dissipation.

For these reasons alone the conversion of the transmitter circuitry to CMOS is strongly recommended.

The methods used for mounting passive components on the wire wrap boards is not reliable at present and proper component carriers should be used. In the longer term if the project is considered worthwhile the use of custom VLSI chips should be investigated. This would lead to very significant reductions in power, heat dissipation, circuit complexities and physical size.

With the transducers mounted on the metal bin, any bin resonances will be superimposed with the vibration of the skip. To overcome this, direct mounting of the transducers onto the skip is recommended. This was not originally done as it required drilling and tapping of the skips consuming valuable and limited testing time.

The recommended mounting arrangement uses a mounting block which would bolt onto the bottom of the skip. The block should be rectangular with two bolts to hold it on to the skip and a pin to locate it. Figure 36 shows a possible construction. The pin would ensure the correct orientation of the block each time it is attached to the skip. The mounting block would also allow new locations to be tried.

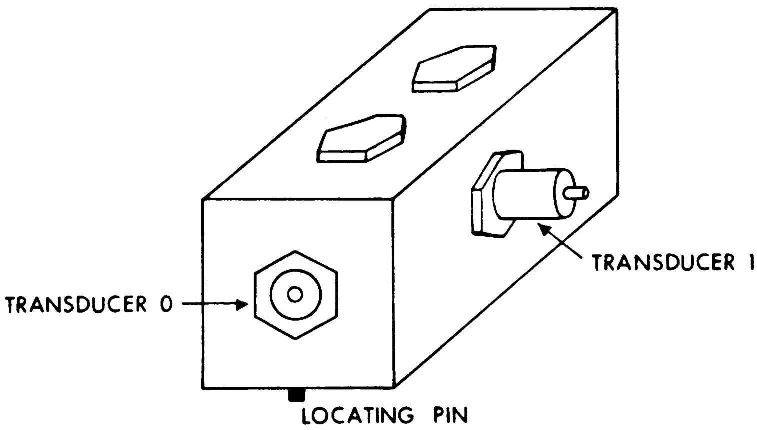

Figure 36

Mounting Block Arrangement

CHAPTER 4

THE RECEIVER

This chapter deals with the design of the receiver, decoding circuitry and interface to the computer. Figure 37 shows a block diagram of the receiver. The receiver's functions are to reliably decode the received signal and pass the data to the computer. Along with these main functions there are two important secondary tasks:

a) to take distance measurements and pass these to the computer, and

b) to collect error counts when the pseudo-random sequence is being transmitted.

The receiver circuitry is divided into four main sections corresponding to these major functions:

a) Signal reception and demodulation.
This area is responsible for detecting the signal, amplifying it and then decoding it back into a sequence of 10 bit words as originally transmitted.

b) Error Detection and Counters.
This circuitry operates when the pseudo-random sequence is transmitted. Its function is to detect when an error occurs, determine how many symbols are in error and to keep a tally.

c) Distance Measuring Equipment.
This is responsible for gathering accurate information on the location of the skip in the shaft.

d) Interface to the Computer.
This stores the information, obtained from sections a) and c) above, and passes it to the computer for storage in a disc file.

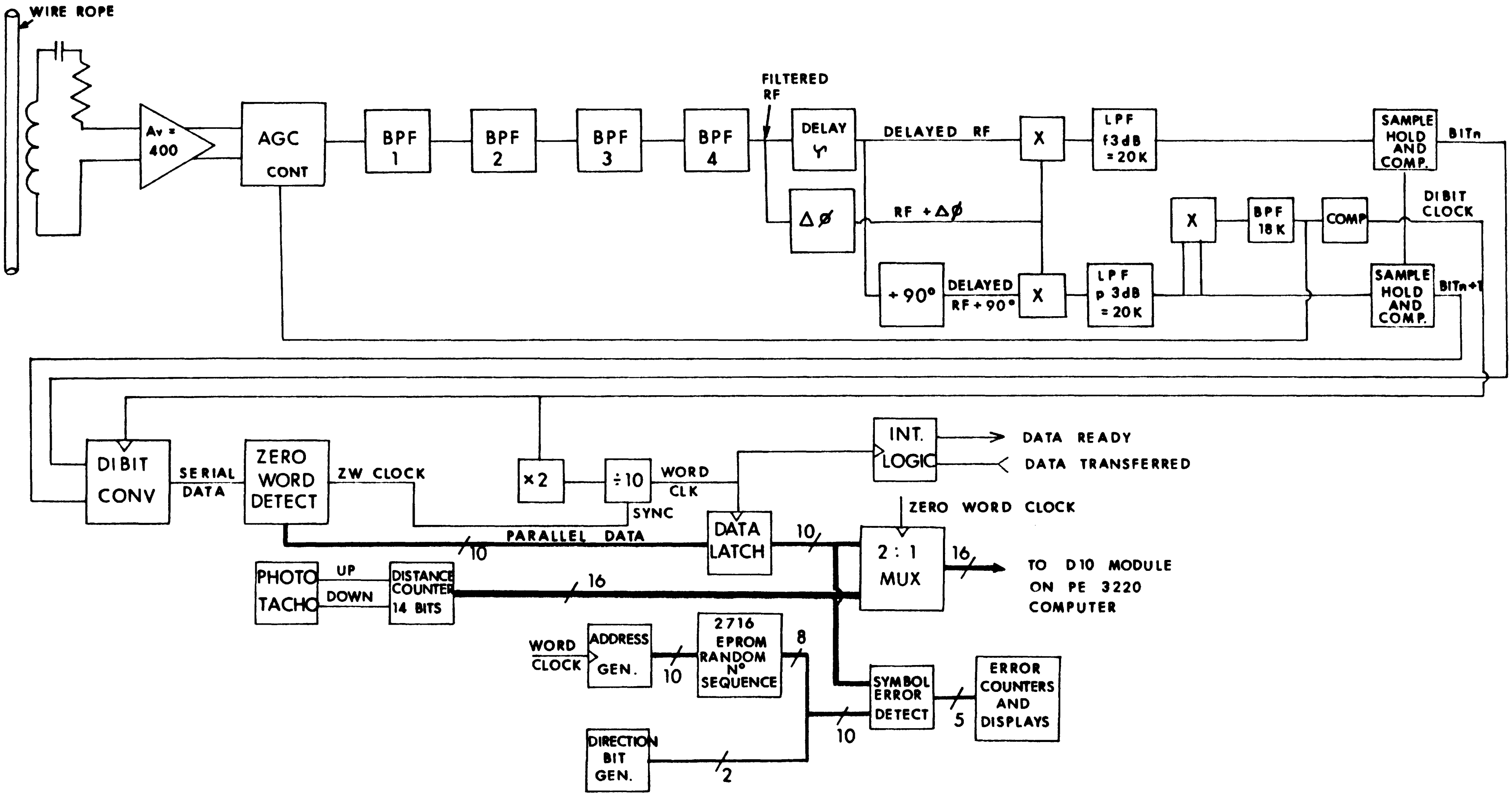

Figure 37

Block Diagram of Receiver Circuit

4.1 SIGNAL RECEPTION AND DEMODULATION

The design of this section follows conventional lines with the received signal passing through:

a) Tuned signal coupler and high gain front-end amplifier.

b) Automatic gain control amplifier and narrow band filter.

c) Demodulation circuit for QDPSK signals.

4.1.1 THE RECEIVER FRONT END

The signal is picked up, from the wire rope, by a signal coupler just below the sheave wheel. Due to the vibrations of the wire rope a gap of some 10 - 15 cm must be left between the rope and the signal coupler. The coupler has some local tuning to increase its sensitivity to the frequencies of interest. A 100 - 150 metre shielded cable connects the signal coupler to the receiver in the computer room. The first stage of the receiver utilises a wide band video amplifier with differential inputs and outputs to minimise the effects of common mode noise. There is some limited filtering on both the inputs and outputs of the video amplifier to help reduce the effects of normal mode noise. The overall sensitivity of receiver, which is mainly determined by the first stage, is 6 μV RMS for a 6 dB SNR. The output of the differential amplifier is fed to a monolithic Automatic Gain Control (AGC) amplifier with a single ended output. The reaction time of the AGC is designed to be short so that it will react quickly to fluctuations in amplitude.

Normally AGCs with short reaction times are badly affected by impulsive noise. To ensure that impulsive noise had the minimum effect the control signal for the AGC is derived after filtering and decoding.

This process of generating the control signal is described in Section 4.1.2, which deals with the decoder.

The AGC is followed by four cascaded second order band-pass filters. The response curves are designed to be overlapping in order to achieve the required bandwidth and steep roll off. The frequency responses of each of the four stages and the combined response are shown in Figure 38.

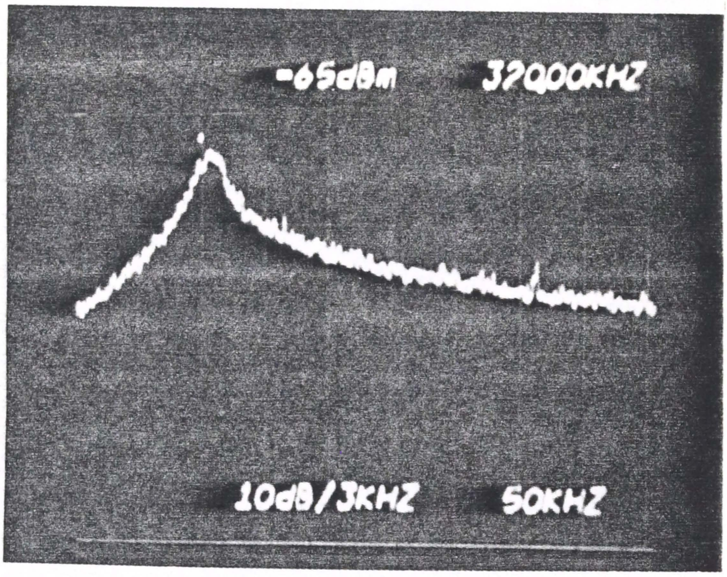

Stage 1

Frequency Response

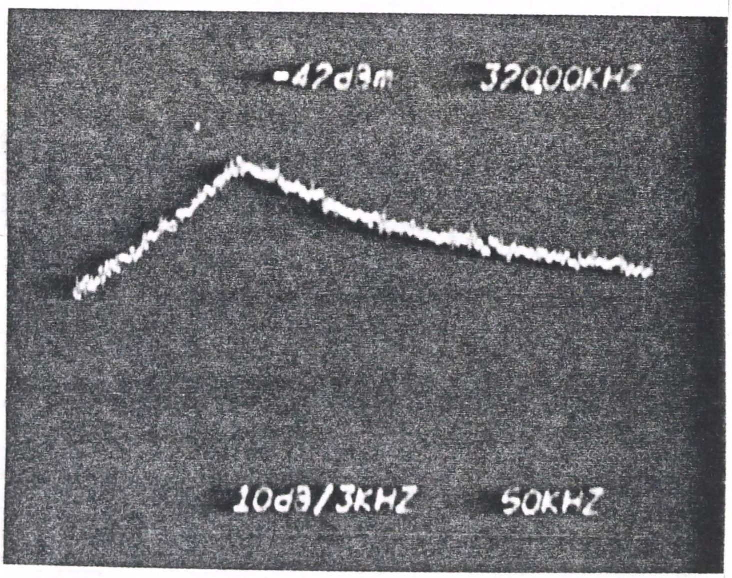

Stage 2

Frequency Response

Figure 38

Frequency Responses of Band-Pass Filters

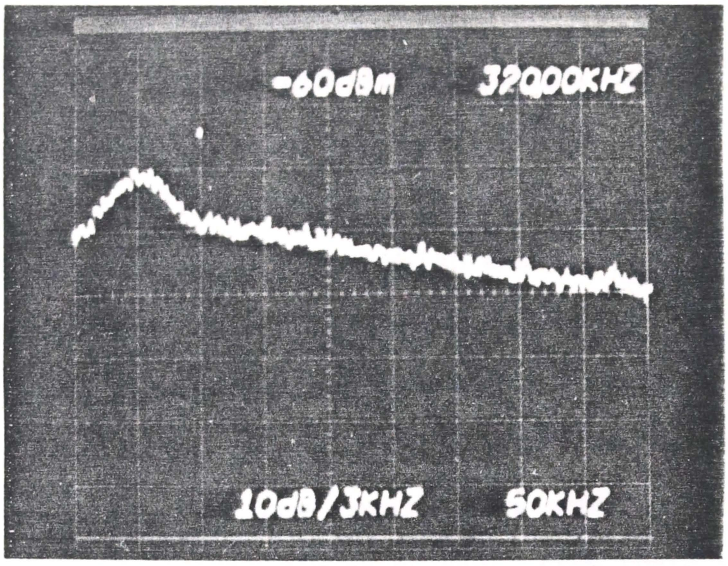

Stage 3

Frequency Response

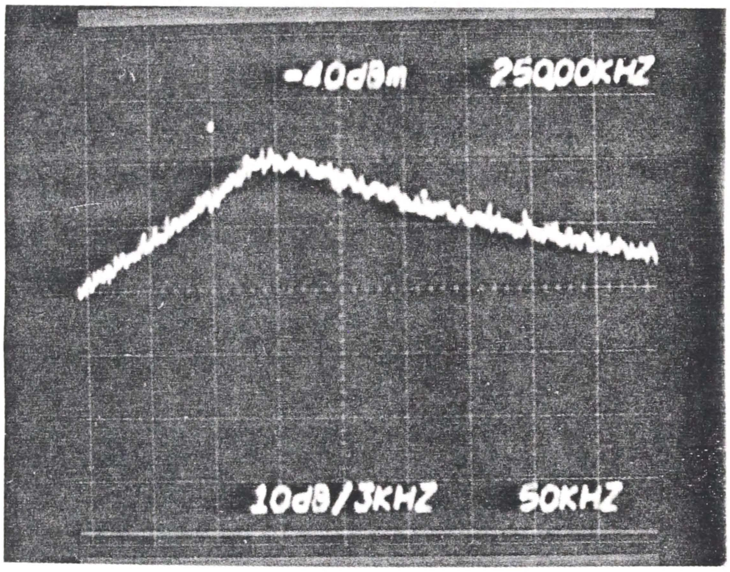

Stage 4

Frequency Response

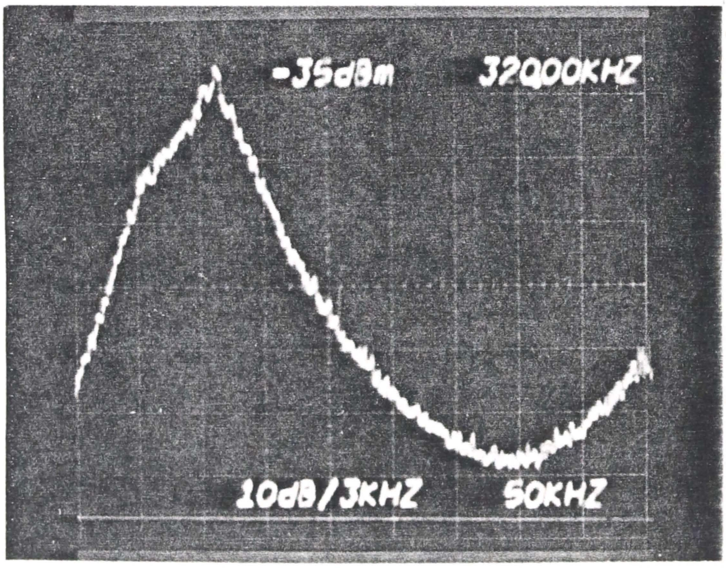

Combined

Frequency Response

Figure 38 Continued

4.1.2 THE PHASE DECODER

The decoder is a classical QDPSK decoder as detailed in [32], a block diagram is shown in Figure 39. To achieve the one symbol delay required, by differential decoding, a pair of Charge Coupled Devices (CCDs) are used as an analog delay line. The delay can be accurately controlled by using a crystal clock for the CCDs. The $\Delta\phi$ phase shifter is used to ensure that there is exactly one symbol period delay. The Dibit clock is derived by squaring the output of one of the bit wave forms before sampling. The squared wave form is fed into a band-pass filter. From there it goes to control the gain of the AGC and to a comparator to produce the Dibit clock. Generating the control signal for the AGC in this manner ensures impulsive noise has the minimum effect.

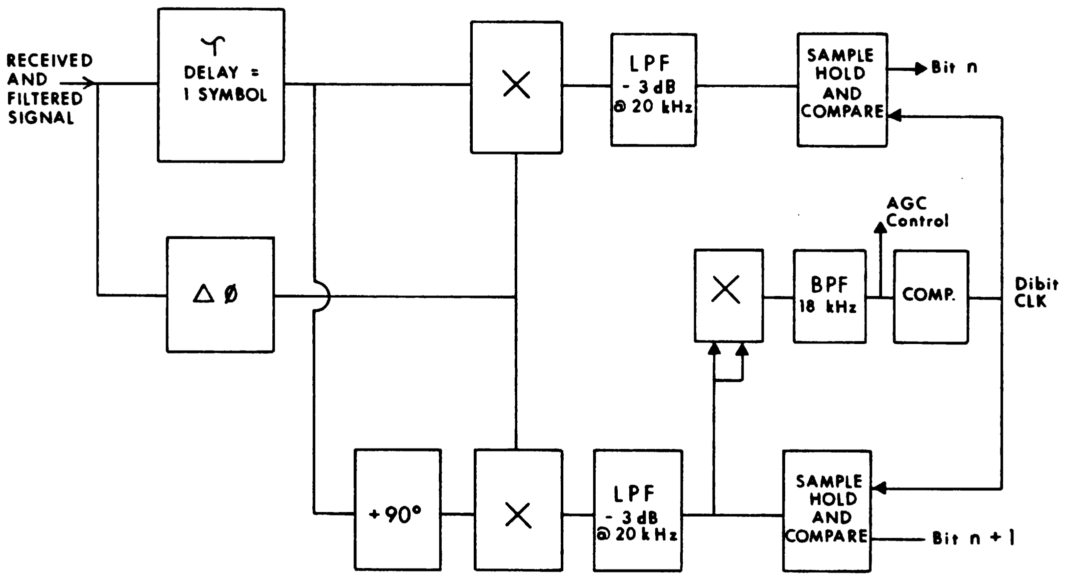

Figure 39

Block Diagram of Phase Decoder

The low pass filters are second order Butterworth active filters followed by a single order RC low pass stage giving an overall -3 dB point of 20 kHz. The filter outputs feed into sample and hold circuits which are clocked by the Dibit clock.

These feed into voltage comparators with threshold values of zero volts. The outputs are Bits n and n+1 respectively. The Dibit clock is generated by taking the output of 18 kHz Band-pass filter and feeding into a voltage comparator with a threshold of zero volts. A dual monostable is set up to fire on both the rising and falling edges of the Dibit clock. The outputs of the mono stables are "OR"ed together to produce the bit clock.

4.1.3 SYNCHRONISATION DETECTOR

A Synchronisation Word containing all zeros (a zero word) is transmitted every half second. To detect this word and synchronise the receiver a ten stage shift register is used with all the outputs "NAND"ed together. When all the NAND gate inputs are low the output goes high, generating the signal Zero Word Detect (ZWD). This signal is used to synchronise:

a) the word clock,

b) the start of the data transfer to the computer,

c) the reading of the distance recorder.

4.1.4 THE OUTPUT REGISTER

The outputs of the ten stage shift register described in 4.1.3 above are also fed to two parallel D registers (74378s). These registers produce the final form 10 bit word in the same format as that transmitted. The outputs of the D registers remain fixed until the next complete word has been received and decoded. The output register feeds into the error detection and counting circuit, as well as the computer interface circuit.

4.2 THE ERROR DETECTION AND DISPLAY SECTIONS

This circuit complements the test data section in the transmitter. When the transmitter is sending the pseudo-random sequence this circuit compares the received data with the known sequence. Any differences (errors) are analysed and the number of symbols in error determined. The appropriate counter is then incremented. While the displays will always show numbers they will only be meaningful when the pseudo-random sequence is being transmitted. The block diagram for this section is shown below in Figure 40.

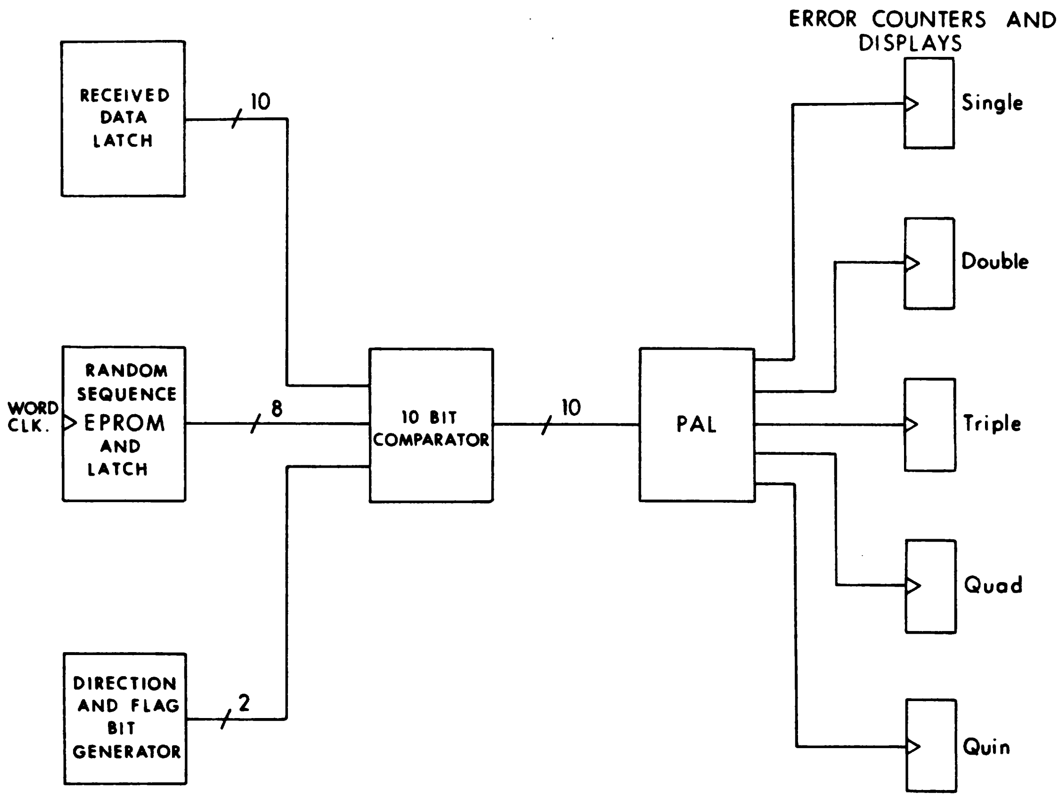

Figure 40

Block Diagram of Error Detection and Display Section

The random sequence EPROM is a copy of that used in the transmitter. The address generator for the EPROM is synchronised with the transmitter by the ZWD signal, ensuring the correct words are being compared.

The comparator produces a high output on the lines corresponding to the bits in error, eg line 8 goes high if bit 8 is in error. The Programed Array Logic (PAL), a 2716 EPROM, decodes those lines working out how many symbols, in a word, were in error. Then it clocks the appropriate counter and turns on an error LED.

4.3 DISTANCE RECORDING EQUIPMENT

The function of this portion of the system is to accurately measure the position of the skip down the shaft. It interleaves these measurements in the proper places amongst the acceleration measurements. Having an accurate position record enables high resolution statistical comparison techniques to be used to analyse the data.

4.3.1 THE MEASURING TECHNIQUE

The technique used employs a photo tachometer driven by an auxiliary winder shaft. The auxiliary shaft is in turn connected to the main winder drum shaft. Thus the output pulses of the photo tachometer accurately represent the rotation of the winder drum.

The winders are conventional using double cylindrical drums, one for each skip, with the skips operating in counter balance. The ZC winders, as with other conventional drum winders, use two layers of winding rope, giving two different effective drum circumferences. Therefore, the pulses from the photo tachometer can represent two distance increments. This should not cause any significant errors as an accurate survey run will calibrate the distance recording equipment and locate the change over point. The change over point should always occur in the same place within one or two metres hence not significantly affecting the measurement accuracy. Driving the photo tachometer from the winder was selected in preference to other methods, (eg., from sheave wheels), because of:

a) ease of access,

b) shelter of equipment from the outdoor environment,

c) ease of connection to driving mechanism.

The photo tachometer used is bi-directional producing two sine waves differing in phase by $\pm$ 45° + ve for one direction -ve for the other, Figure 41 demonstrates.

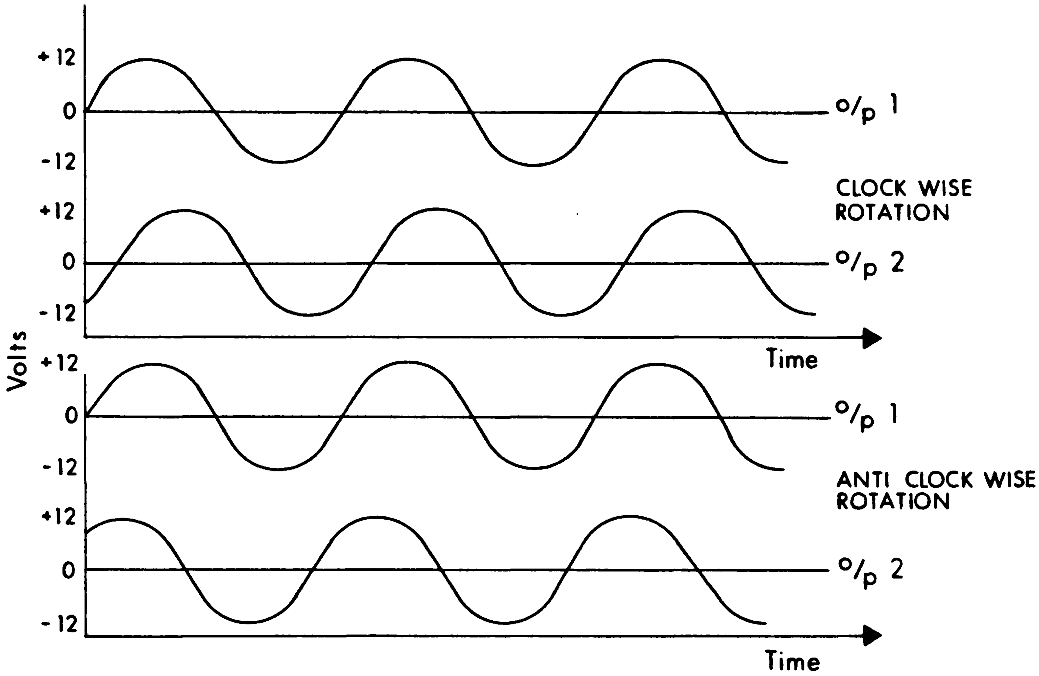

Figure 41

Output Wave Forms for the Photo Tachometer

The frequency of the wave forms are directly proportional to rotational speed. The outputs are fed into voltage comparators to produce TTL compatible pulses. Feeding these pulses into a simple logic circuit generates separate up and down clocks. The clocks drive a presetable up down counter ie., the distance register.

4.3.2 THE DISTANCE REGISTER

The distance register is a 15 bit up-down counter. Hence the physical properties of the winder, skip and shaft should determine the distance resolution rather than the electronics. As the equipment has yet to be commissioned the actual resolution has not been determined. The output of the distance register is loaded into the computer interface ready for transferring to the computer each time a synchronisation word is detected ie., every half a second.

The distance register will count up when the east skip travels down the shaft and the west skip travels up. The register will count down when the situation is reversed. A known start value needs to be loaded into the distance register so that over or under flow is avoided. The value selected, 4000_{16}, is the half range value for the register. This value is loaded into the register each time the receiver is manually reset, generally at the start of a run.

4.3.3 DETERMINING DISTANCE

In the raw data file collected on the PE computer will be readings of the distance register taken every half a second. Comparing these readings with a reference file, an accurate calculation of skip position at the reading time can be made.

By using interpolation methods intermediate positions can be accurately calculated. This will allow pin-pointing of skip disturbances. As the time between distance readings is accurately known, winding velocity and acceleration profiles can easily be calculated from these readings.

4.4 THE INTERFACE TO THE PERKIN-ELMER COMPUTER

The transferring of data to the PE computer is handled by:

a) A 16 bit parallel interrupt driven Digital Input Module on the PE.

b) An assembler program to store the collected data on a disc file.

c) Logic on the receiver to generate and control the interrupts sent to the input module.

d) A single interface register in the receiver to output the data to the PE computer.

There are two sources of data for the interface register:

a) The output register of the receiver see section 4.1.4.

b) The Distance register see section 4.3.2.

A block diagram of the computer interface section appears in Figure 42.

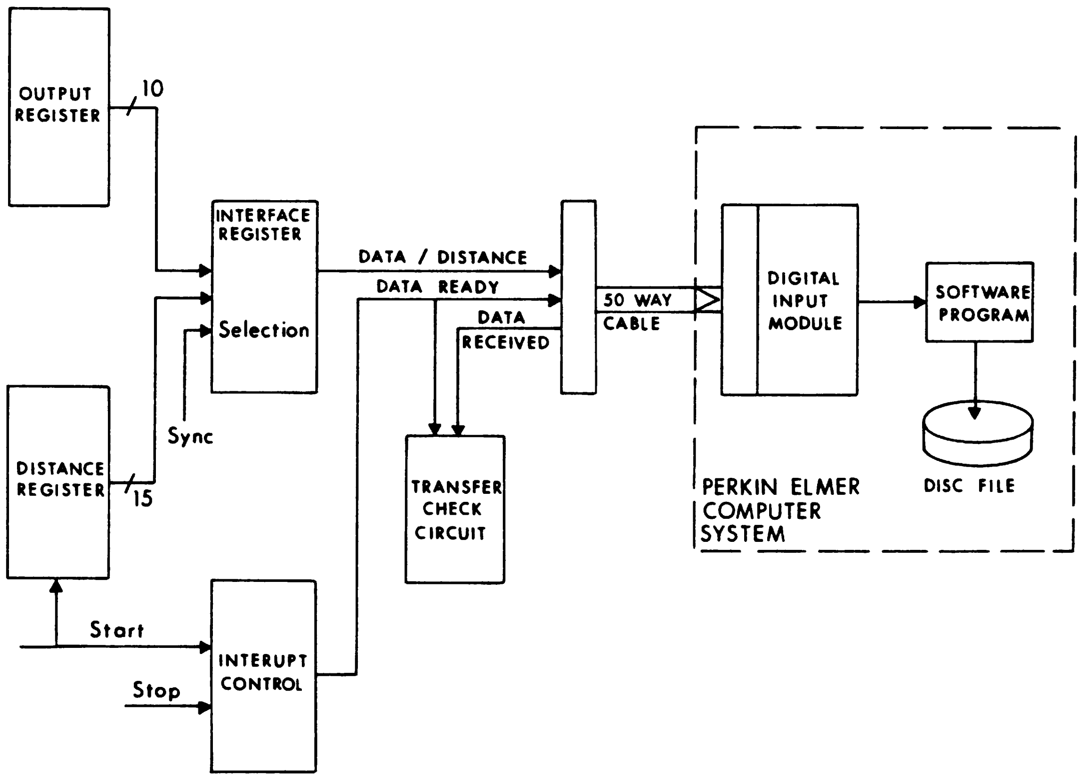

Figure 42

Block Diagram of Perkin Elmer Computer Interface

4.4.1 DIGITAL INPUT MODULE FOR THE PERKIN-ELMER COMPUTER

This module is a 16 bit parallel input module which can either be interrupt or program driven. The module's input and control lines are Transistor Transistor Logic (TTL) compatible. For the accelerometer the interrupt driven mode is selected to give control to the receiver and ensure all data is collected.

In interrupt mode the module carries out a hand-shaking transfer of data. The receiver, having data to transfer, sends an interrupt to the module. If the module has been requested, by a program, to read it's inputs, it will proceed with that read on receipt of an interrupt. Having completed the read it will send back to the receiver a Data Received pulse, signalling completion of the transfer. The specification sheet for the input module appears in Appendix Four.

4.4.2 THE STORAGE SOFTWARE

The storage software consists of an assembler program whose function is to read the data presented to the I/O module and either store or ignore it. It makes this decision based upon the state of the transfer bit as described in section 4.4.4.

The program uses two buffer areas to collect the data. While it is reading data into one area it is writing data from the other out to the disc file. The output disc file has a contiguous record length of 41000 bytes, (20500 readings). These factors ensure that the program is able to operate as fast as possible ensuring the minimum risk of missing a reading.

Once the program has initialised the reading of data into a buffer, the hardware handles all aspects until the buffer is full.

The time taken for the hardware to handle an interrupt, read the data and store it in memory, is usually in the order of 50 microseconds.

This ensures the risk of missing a reading is kept to a minimum. The only real risk of missing a reading comes about when a buffer is filled and the data storage is transferred to the other buffer. This usually takes approximately 200 microseconds but can stretch to over 280 microseconds at times. With a link speed of 36 kbits per second the time between two readings being received is 280 microseconds if the interrupt is not handled by the computer in this time the reading is lost. The error will be detected by both the receiver hardware and software, and the system will stop. A sixteen stage FIFO buffer is planned to be incorporated (see section 4.4.4) to allow the computer to catch up without losing data.

With a length of 41000 bytes it takes some 4.75 seconds to fill the buffer. This gives plenty of time for the computer to initiate and complete the writing of the other buffer to disc. The transfer of data from the receiver to the computer is stopped by the user pressing the stop button on the receiver. This resets the transfer bit after the next Zero Word (or synchronising word), and when the software discovers that the transfer bit is no longer set it stops and displays how many buffers have been transferred and stored.

4.4.3 RECEIVER INTERRUPT AND CONTROL LOGIC

This circuitry is responsible for generating, at the correct time, the interrupts to the input module in the computer. As well it also checks that the computer has acted upon the interrupt before the next one is generated.

The interrupt signal is simply a delayed and gated version of the receivers word clock. Each time the receiver has gathered in a word (10 bits) a clock pulse is generated. This pulse is delayed to allow outputs of the various registers to settle before being used as the interrupt pulse. Before it is finally sent to the computer the pulse is gated with the Transfer Enable line. The reset button, pressed by the user to start the transfer of data, sets the Transfer Enable line high. Hence the interrupts will only be sent to the computer if the reset button has been pressed.

In the receiver a small circuit checks that an interrupt has been served by the time the next is generated. If this is not the case a red LED labelled 'Data Not Transferred' is illuminated. The circuit consists of two monostables, see Appendix Three. The first monostable is fired, when the interrupt is generated, enabling the second. The first is cleared, disabling the second by the data received pulse from the computer. The second monostable if enabled at the time, will be fired by the next interrupt pulse. This will illuminate the Data Not Transferred LED. The second monostable can only be fired if two successive interrupts are generated with no intervening data received pulse.

4.4.4 INTERFACE REGISTER

The data to be transferred to the computer is placed in the interface register. This is a 16 bit parallel register. The source for its data is either the output or distance registers. The selection is determined by the synchronising pulse which is generated on the reception of the synchronising word. When a synchronising pulse is generated the interface register will be loaded with the contents of the distance register. At all other times it will be loaded from the output register.

Data is transferred to the computer in 16 bit words and the data received is in 10 bit words giving six spare bits. These spare bits are used to signal special conditions and to give greater accuracy to the distance measurements. Tables 8 and 9 below set out the format for the 16 bits transferred to the computer.

The word can have two interpretations, based on the value of bit 15 (MSB). If bit 15 is high then bits 14-0 are the 15 bits of the distance measurement, otherwise the bits represent an acceleration reading of 8 bits resolution plus three special bits:

a) Bit 14 the transfer bit, is used by the assembler program to determine whether the data should be stored (Bit 14 high) or ignored (Bit 14 low).
b) Bit 1 - the direction bit signifies from which transducer the measurement was taken.
c) Bit 0 - a flag bit always high

TABLE 8

Transferred Word Format (Distance)

Bit No.	Description	Bit No.	Description
15 (MSB)	Distance (High)	7	Bit 7 of Distance
14	MSB of Distance	6	Bit 6 "
13	Bit 13 "	5	Bit 5 "
12	Bit 12 "	4	Bit 4 "
11	Bit 11 "	3	Bit 3 "
10	Bit 10 "	2	Bit 2 "
9	Bit 9 "	1	Bit 1 "
8	Bit 8 "	0 (LSB)	Bit 0 "

TABLE 9

Transferred Word Format (Acceleration)

Bit No.	Description	Bit No.	Description
15 (MSB)	Acceleration (Low)	7	Bit 5 of Accel
14	Transfer Bit	6	Bit 4 "
13	Low	5	Bit 3 "
12	Low	4	Bit 2 "
11	Low	3	Bit 1 "
10	Low	2	Bit 0 LSB Accel
9	Bit 7 of Accel (MSB)	1	Direction Bit
8	Bit 6 "	0 (LSB)	Flag Bit (High)

The transfer bit is set high by the user pressing the reset button. Currently there is only one interface register. If the computer has not read the output of this register before it is next updated, 280 microseconds later, then the data has been irretrievably lost. This situation is detected by the check circuit mentioned in 4.4.3. To overcome the loss of data it is planned to replace the current interface register with a sixteen stage First In - First Out (FIFO) buffer. This will allow the computer time to catch up with the receiver after swapping program buffers. The addition of the FIFO should completely overcome the data loss that is now experienced from time to time.

4.5 MOUNTING AND CONSTRUCTION DETAILS

The same construction methods (wire wrap) were used for the receiver as for the transmitter. However the mounting arrangement for the receiver coupler is quite different to that used for the transmitter. The coupler has to be placed as close as possible to the wire rope without ever coming into contact with it.

The coupler is mounted on a wooden frame used to mount two couplers for other shaft communications equipment. Figure 43 shows the arrangement.

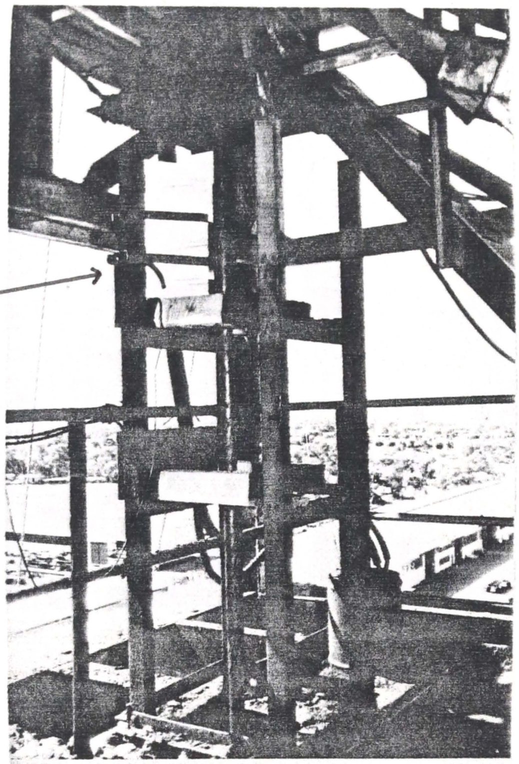

Figure 43

Receiver Coupler Mounting Arrangement

The mounting location is just below the sheave wheel at the top of the head frame. The arrow in Figure 44 shows the location of the mounting frame detailed in Figure 43.

The receiver is located in the computer room some 150 metres away. A single four core shielded cable connects the coupler to the receiver. The cable runs down the side of the headframe then via ducts to the office block and into the computer room. The cable reduces the signal level to the receiver by a factor of 15.7. This is due to the high output impedance of the receiver coupler and the high capacitance of the long cable run. By locating the receiver front end at the headframe this loss would be reduced to almost zero.

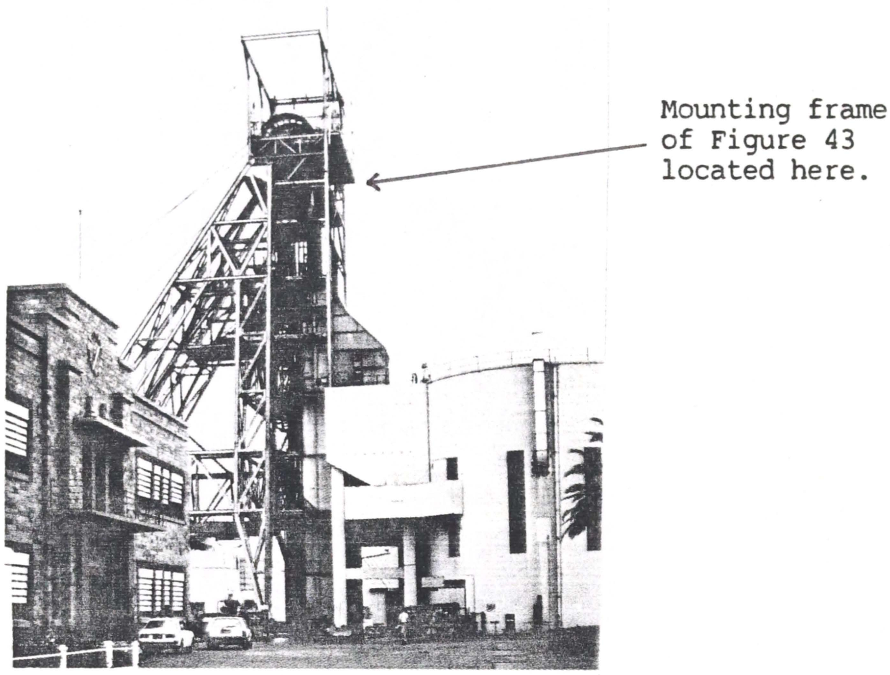

Figure 44

ZC Mines Head Frame

The receiver power supplies are conventional series regulator types. The nominal voltages are ± 5, ± 15 and ± 24 volts un-regulated. The source voltage is 240 V 50 Hz.

The distance recording equipment, consisting of a photo tachometer and associated electronics, is located in the winder house. The photo tachometer is mounted on a rubber spring base and located directly below an auxiliary shaft see Figure 45. The shaft drives the photo tachometer via a toothed vee belt.

A cable from the computer room supplies DC power to the photo tachometer and takes the output pulses to the receiver.

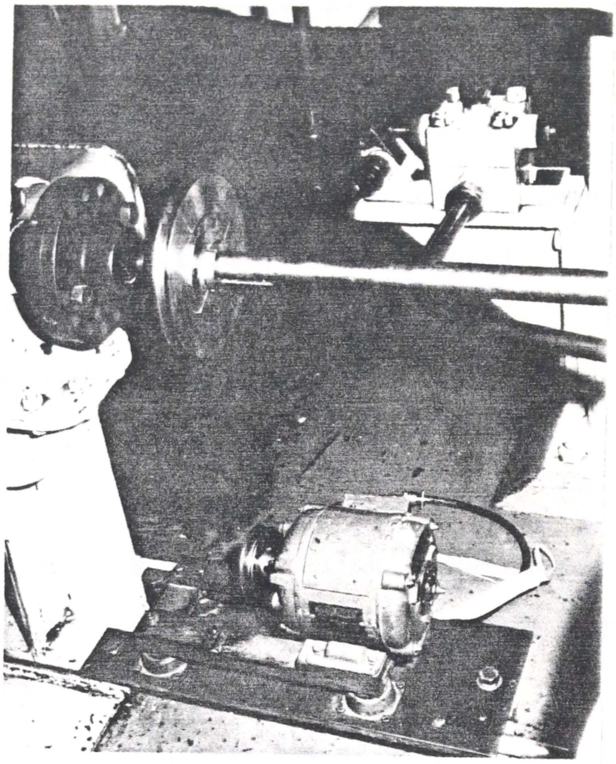

Figure 45

Photo Tachometer Mounting Arrangement

CHAPTER 5

TESTS AND TRIALS

This chapter details the practical trials conducted with the accelerometer. Two sets of trials were conducted:

a) Data link tests.

b) Accelerometer test runs.

5.1 DATA LINK TESTS

During the development of the data link a number of practical tests were performed. These tests were used to provide design feedback on the operation of the link. The main tests were:

a) Received signal level tests.

b) Error rate tests.

5.1.1 THE RECEIVED SIGNAL LEVEL TESTS

These were used as a guide to the design of the receiver front end. The test signals consisted of:

a) One pulse (symbol) in five being transmitted.

b) Transmitting the normal signal wave form.

The above signals, shown in Figures 46 and 47 below, enabled a quick visual check of ISI problems as well as signal strength. The test involved attaching the transmitter to the skip and having it travel up and down the shaft while observing the received signal on an oscilloscope.

The first tests indicated that ISI and signal level were unlikely to be major problems (see Figure 48,49 and 50 below). A comparison between these practical results and those predicted by the theory is documented in Section 2.3.3.

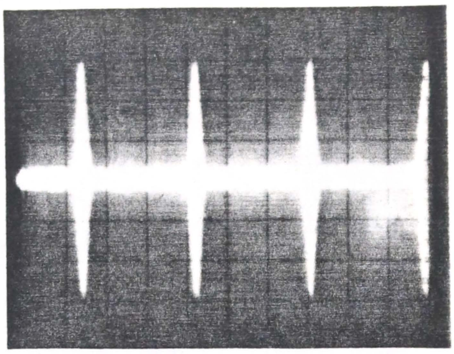

Figure 46

Received Level Test Signal ("Single Pulse")

Top trace - Output of RF filter - 2 V/div

Time base - 0.1 ms/div

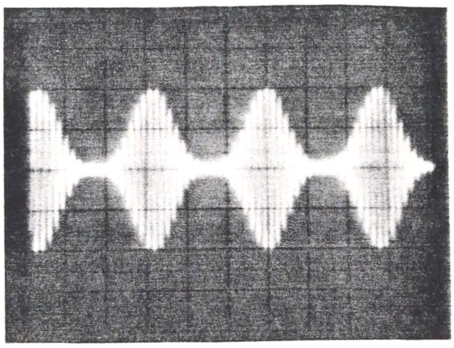

Figure 47

Received Level Test Signal (Continuous)

Top Trace - Output of RF filter - 2 V/div

Time base - 20 μs/div

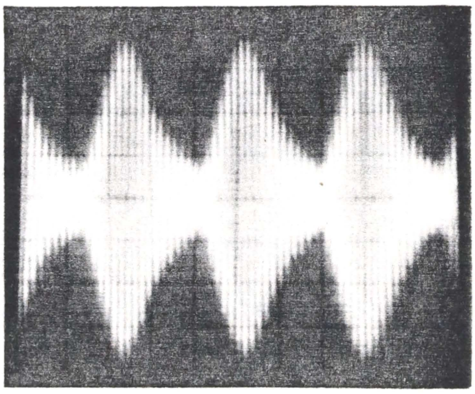

Figure 48

Example of ISI in Received Signal

Top trace - Output of RF filter - 2 V/div

Time base - 20 μs/div

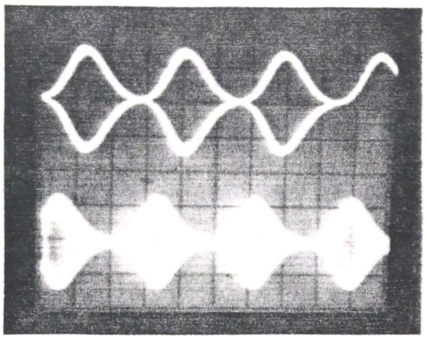

Figure 49

Received Signal Eye Pattern

Top trace - Output of demodulator filter - 5 V/div

Bottom trace - Output of RF filter - 2 V/div

Time base - 20 μs/div

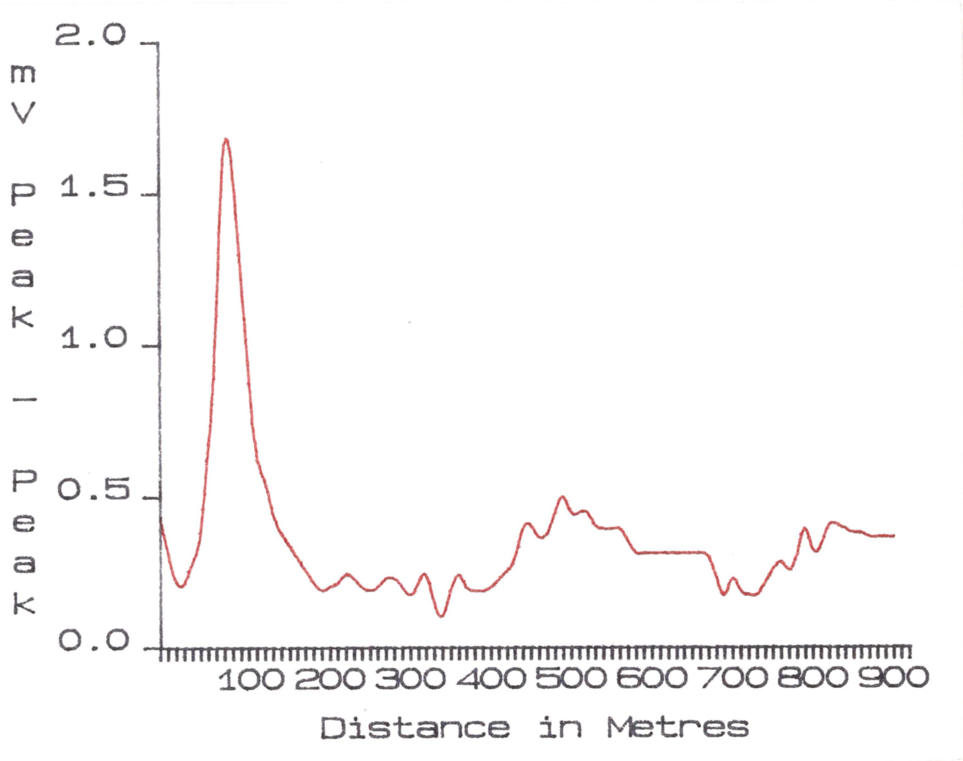

Figure 50

Received Signal Level Vs Shaft Depth

However, it was found that interference from other shaft radio communication units and the impulsive nature of RF noise in the shaft did cause problems.

Figures 51 and 52 show the effects of these two aspects. In Figure 51, the top trace is the output of the first receiver stage ie., the received signal is only amplified not, filtered or put through the AGC. The bottom trace is the RF filter output after the AGC and the amplitude reduction is evident. In Figure 52 the top trace is the output of the clock filter while the bottom is that of the RF filter and AGC. The effect of impulsive noise is very evident in the large signal loss and the long recovery time for the AGC.

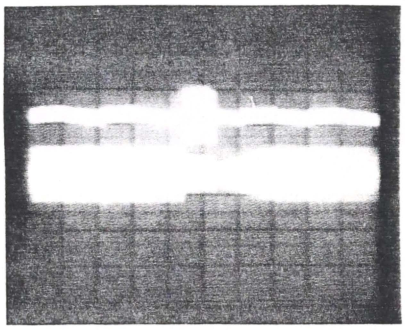

Figure 51

Effect of Interference on the AGC (Original Circuit)

Top trace - Output of 1st amplifier stage - 50 mV/div

Bottom trace - Output of RF filter - 5 V/div

Time base - 10 ms/div

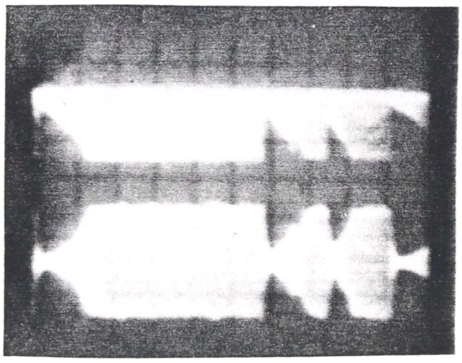

Figure 52

Effect of Impulsive Noise on AGC (Original Circuit)

Top trace - Output of demodulator filter - 5 V/div

Bottom trace - Output of clock filter - 1 V/div

Time base - 5 ms/div

To overcome these problems two additional band pass filter stages were added and the AGC control signal was sourced after filtering and decoding (see section 4.1.2). The effects of interference and noise were significantly reduced, as evident from Figures 53 and 54.

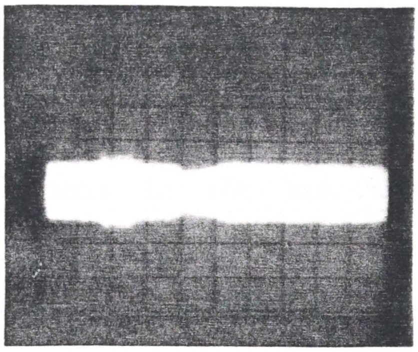

Figure 53

Effect of Interference on the AGC (New Circuit)

Top trace - Output of RF filter - 5 V/div

Time base - 5 ms/div

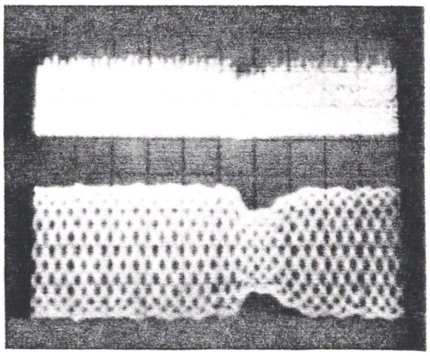

Figure 54

Effect of Impulsive Noise on the AGC (New Circuit)

Top trace - AGC control voltage - 1 V/div

Bottom trace - Output of clock filter - 1 V/div

Time base - 1 ms/div

5.1.2 ERROR RATE TESTS

Once the receiver design and construction was completed a further set of tests measured the actual error rate of the whole data link. The results were used in two ways:

a) to guide fine adjustment of the circuit designs,

b) to determine the reliability of the link and the collected data.

The test data sections in the transmitter and receiver, as described in Sections 3.3.4 and 4.2, were used to transmit and check known data for errors. Two methods were used for checking the reliability of the link with the transmitter attached:

a) The skip was lowered down the shaft to the position of lowest signal strength.

b) The skip travelled up and down the shaft at normal operating speeds.

Each of the above had their purposes. Test a) was best if:

i) a particular location in the shaft needed closer investigation, and

ii) circuit modifications were carried out and quantitative comparisons were required.

Test b) was used when the reliability and performance of the link needed to be tested under normal operating conditions.

The final system has an error rate of approximately one word in every 258,000 transmitted (or one error in every 710,000 symbols). This is considered more than adequate for a data link of this nature. The error rate was arrived at by carrying out a series of tests on both skips (east and west) with each test lasting 10 to 20 minutes. At the end of each test the error counters were recorded and the error rate calculated.

$$\text{Error rate (words)} = \frac{\text{No. of Words in ERROR}}{\text{Total No. of Words Transmitted}}$$

$$\text{Error rate (symbols)} = \frac{\text{No. of Symbols in ERROR}}{\text{Total No. of Symbols Transmitted}}$$

For example in one test the following results were recorded:

TABLE 10.

Error Rate Test Results

Elapsed	Symbols in Error in a Word					Error Totals		Total Transmitted	
Time Min	One	Two	Three	Four	Five	Words	Symbols	Words	Symbols
5	1	2	2	0	0	5	11	1.1×10^6	5.5×10^6
10	1	2	2	0	0	5	11	2.2×10^6	11×10^6
20	11	8	4	1	0	24	43	4.4×10^6	22×10^6
30	18	10	5	1	0	34	57	6.6×10^6	33×10^6

From the above Table it can be determined that in the first five minute slot the following error rates were obtained:

Word error rate : 1 in 220,000

Symbol error rate : 1 in 500,000

In the second five minute slot the rates are:

Word error rate : 0 in 1.1 million

Symbol error rate : 0 in 5.5 million

Looking at the 10 minute slots the rates are:

1st slot - word rate : 1 in 440,000

- symbol rate : 1 in 1,000,000

2nd slot - word rate : 1 in 116,000

- symbol rate : 1 in 344,000

3rd slot - word rate : 1 in 220,000

- symbol rate : 1 in 786,000

The average 10 minute word error is 1 error in every 258,000 words transmitted while the symbol rate is - 1 in every 710,000 symbols.

5.2 ACCELEROMETER TRIALS

With all aspects of the accelerometer functioning, except the distance recording equipment, it was possible to conduct a number of trial runs. These took two forms:

a) sending and storing the test data random sequence, or

b) measuring and storing real forces.

Trial a) made it easy to use the computer to check and report on any errors and was used to test the whole instrument (except for the distance recording equipment). Meanwhile trial b) was used to:

i) gain an insight into the forces experienced by the skip and to collect some real data, and

ii) determine if the gain of the transducer amplifier needed changing.

5.2.1 TEST RUNS USING THE RANDOM NUMBER SEQUENCE

With this test, the whole instrument, (transmitter, receiver, computer interface and software) was tested. The only difference from normal use was that rather than transmitting the acceleration measurements, the known test data was continuously transmitted.

The created disc file contained the received sequences making it easy to check for any errors. A program CDATA was written to check through the disc file looking for and listing any errors. The types of errors looked for were:

a) wrong data received ie., error in one or more of the eight data bits,

b) wrong direction ie., error in direction bit,

c) flag bit error,

d) synchronising word in the wrong place.

Two runs for each skip were carried out. These tests demonstrated that the basic instrument functioned well, though some improvements were needed. The area that specifically needed improvement was the output register. At present with only a single stage output register, overwriting of the contents can occur, causing errors, as discussed in Section 4.4.2. The addition of a sixteen-stage FIFO output register will overcome this problem.

5.2.2 MEASURING REAL FORCES

A number of runs for each skip were carried out while measuring and storing the acceleration measurements. Both full and empty skips were used so that the transducer scaling could be checked for both cases. Indicative information of the differences in behaviour between full and empty skips was also obtained. Originally the sensitivity was selected to give the specified range of ± 2 g. This was found to be small and a larger range of ± 5 g was selected which reduced the resolution to ± 0.04 g.

5.2.2.1 Early Plotting and Analysis Software

Some limited plotting and analysis software was written to aid in the initial analysis of the data. The plotting software will display half a second (the data collected between two synchronising words), on a colour graphics screen. The analysis software takes the raw data and produces:

a) the magnitude ie., |acceleration| in both the N-S and E-W directions,

b) joins the peaks of the magnitude together ie., peak |acceleration| in both directions.

Figures 55, 56 and 57 show the same half-second plotted as:

a) Raw data ie., acceleration,

b) |acceleration|,

c) peaks of |acceleration|.

Currently the scale for all these Figures is 1 millimetre = 2.5 milliseconds. Alternatively one can think of the scale in frequency terms. It can be shown that for the above time scale the frequency of vibration f is given by: $f = 400\ \lambda$ where λ is the wavelength measured in millimetres on the plot. This is useful for quickly determining the frequency of vibration.

With the current scaling each plot displays a maximum of five metres of the shaft, with the skip travelling at its maximum rate of 10 metres per second. Hence, over 200 plots are required to trace out the whole shaft. This number of plots is impractical. What is required for a first stage analysis is a small number of plots, showing all the shaft, highlighting areas of high acceleration. The analyst can use these plots to determine areas that require further more detailed analysis.

To achieve this small number of plots, a reduction in the scale by a factor of at least 20 is required. Hence, much of the fine detail must be taken out to avoid cluttering the plots.

The first stage in reducing the fine detail and making the plots easier to interpret was to plot the absolute value of the accelerations ie., |acceleration|. With this plot it is easier to distinguish the areas of high acceleration. But it would be difficult to shrink the x scale much further. The next stage in producing the clear overview plots was to reduce the fine high frequency detail without losing the acceleration peaks.

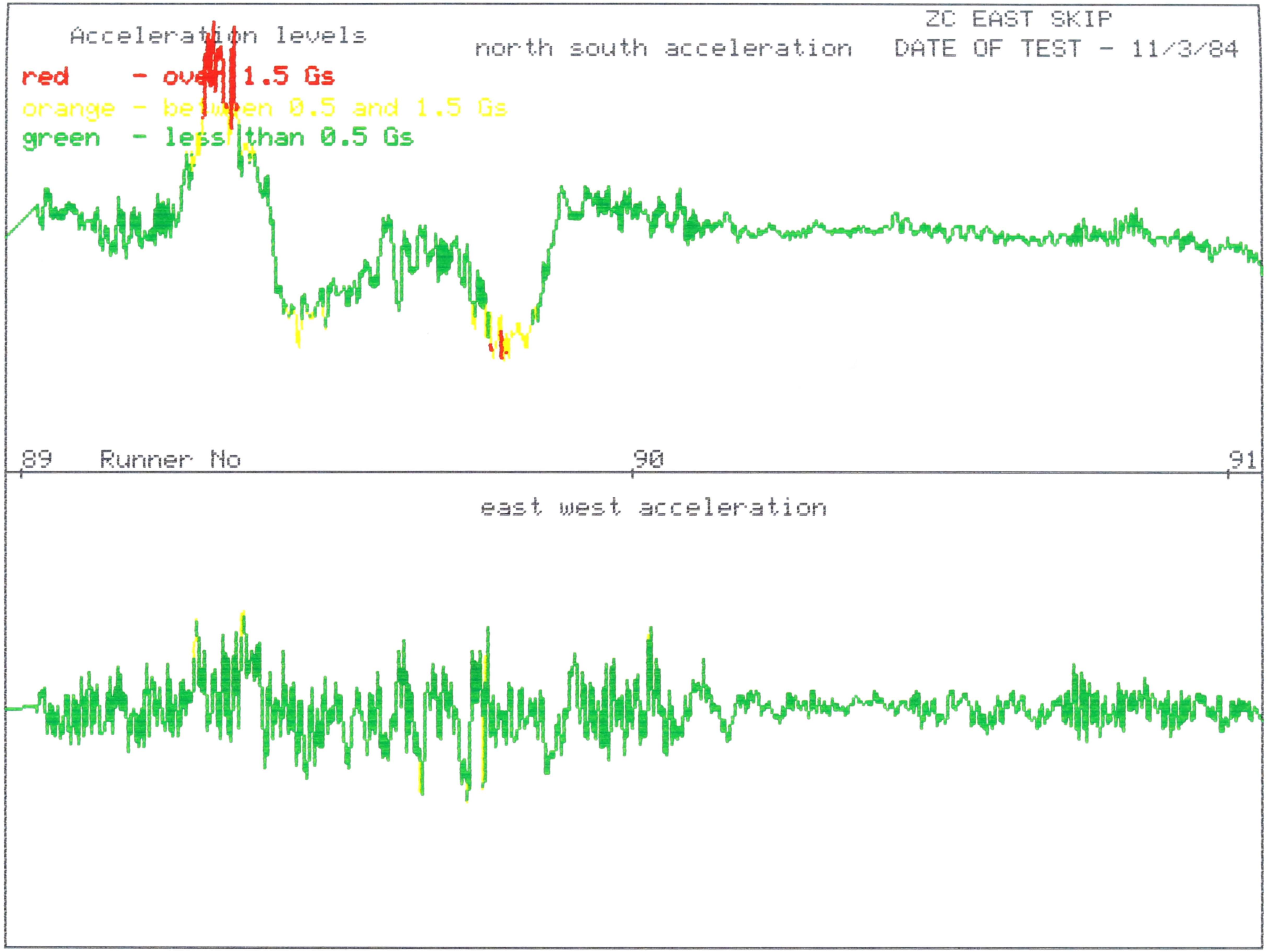

Figure 55

Plot of Raw Data from East Skip Test (Empty)

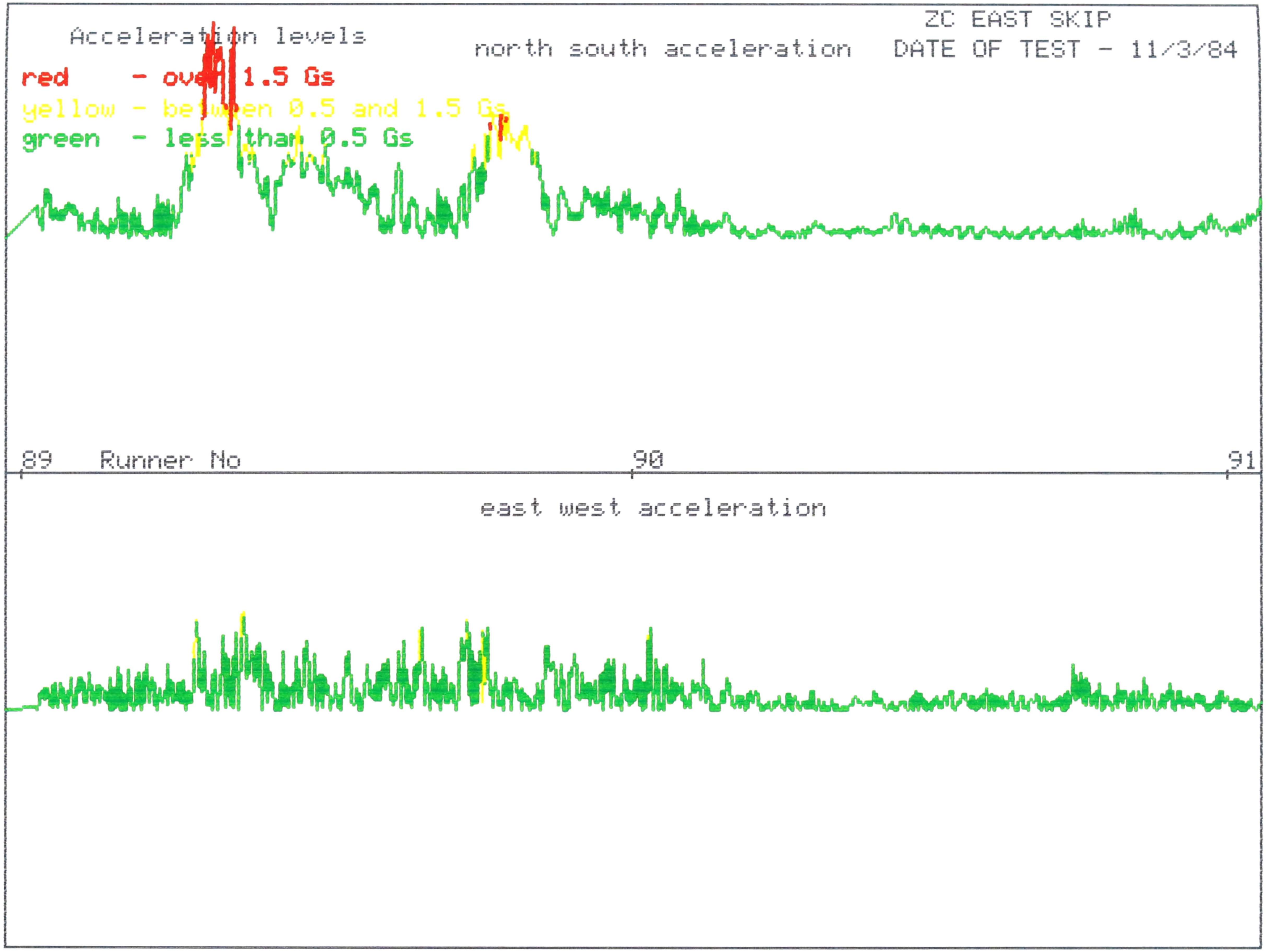

Figure 56

Plot of |Raw Data| from East Skip Test (Empty)

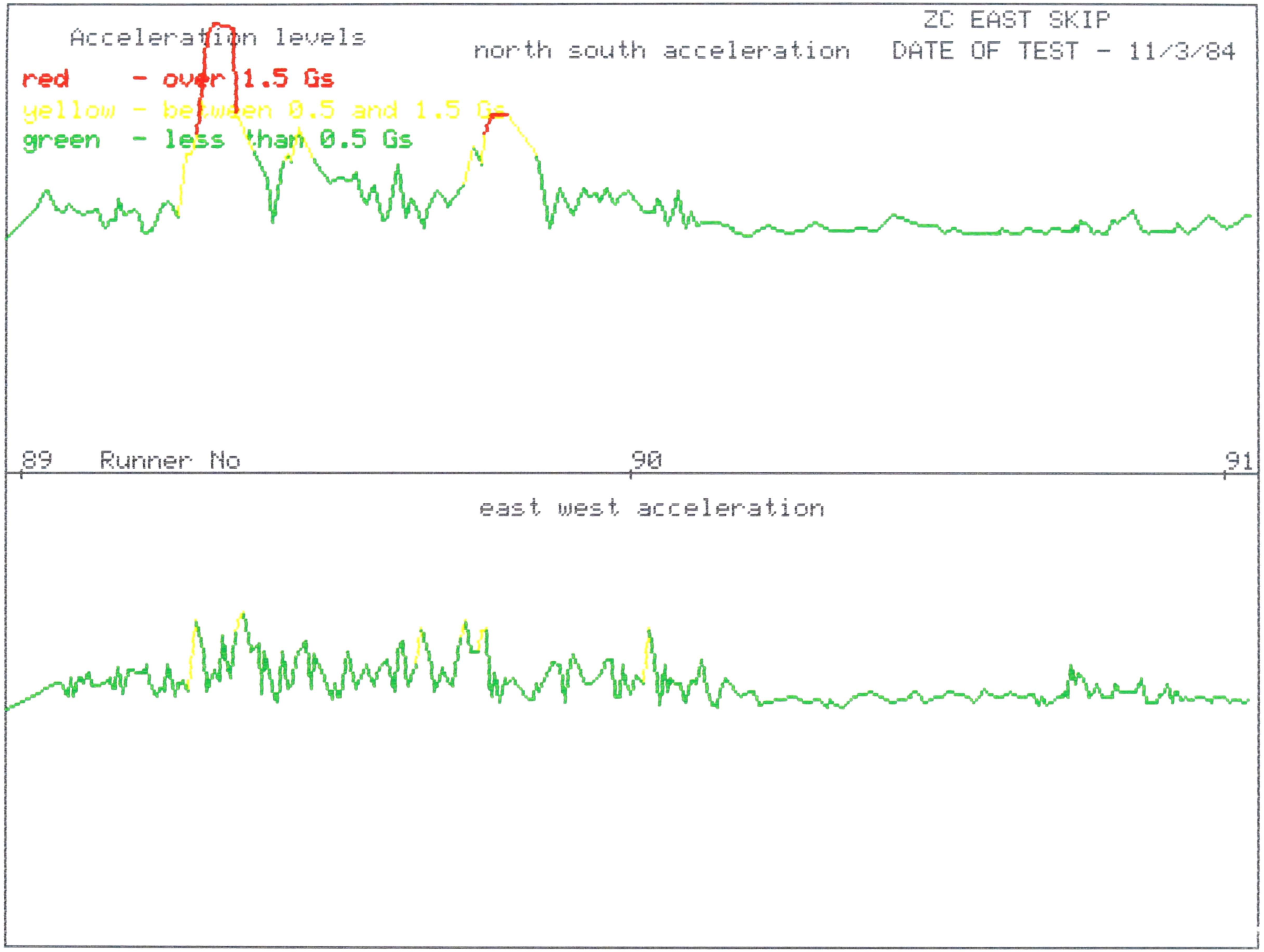

Figure 57

Plot of Envelope of |Raw Data|

It was considered important to retain the peaks as a guide to shaft conditions. Thus the envelope of Figure 56 (ie., all the peaks joined together) was used to produce Figure 57 which is significantly less cluttered than Figures 55 or 56. The scale could comfortably be reduced by a factor of 10. Additional work to enable a further reduction in scale is necessary.

5.2.2.2 Observations on the Collected Data

From the limited data so far collected some interesting observations can be made:

a) High Amplitude Accelerations.

Accelerations in the order of ± 3 g have been recorded. Mostly these have been of a low frequency nature indicating flexing in the supporting timbers and guides. Looking at Figure 56, the top trace shows a peak in the order of 3 g. The low frequency wave form that forms the base of the shape has a frequency of approximately 13 Hz. In all the tests carried out so far accelerations of this nature have been present.

b) High Frequency Vibrations.

It can be seen from Figures 55 and 56 that there can be a significant high frequency content (100 - 400 Hz). This is often related to a major acceleration in the other channel. For example, in Figure 55 the top trace shows a large low frequency dip about midway across. The bottom trace at the same point goes into high frequency oscillations in sympathy. The high frequency components could be due to mechanical resonances in the transmitter and transducer mounting arrangement.

Further work is necessary to confirm this, and testing of alternative mounting arrangements for the transducers should be undertaken.

c) Further Study.

Obviously further work is required to explain the data gathered so far. To do this, firstly the distance equipment must be commissioned so that runs can be correlated; then further data gathered to allow detailed analysis to commence. As mentioned in section 5.2.2.1 further work on the methods of displaying the data is required.

CHAPTER 6

CONCLUSION

This thesis has documented the development of a system that significantly improves the state of the art in accelerometers used in mine shafts. The work presented here, and the accelerometer developed form a sound foundation for the further development of analysis techniques for accelerations experienced by shaft vehicles.

The research and development conducted during this project have led to advances in the following areas:

a) Mine shaft accelerometers through:

   i) The real time collection of data by computer.

   ii) An improvement in frequency response and resolution of sixteen and thirty two times respectively.

   iii) The ability to carry out analysis of the data using computer based techniques.

b) Radio Communications in mine shafts, through the development of a 36 kbaud digital radio link.

It appears that a number of firsts may be attributable to this project, they are:

a) The first medium speed digital radio link for mine shafts.

b) The first digital shaft vehicle accelerometer.

c) The use of stored profiles for use in shaping transmitted symbol pulses.

6.1 MAJOR FINDINGS

From the theory developed in Chapter Two and Appendix One it is evident that:

a) ISI does not constitute a serious problem for digital radio links in mine shafts if appropriate pulse shaping is used.

b) The large system losses, in the order of 130 dB are mostly due to poor signal couplers and termination impedances (108 dB). Shaft propagation losses are minimal ~4 dB/km at 321 kHz and 16 dB/km at 1 MHz.

c) Poor termination impedance matching does result in standing wave patterns with a peak to trough ratio in the order of seven. This in the wider picture of overall system losses is very small.

d) Higher carrier frequencies than those often used for analog radio links [6,8,9] offer advantages in system efficiency by:

   (i) lowering the transmitted power requirements, and

   (ii) increasing the receiver coupler transfer impedance.

Therefore future efforts should be directed at minimising system losses by concentrating on maximising signal coupler efficiency.

6.2 SUMMARY OF RESULTS

This project set out to develop an accelerometer, for mine shaft vehicles, with greatly improved specifications. This was achieved, a comparison between the design specifications and the measured results appears in Table 11.

TABLE 11

Comparison Between Design and Measured Specifications for Accelerometer

Parameter	Specified	Achieved	Notes
Frequency Response	5-500 Hz(-3 dB)	5-500Hz (-5 dB)	section 3.2.1
Range	±2 g nominal	±5 g nominal	±2g was too low
Resolution	±.02g(1 in 256)	±.04g (1 in 256)	section 5.2.2
Distance Resolution	±1 metre	Yet to be tested	
Digital Link Speed	40 kb/s	36 kb/s	
Error Rate	-	1 in 710,000	section 5.1.2

The additional loss at 500 Hz of 2 dB (20%) is not considered significant as it applies to less than 5% of the overall bandwidth. The original range specification of ±2 g was found impractical as the actual forces measured by the accelerometer were in the order of ±3 g. So to give a reasonable degree of headroom ±5 g was selected as the range. The resolution is directly determined by the range and so it increased from ±0.02 g to ±0.04 g.

The data link speed was not limited by the characteristics of digital transmission in mine shafts, but by the transmitter clock speed. It is considered feasible to develop a digital link with a speed of 60 kbits per second using the same techniques.

While the speed of the link is 4 kbits per second lower than specified it is more than fast enough to avoid aliasing effects. The minimum link speed required to avoid aliasing, using the developed filter was 34 kbits per second.

6.3 FURTHER AND FUTURE WORK

The development of computer based analysis tools is the next major work required for this project. This will release the full benefits of the accelerometer to the user. Along with the development of the analysis tools some small refinements are also required. For completeness, the refinements are summarised below:

a) Addition of a FIFO buffer to the computer interface.

b) Better wire wrap boards especially for the transmitter.

c) The evaluation of different mounting locations and methods of the transducers.

ACKNOWLEDGEMENTS

I would like to thank firstly, ZC Mines Ltd. for supporting this work in all respects during the practical development phase; secondly, Kembla Coal and Coke Pty. Limited who have provided the computing and typesetting resources so necessary for completing the thesis.

Also I would like to thank Dr. Chris Phillips and Prof. Harvey Holmes, my supervisors, for their helpful comments and encouragement over the years.

REFERENCES

[1] **Operations Handbook**, The Zinc Corporation Ltd, New Broken Hill Consolidated Ltd, The Southern Power Corporation Pty Ltd., 1978

[2] F.J.J Blaauw, "The 1978 calamitous bunton failure," **Coal, Gold and Base Minerals of Southern Africa**, Vol. 28, No. 9, pp. 102-123, November 1980.

[3] L.C. Galloway and P.M. Tiley, "The performance of fixed guidance systems in mine shafts," **CIM Bulletin**, Vol. 75, No. 847, pp. 54-60, November 1982.

[4] K. Jones and L. Albert, "The value of decelerometer testing," in **Proceedings of the Canadian Institute of Mining and Metallurgy 85th Annual General Meeting**, Winnipeg, Manitoba, April 17-20, 1983, pp. 1-19.

[5] S.H. Crandall and W.O. Zhu, "Random vibration: a survey of recent developments," **Transactions of the ASME**, Vol. 50, No. 4B, pp. 993-962, December 1983.

[6] J.R. Wait and D.A. Hill, "Theory of the transmission of electromagnetic waves down a mine hoist," **Radio Science**, Vol. 10, No. 6, pp. 625-632, June 1975.

[7] R.L Lagace, "Emergency and operational mine communications," in **Final report, Bureau of Mines contract H0122026**, Vol. 1, A.D. Little, Inc., Cambridge, Mass., January 1974, ch. 5.

[8] R.L. Lagace, M.L. Cohen, A.G. Emslie and R.H. Spencer, "Lf hoist phone communication in deep hoist shafts," in **Technical Services for Mine Communications Research, Report to US Bureau of Mines, contract H0346045**, A.D Little, Inc, Cambridge, Mass., October 1975, ch. 5.

[9] D.T. Anderson and J.A. Vanous, "A frequency diversity communication system for mines," in **Proceedings of the Second WVU Conference on Coal Mine Electrotechnology**, Morgantown, West Virginia, June 12-14, 1974, pp. 11.1-11.13.

[10] J.R Wait, "Theory of e.m. wave propagation through tunnels," **Radio Science**, Vol. 10, No. 7, pp. 753-759, July 1975.

[11] J.R. Wait and D.A. Hill, "Coaxial and bifilar modes on a transmission line in a circular tunnel," **Applied Physics**, Vol. 4, No. 4, pp. 307-312, 1974.

[12] R.J. Pogorzelski, "Electromagnetic propagation along a wire in a tunnel - approximate analysis," **IEEE Transactions on Antennas and Propagation**, Vol. AP-27, No. 6, pp. 814-819, November 1979.

[13] P. Delogne, "Basic mechanics of tunnel propagation," **Radio Science**, Vol. 11, No. 4, pp. 295-303, April 1976.

[14] J.R. Wait and D.A. Hill, "Guided electromagnetic waves along an axial conductor in a circular tunnel," **IEEE Transactions on Antennas and Propagation**, Vol. AP-22, No. 4, pp. 627-630, July 1977.

[15] S.F. Mahmoud, "Characteristics of electromagnetic guided waves for communication in coal mine tunnels," **IEEE Transactions on Communications**, Vol. Com. 22, No. 10, pp. 1547-1554, October 1974.

[16] D.A. Hill and J.R. Wait, "Propagation along a braided coaxial cable located close to a tunnel wall," **IEEE Transactions on Microwave Theory and Techniques**, Vol. MTT-24, No. 7, pp. 476-480, July 1976.

[17] D.A. Hill and J.R. Wait, "Analysis of radio frequency transmission along a trolley wire in a mine tunnel," **IEEE Transactions on Electromagnetic Compatibility**, Vol. EMC-18, No. 4, pp. 170-174, November 1976.

[18] S.F. Mahmoud and J.R. Wait, "Theory of wave propagation along a thin wire inside a rectangular wave guide," **Radio Science**, Vol. 9, No. 3, pp. 417-420, March 1974.

[19] D.B. Seidel and J.R. Wait, "Radio transmission in an elliptical tunnel with a contained axial conductor," **Journal of Applied Physics**, Vol. 50, No. 2, pp. 602-605, February 1979.

[20] E.F. Kuester and D.B. Seidel, "Low-frequency behaviour of the propagation constant along a thin wire in an arbitrarily shaped mine tunnel," **IEEE Transactions on Microwave Theory and Techniques**, Vol. MTT-27, No. 8, pp. 736-741, August 1979.

[21] S.F. Mahmoud and J.R. Wait, "Calculated channel characteristics of a braided coaxial cable in a mine tunnel," **IEEE Transactions on Communications**, Vol. COM-24, No. 1, pp. 82-87, January 1976.

[22] J.R. Wait, "Quasi-static limit for the propagating mode along a thin wire in a circular tunnel," **IEEE Transaction on Antennas and Propagation**, Vol. AP-25, No. 3, pp. 441-443, May 1977.

[23] J.R. Wait, **Electromagnetic Waves**, New York: Harper and Row, 1985, ch. 5, pp. 197-224.

[24] J.J. Brophy, **Basic Electronics for Scientists**, Tokyo: M^cGraw Hill Kogakusha, 1972, ch. 10, pp. 380-389.

[25] M.K. Mills, "Self inductance formulas for multi-turn rectangular loops used with vehicle detectors," in **Conference Record of Papers Presented at the Thirty Third Annual Conference**, IEEE Vehicular Technology Conference, Toronto, Ontario, May 25-27, 1983, pp. 65-73.

[26] W.R. Smythe, **Static and Dynamic Electricity**, 2^{nd} Edition, New York: M^cGraw Hill, 1950.

[27] M. Kanda, "Time and amplitude statistics for electromagnetic noise in mines," **IEEE Transactions on Electromagnetic Compatibility**, Vol. EMC-17, No. 3, pp. 122-129, August 1975.

[28] B.W. Kerninghan and P.J. Plauger, **Software Tools**, New York: Yourdon Inc., 1976.

[29] D.J. Fitzgerald, "**The Via Utility**," Personal Communications.

[30] D.J. Fitzgerald, "**The Know 1 Data Base**," Report to the General Manager The Zinc Corporation Ltd., 1982.

[31] F.J. Harris, "On the use of windows for harmonic analysis with the discrete Fourier transform," **Proceedings of the IEEE**, Vol. 66, No. 1, pp. 51-83, January 1978.

[32] A.B. Carlson, **Communication Systems**, Tokyo: McGraw Hill Kogakusha, 1975, ch. 10.

[33] A.P. Clark, **Principles of Digital Data Transmission**, London: Pentech Press, 1976.

[34] R.F.W. Coates, **Modern Communications Systems**, London: The Macmillian Press Ltd. 1975, pp. 184-186

[35] **Linear Data Book 1982**, National Semiconductor Ltd., pp. 3.213

[36] P.A. Baker, "Phase-modulation data sets for serial transmission at 2000 and 2400 bits per second," **AIEE - Transactions**, Vol. 81, pt. 1, No. 61, pp. 166-171, July 1962.

[37] B. Glance, "Power spectra of multilevel digital phase-modulated signals," **The Bell System Technical Journal**, Vol. 50, No. 9, pp. 2857-2878, November 1971.

[38] **Program Manual BA1, Basic Library**, Texas Instruments Ltd., 1975, pp. 56.

[39] B.E. Brooks and J.E. Burton, "The winder safety monitor shaft communication system," **Mining Technology**, Vol. 62, No. 712, pp. 75-83, February 1980.

[40] H.K. Sacks and R.L. Chufo, "Hoist radio communications," in **Underground Radio Communications**, US Bureau of Mines IC 8744, 1977, pp. 28-41.

[41] S.D. Conte and C. deBoon, **Elementary Numerical Analysis an Algorithmic Approach**, 3rd Edition, Singapore: McGraw Hill, 1981, pp. 120-127.

[42] CRA Exploration, Private discussions, Broken Hill, 1983.

[43] G.D. Bergland, "A guided tour of the fast Fourier transform," **IEEE Spectrum**, Vol. 6, pp. 41-52, July 1969.

[44] M. Abramowitz and I. Stegun, **Handbook of Mathematical Functions**, New York: Dover Publications, 1964, pp. 358-379.

APPENDIX 1

APPENDIX 1

PROPAGATION OF RADIO WAVES IN MINE SHAFTS

This appendix provides background and comparative information for chapter two. It deals with:

a) The model for calculating Γ for a rectangular mine shaft.

b) Results for the circular model for a range of parameter values.

c) Transmission line equations for a mine shaft and a discussion signal coupler design and efficiency.

d) Results of the SigLev program using a range of parameter values.

A1.1 PROPAGATION COEFFICIENT - RECTANGULAR MODEL

Mahmoud and Wait [18] have derived a modal equation for a rectangular tunnel with an arbitrarily located thin axial conductor. The modal equation relates to a rectangular tunnel of cross-section 2a × 2b (with 2a being the larger) and infinite length. The shaft sides are formed by two planes which are assumed to be perfectly electric (ie., infinite conductivity) or perfectly magnetic (infinite permeability). The media above and below the wider walls is a lossy dielectric with a conductivity σ_e, permeability μ_e and permittivity ε_e. The tunnel is assumed to contain air with the normal free space values of ε_o, μ_o and zero conductivity. Located in the tunnel is a thin conductor of radius ρ and permittivity ε_w, permeability μ_w and conductivity σ_w. The conductor runs parallel to the tunnel centre line and is located at $x = x_o$, $y = y_o$. In the equations that follow the factors e^{-jwt} and $e^{-\Gamma z}$ are assumed but not included for reasons of brevity. Figure 58 shows the model geometry for a rectangular tunnel.

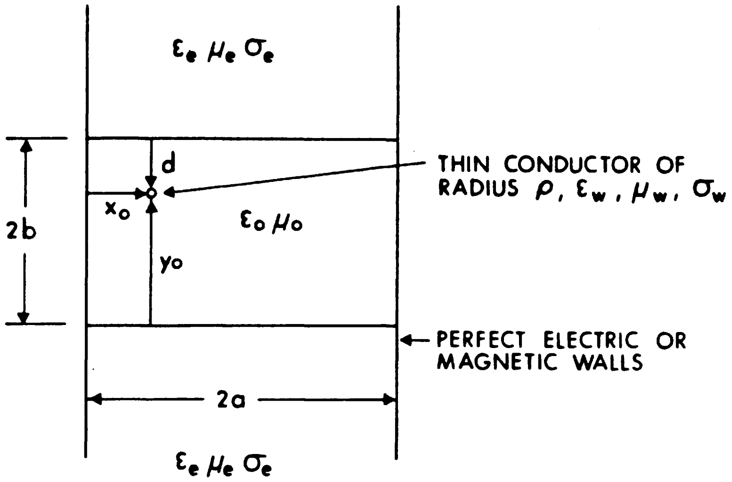

Figure 58

Geometry of Rectangular Shaft Model

The modal equation is:

$$\frac{-Z_w \pi}{(j\omega\mu_o)} = \left(1 + \frac{\Gamma^2}{k_o^{\,2}}\right)\cdot\Sigma\, P_m(x_o;x_o)\cdot f_m(y_o)\cdot f_m(d-\rho)\ /\ U_m\cdot\Delta_m\ -$$

$$(\Gamma/k_o^{\,2})\cdot\Sigma\, P_m(x_o;x_o)\ \cdot\ R_m^{\,*}[f_m(y_o)\cdot g_m(y_o+\rho)\ +\ f_m(d)\cdot g_m(d-\rho)]/\Delta_m{}^*\Delta_m \quad \text{(A1.1)}$$

Where $f_m = 1/2[e^{Umy} + R_m e^{-Umy}]$ $\qquad g_m = 1/2[e^{Umy} - S_m e^{-Umy}]$

S_m, R_m and $R_m^{\,*}$ represent the reflection and transmission factors and are given by:

$$R_m = (U_m - U_{m1})/(U_m + U_{m1}) \qquad S_m = \frac{(k_1^{\,2}U_m - k_o^{\,2}U_{m1})}{(k_1^{\,2}U_m + k_o^{\,2}U_{m1})}$$

$$R_m^{\,*} = 2\Gamma\left[(U_m + U_{m1})^{-1} - \frac{k_o^{\,2}}{(k_1^{\,2}U_m + k_o^{\,2}U_{m1})}\right]$$

$$\Delta_m = e^{(2Umb)}[1 - R_m^{\,2}e^{(-4Umb)}] \qquad \Delta_m^{\,*} = e^{(2Umb)}[1 - S_m^{\,2}e^{(-4Umb)}]$$

$$U_m = [-k_o^{\,2} - \Gamma^2 + (m\pi/2a)^2]^{1/2} \qquad U_{m1} = [-k_1^{\,2} - \Gamma^2 + (m\pi/2a)^2]^{1/2}$$

k_o, k_1 and γ_w are the propagation coefficients for air, the surrounding rock and the conductor material respectively:

$$k_o^2 = \omega^2 \varepsilon_o \mu_o \qquad\qquad k_1^2 = \omega^2 \mu_e (\varepsilon_e - j\sigma_e/\omega)$$

$$\gamma_w = [j\mu_w \omega(\sigma_w + j\varepsilon_w \omega)]^{1/2}$$

The series impedance of the conductor is given by:

$$Z_w = [j\mu_w \omega/(\sigma_w + j\varepsilon_w \omega)]^{1/2} \frac{I_o(\gamma_w \rho)}{2\pi\rho I_1(\gamma_w \rho)}$$

For the steel conductors and the frequency range of interest it can be assumed that $\mu_w = \mu_o$ [8,17].

For perfectly electric walls:

$$P_m(x;x_o) = \frac{2\pi}{a} \sin\left(\frac{m\pi x}{2a}\right) \sin\left(\frac{m\pi x_o}{2a}\right)$$

While for perfectly magnetic walls:

$$P_m(x;x_o) = \frac{2\pi}{a} \varepsilon_m \cos\left(\frac{m\pi x}{2a}\right) \cos\left(\frac{m\pi x_o}{2a}\right) \qquad \begin{array}{ll} \varepsilon_m = 1/2 & m = 0 \\ = 1 & m > 0 \end{array}$$

The equations presented above for S_m and U_{m1} differ from those in [18] and follow those presented by Mahmoud in [15]. The differences take into account the finite conductivity of the rock in region 1.
The equation was solved numerically using Mullers Method [41]. For a complete derivation of the above equation (A1.1) the reader is referred to [15,18].

Figure 59 shows the dimensions of the ZC shaft used in solving (A1.1). The calculated results for α and β for the shaft for both the east and west skips in a frequency range of 100 kHz to 3 MHz are shown in Figures 60 and 61.

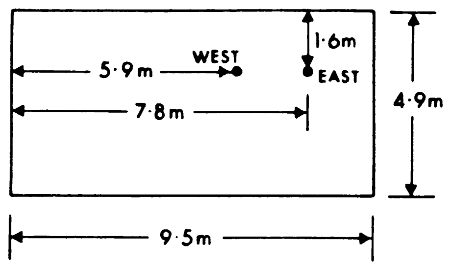

Figure 59

ZC Shaft Measurements for Rectangular Model

On the surface, the results in Figure 60 contradict the general observations made in Chapter Two, in that α decreases as the rope approaches the eastern shaft wall. However, this wall is modelled as a perfect electrical plane. As the conductor moves closer to the plane α will approach a lower, more ideal, value since the lossy wall will exert less influence. It was also noted that the attenuation rate determined from the rectangular model was at least a factor of five smaller than that predicted by circular models of equivalent cross sectional area.

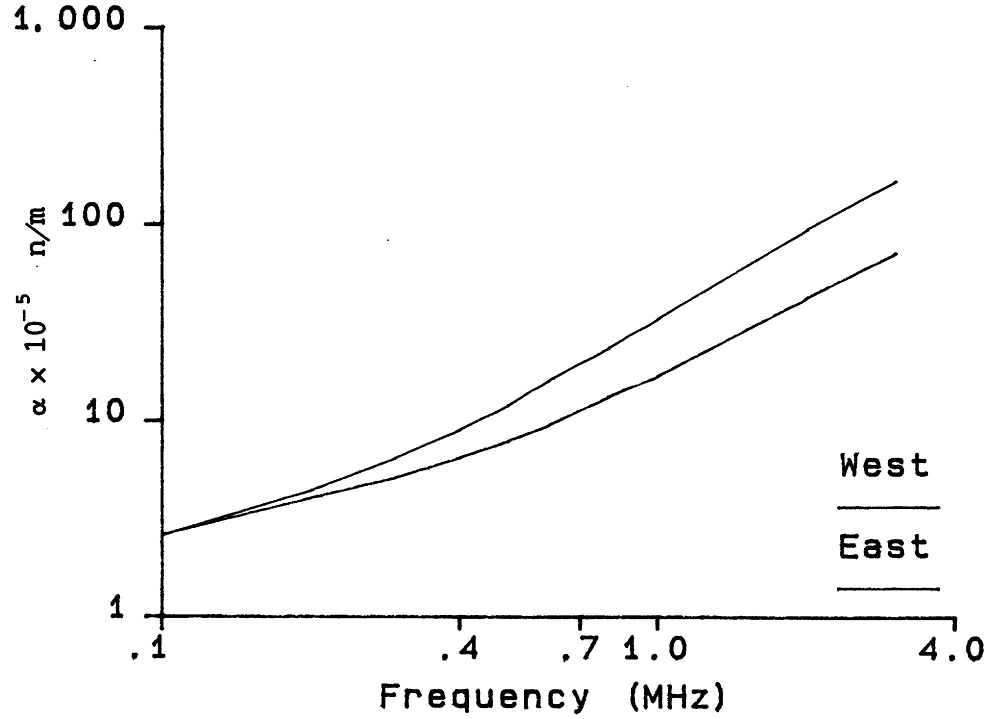

Figure 60

Attenuation Coefficient (α) vs Frequency (Rectangular Model)

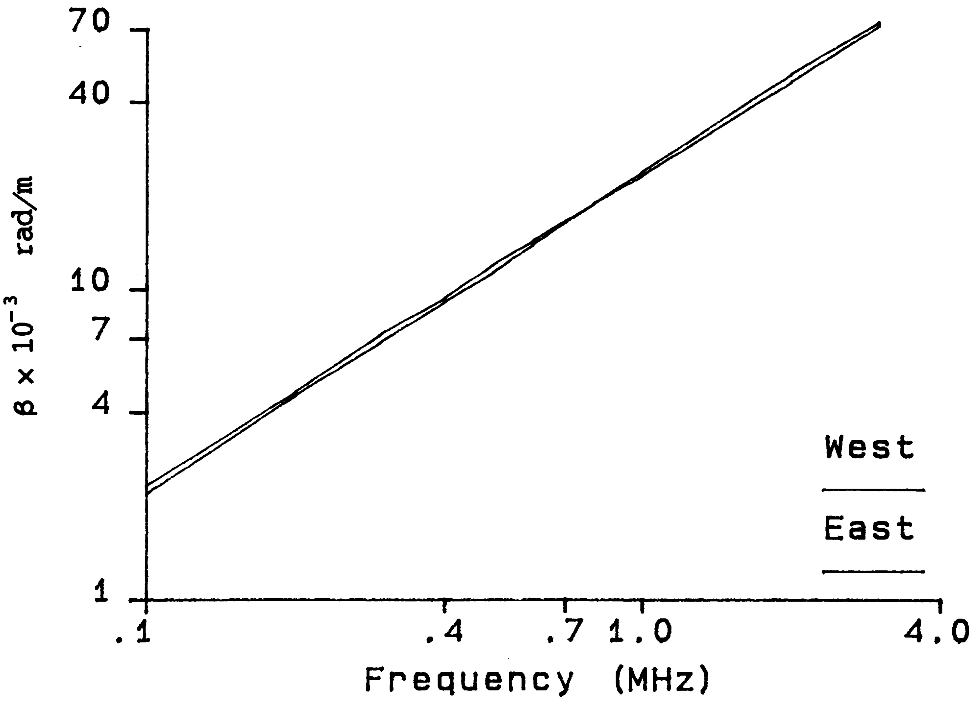

Figure 61

Phase Change (β) vs Frequency (Rectangular Model)

As the propagation coefficient Γ is largely independent of cross-sectional shape for low frequencies [20] it was considered that the rectangular model was unsuitable.

A1.2 PROPAGATION COEFFICIENT - CIRCULAR MODEL RESULTS

For the circular model (see section 2.1.1) the geometric parameters for the model were determined in the following manner:

a) Shaft radius was selected to give the same cross sectional area as the ZC Mines shaft.

b) The position of the axial conductor was determined graphically making a value judgement on how far the conductor should be placed from the wall of the circular shaft. In making this judgement the minimal radial distance from the conductor to the circular model wall was kept very similar to the minimum distance to the real wall.

A second location for the east skip was tried with the wire located closer to the wall (p_o = 2.4 rather than 2.1 metres).

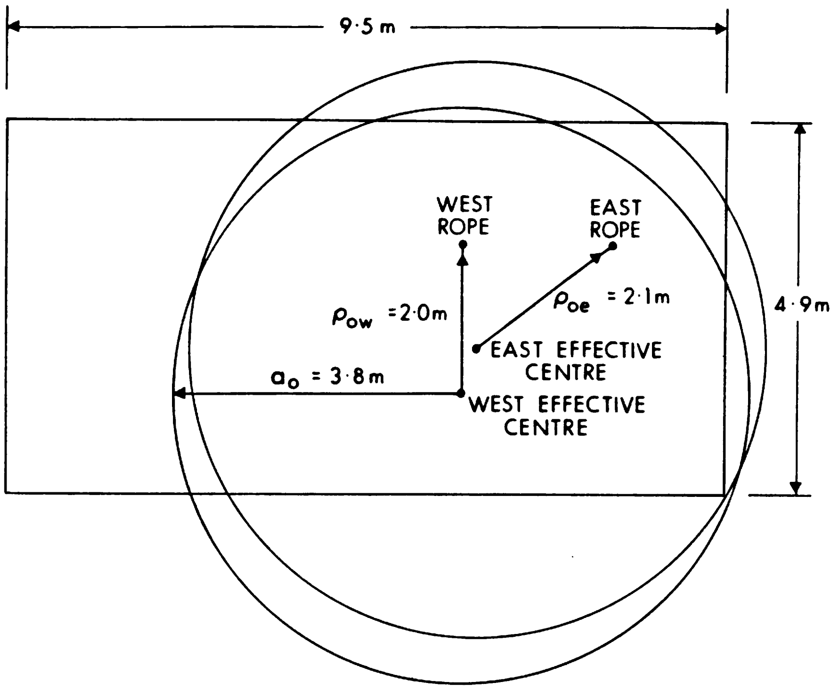

Figure 62

Determination of Measurements for ZC Mines Shaft

The coefficients α and β were calculated for a range of parameters listed in Table 12. The results are shown in Figures 63 and 64.

TABLE 12

Geometric and Electrical Parameters for Circular Model

Parameter	Curve 1	Curve 2	Curve 3
Shaft Radius	3.8 m	3.8 m	3.8 m
Rope Radius	2.4 cm	2.4 cm	2.4 cm
Rope Offset	2.1 m	2.1 m	0.0 m
Rock Conduct.	0.001 S/m	0.01 S/m	0.01 S/m
Wire Conduct.	1×10^5 S/m	1×10^5 S/m	1×10^5 S/m

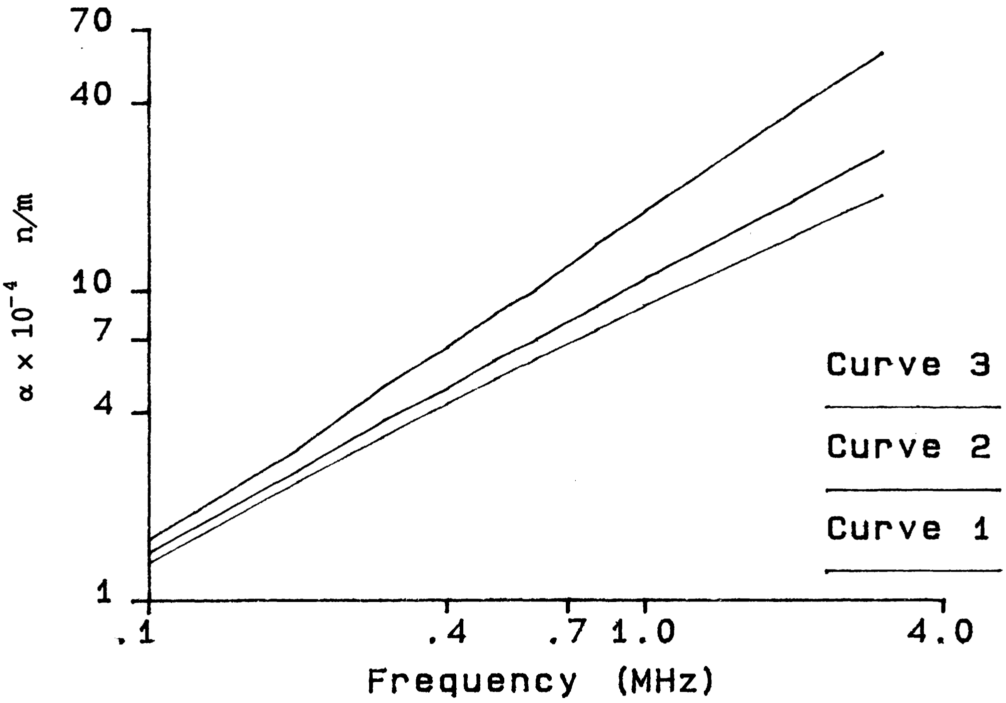

Figure 63

Attenuation (α) vs Frequency (Circular Model)

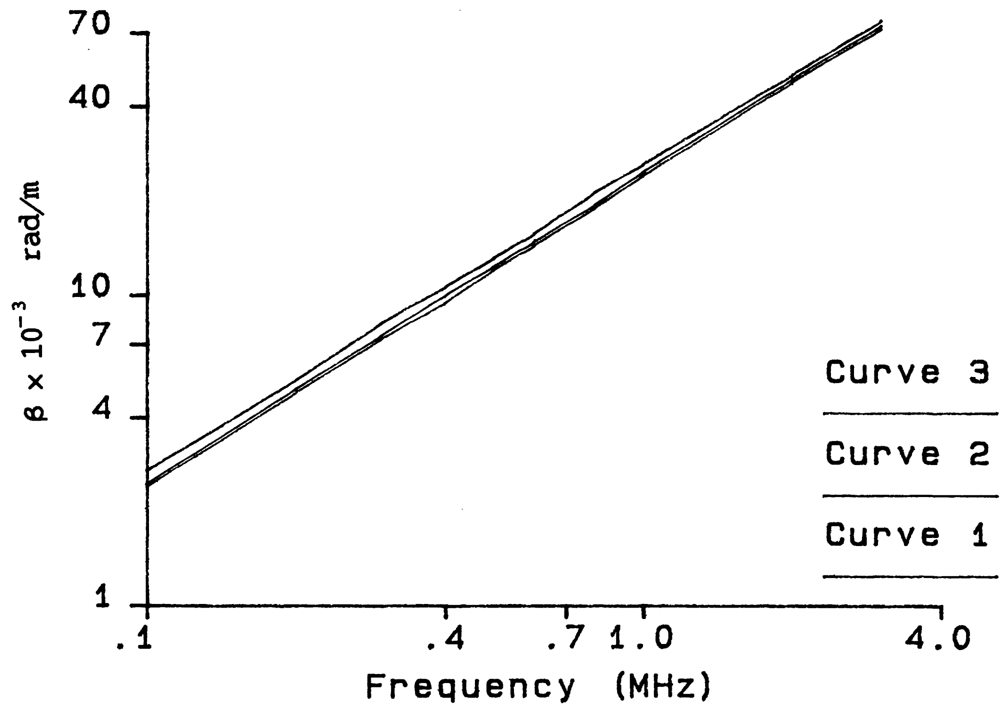

Figure 64

Phase Change (β) vs Frequency (Circular Model)

Observations from the above graphs:

(i) While conductor location does effect the value of Γ (both α and β) its sensitivity is quite weak compared to the effect of σ_e until the conductor is very close to the wall. The results for a rope offset of 2.4 metres were indistinguishable from those for 2.1 metres.

(ii) Lowering the conductivity of the rock raises the losses (α) by a factor logarithmicly dependent on frequency.

The shaft propagation losses are low and are detailed in Table 13.

TABLE 13

Propagation Loss for a Circular Model

Frequency Hz	Rock Cond. S/m	Loss dB/km
100 k	0.01	1.3
100 k	0.001	1.4
300 k	0.01	3.2
300 k	0.001	4.0
1 M	0.01	9.0
1 M	0.001	14.6

A rock conductivity in the order of 0.001 siemens per metre is considered the most realistic by geophysicists familiar with the Broken Hill region [42].

A1.3 TRANSMISSION LINE EQUATIONS

From section 2.1 the received voltage is given by equation (2.1)

$$V_r = \frac{V_r}{V_{ri}} \cdot \frac{V_{ri}}{i_r} \cdot \frac{i_r}{i_t} \cdot \frac{i_t}{V_o} \cdot V_o$$

Where V_r/V_{ri} represents the losses due to the cable between the signal coupler and the receiver. There is approximately 150 metres of cable and the loss was measured at 24 dB.

The factor V_{ri}/i_r represents the receiver coupler, therefore:

$$V_{ri} = M_r \frac{di_r}{dt} \quad \text{and} \quad \frac{V_{ri}}{i_r} = M_r \ \omega$$

for $M_r = 2.08\ \mu H$ and $\omega = 2\pi \times 321$ kHz, $V_{ri} = 4.2$

The factor i_r/i_t represents the transmission line and is given by:

$$\frac{i_r}{i_t} = \frac{e^{-\Gamma}[1 - \rho_r]}{[1 - \rho_r \rho_t e^{-2\Gamma z}]}$$ for steady state signal level conditions,

and by:

$$\frac{i_r}{i_t} = e^{-\Gamma z}[1 - \rho_r] \cdot \sum_{n=0}^{\infty} (\rho_r \rho_t e^{-2\Gamma z})^n$$ when considering pulse shapes.

The transmitter coupler and induction of the signal onto the hoist rope is represented by i_t/V_o from Figure 3 of Chapter Two it can be seen that:

$$i_t = \frac{M_t \dfrac{di_o}{dt}}{|Z_o + Z_t|} \qquad \text{giving} \qquad \frac{i_t}{V_o} = \frac{M_t}{L_t \ |Z_o + Z_t|}$$

For $M_t = 3.72\ \mu H$ $L_t = 1.15$ mH $Z_o = 343 - j\ 19\ \Omega$ and $Z_t = -\ j2934\ \Omega$

$$\left|\frac{i_t}{V_o}\right| = 1.09 \times 10^{-6}$$

Therefore the losses due to the signal couplers alone amounts to some 107 dB out of a total system loss of approximately 130 dB.

The system losses are reduced by 12 dB each time the turns for the transmitter coupler and receiver couplers are halved and doubled respectively. However halving the turns for the transmitter coupler has the adverse effect of increasing the power drain by a factor of four. A better method of reducing the system loss would be to develop an higher efficiency transmitter coupler using either a ferrite or iron core.

A1.4 SIGLEV PROGRAM RESULTS

The program was run for the following sets of parameters:

$\Gamma = 3.71 \times 10^{-4}$ n/m + j7.14×10^{-3} rad/m

Frequency = 321 kHz and $\sigma_e = 0.01$ S/m

$Z_o = (318.3 - j\ 15.0)\ \Omega$

$Z_t = -j\ 2934\ \Omega$ Capacitance of shaft vehicle = 169 pF

$Z_r = 10.0\ \Omega$ Curve 1

$Z_r = (10.0 + j300.0)\ \Omega$ Curve 2

$\Gamma = 4.65 \times 10^{-4}$ n/m + j 7.68×10^{-3} rad/m

Frequency = 312 kHz and $\sigma_e = 0.001$ S/m

$Z_o = (342.7 - j\ 19.3)\ \Omega$

$Z_t = -j\ 2934\ \Omega$

$Z_r = 30\ \Omega$ Curve 3

$Z_r = (30 + j\ 300)\ \Omega$ Curve 4

$Z_r = (50 + j\ 300)\ \Omega$ Curve 5

From the graphs it can be seen that curve 5 is the closest to the measured results (curve 6). Curves 1 and 3 have there first maximum well away from the maximum for curve 6. This strongly suggests the presence of approximately 150 μH of inductance in the headframe and grounding structure.

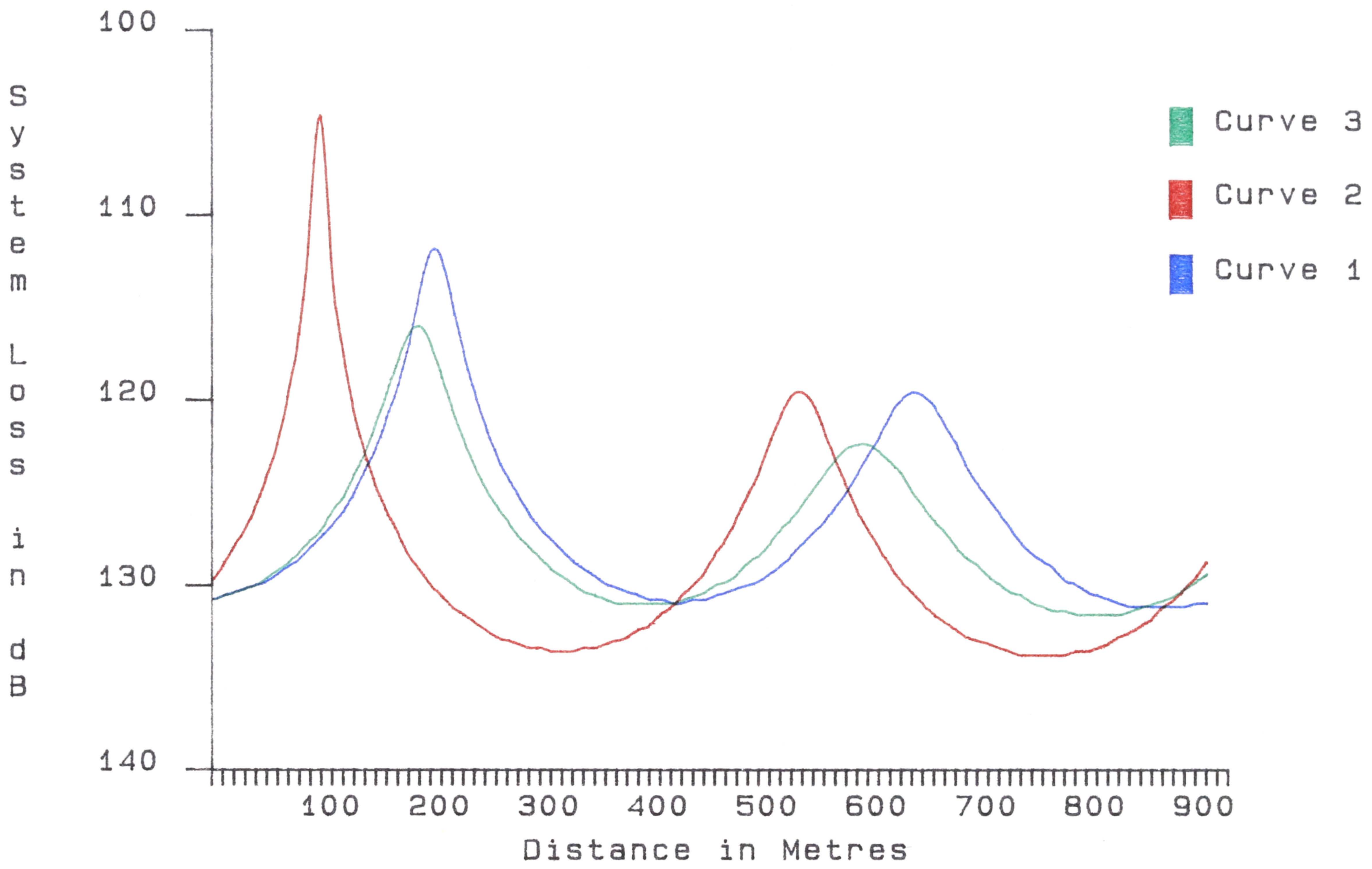

Figure 65

Plot of System Loss (Curves 1,2 and 3)

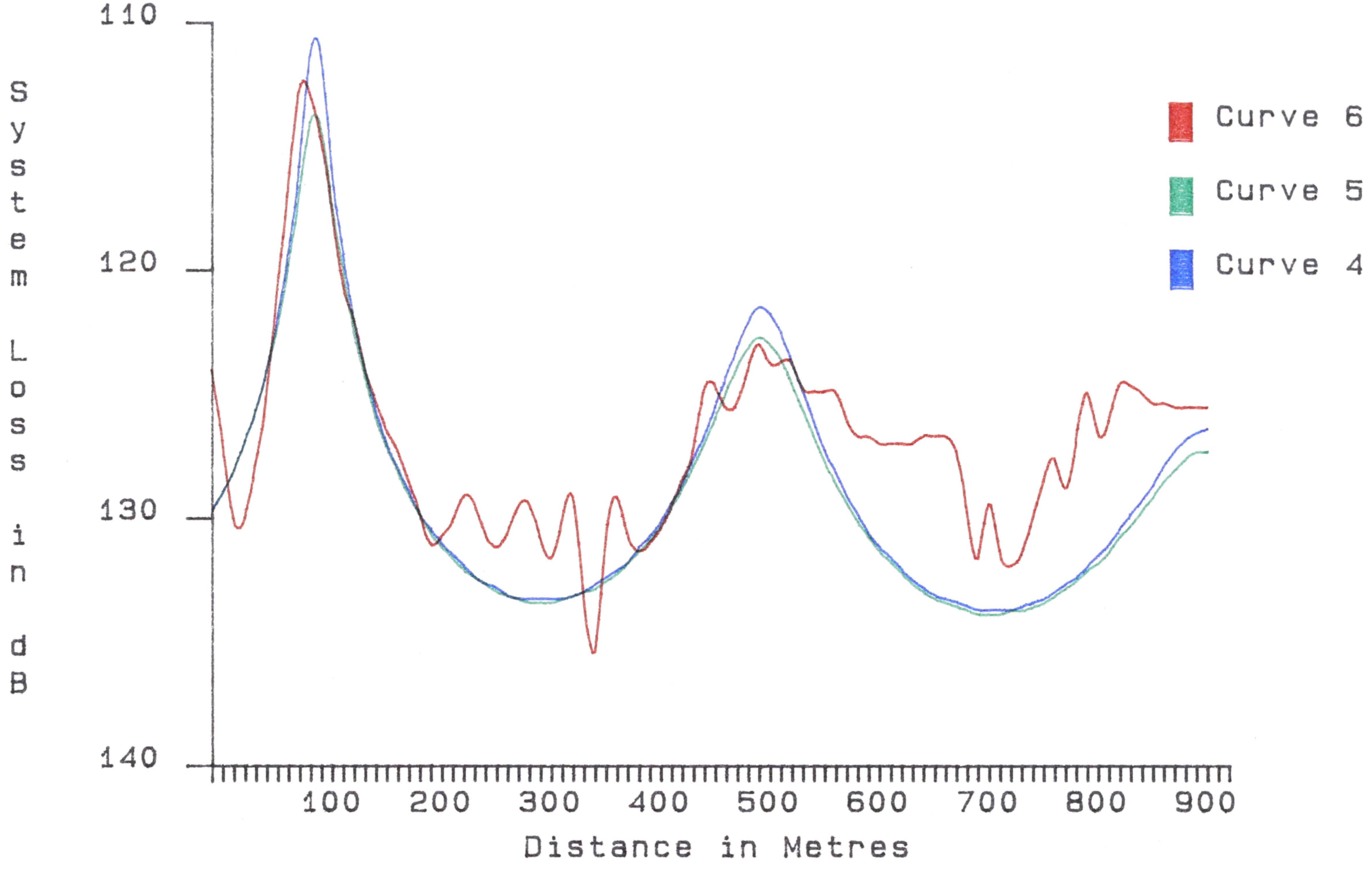

Figure 66

Plot of System Loss (Curves 4,5 and 6)

APPENDIX 2

APPENDIX 2

MODELLING THE DIGITAL RADIO LINK

This appendix details the methods used to model the various aspects of the digital link on a computer. The appendix consisted of two major parts:

a) a discussion of the modelling approach, and

b) a description of the major program sections.

The program listings are not included due to their bulk however, they are available from the author for consultation upon request.

A2.1 MODELLING APPROACH

The model was developed to evaluate equation (2.3) ie:

$$V_r = \frac{M_t \ M_r \ \omega \ e^{-\Gamma z}[1 - \rho_r]}{CF \ L_t \ |Z_o + Z_t|} \cdot \sum_{n=0}^{\infty} (\rho_t \rho_r e^{-2\Gamma z})^n \cdot V_o$$

Using this equation the full effects of standing waves and propagation losses upon the received signal can be evaluated. The equation can be separated into three major portions:

a) The signal generation and transmitter:

$$\text{ie., } i_t = \frac{M_t \ V_o}{L_t \ |Z_o + Z_t|}$$

Where i_t is the current induced into the hoist rope at the transmitter end, see Figure 3, Chapter Two. The factor $M_t/L_t\,|Z_o + Z_t|$ represents the signal transfer impedance of the transmitter coupler and the shaft termination. V_o is the output voltage of the transmitter applied across the signal coupler.

V_o is a function of time and is represented by the equation:

$$V_o(t) = \text{Window}(t) \cdot \text{Vmax} \cdot \sin(\omega t + \text{Phase(Pulse No)})$$

Where window(t) is a function to apply either a rectangular or a four term Blackman Harris window to the transmitted pulse. Phase(Pulse N°) is a QDPSK modulation function for a dibit symbol sequence of 00, 11, 00, 00. Vmax is the peak output voltage of the transmitter ie., 350 volts.

b) The shaft propagation effects:

An equation for these effects can be derived by considering the following. At time zero a current i_t is propagated, from the transmitter end, Z metres up the shaft to the surface receiver. The shaft acts as a lossy transmission line with a propagation coefficient Γ. Each time the signal traverses the shaft it is reduced by a factor $e^{-\Gamma z}$. Hence, when the current i_t reaches the receiver end it will be $i_t e^{-\Gamma z}$. At the receiver a portion $-\rho_r$ is reflected back to the transmitter while the rest $(1 - \rho_r)$ becomes the effective received current. At the transmitter the reflected current, now $i_t e^{-\Gamma z}(-)\rho_r e^{-\Gamma z}$ has a portion $-\rho_t$ reflected back to the receiver. On reaching the receiver the reflected current has a value of $i_t e^{-\Gamma z} \rho_r \rho_t e^{-2\Gamma z}$. Therefore, the received current becomes;
$i_t[1 - \rho_r]e^{-\Gamma z}[1 + \rho_r \rho_t e^{-\Gamma z}]$. On repeating this sequence m times the received current works out to be:

$$i_r = i_t[1 - \rho_r]\, e^{-\Gamma z} \sum_{n=0}^{\infty} (\rho_r \rho_t\ e^{-2\Gamma z})^n$$

Where $e^{-\Gamma z} \sum_{n=0}^{\infty} (\rho_r \rho_t \; e^{-2\Gamma z})^n$ is due to the shaft propagation and reflection effects. The factor $[1 - \rho_r]$, for convenience, is considered as a receiver effect. The above derivation is best summarised by Figure 75.

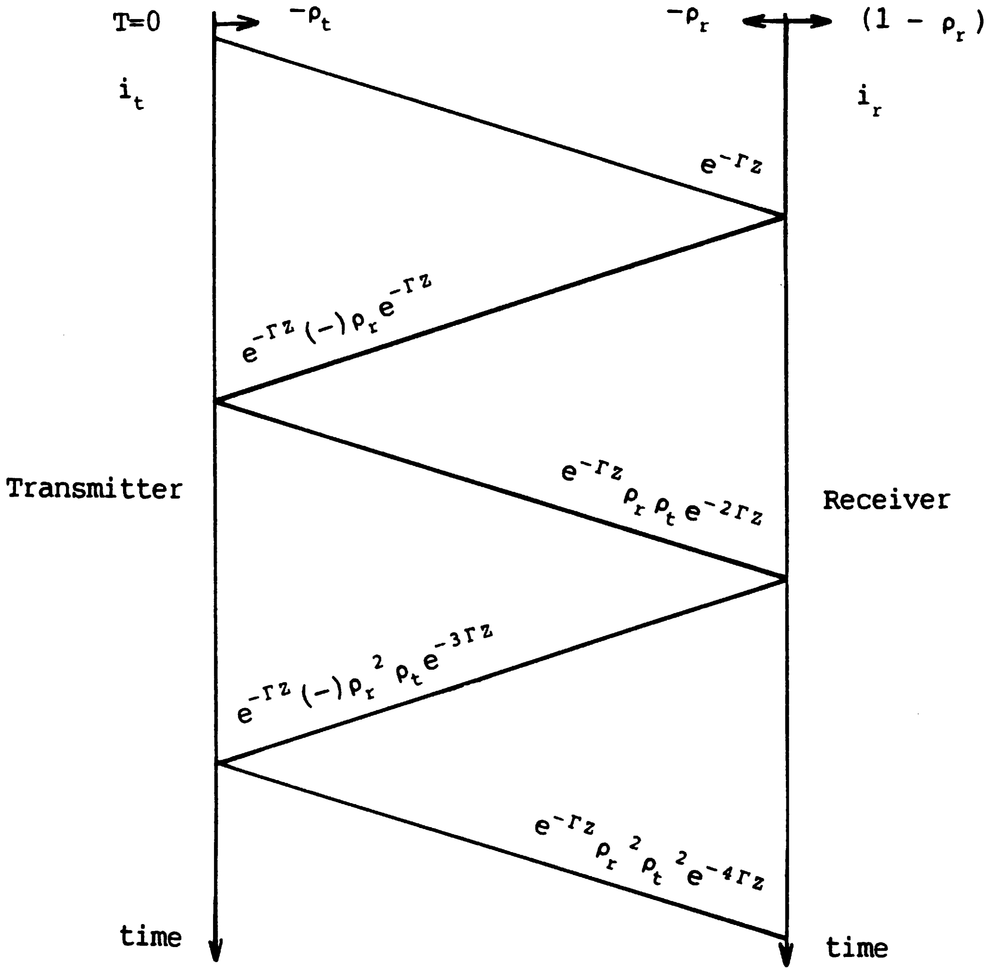

Figure 75

Signal Reflection and Reception for a Lossy Transmission Line

c) The receiver:

As shown above the effective received current is given by the equation for i_r. The received input voltage is in turn given by:

$$V_{ri} = \frac{M_r \; \omega}{CF} \cdot i_r$$

Where $M_r \omega/CF$ represents the receiver coupler and the cable losses between it and the receiver.

The parameters Γ, ρ_r, ρ_t, M_r, L_t, and Z_t are all functions of frequency. As the transmitter output is a modulated signal the transmission line behaviour of the shaft across the frequency spectrum needs to be considered. The easiest method of doing this is to model the link in the frequency domain. This is done by taking the time domain representation of the current i_t and applying a DFT via a FFT algorithm. The sample frequency for the DFT is two megahertz which gives a time window of 2.05 milliseconds and a frequency resolution of 488 Hz. The shaft propagation and reflection effects along with the receiver parameters are then applied in the frequency domain.

The received signal then has an inverse DFT applied so that the signal can be demodulated in the time domain. Demodulation is achieved by multiplying together a series of time samples separated by one symbol period. This corresponds to the Bit n demodulation in Figure 39 of section 4.1.2.

The model result outputs are displayed on a Tektronix 4105 colour graphics terminal. Hard copy plots are available through a Tektronix 4695 ink jet plotter.

A2.2 MAJOR PROGRAM SECTIONS

There are three major sections in the model program:

a) Data entry and recall.

b) Execution.

c) Graphical display.

On starting the model program the data entry section is run, transparent to the user, to set up the default values for all parameters. The program then prompts the user for a command which must be one of:

- l : List the system configuration parameters.
- r : Run the model using the current configuration.
- s : Set up a new configuration.
- m : Modify a system parameter.
- q : Quit
- si : Change the signal characteristics.
- sh : Change the shaft characteristics.
- Re : Change the receiver characteristics.
- Tr : Change the transmitter characteristics.

All of the above with the exception of r and q are associated with the data entry and recall section. The graphical display section is accessed from the execution section at the appropriate stages.

A2.2.1 DATA ENTRY AND RECALL

This section is responsible for controlling the entry or modification of parameters associated with:

a) the transmitted signal,
b) the shaft,
c) the transmitter,
d) the receiver and
e) program execution.

All data is stored and validated through the Knowl relational data base [30]. There are five schema files associated with the model:

a) Model.s - includes information and parameters dealing with the program execution and the graphing of results.

b) Receiver.s - parameter details and validation ranges for receiver parameters.

c) Shaft.s - as above except for the shaft.

d) Signal.s - as above except for the signal.

e) Transmit.s - as above except for the transmitter.

A typical field entry in a schema file is arranged in the following manner:

```
Field_Name    Field_Type and Length  ( eg. F8.2, I4, A10 )
                                          ^    ^    ^
                                       Float Int Alpha
>= Lower_Range   <= Upper_Range  - for the I and F types.
?"  Help String in free format  "
"Units"                          - a text string for the units
= Default_Value
;                                - end of the field definition
```

A field can be set up to have only a number of allowable values. If the user tries to select something different the data base puts out an error message and displays the allowable selection. This is done by enclosing the values and their associated help string in square brackets. A number of examples of this type of field definition appear in the model schema file, model.s, below.

A relation is formed from a number of fields and is arranged as follows:

```
{
 Relation_Name      "File_Prefix.File_Suffix"
 ! File_Name identification
 Field 1
   |
 Field n
}
```

An important characteristic of the model program is that variable parameters only have to be changed in one place, the schema file. This can be done without having to recompile the program. The schema files for the model follow:

```
#file model.s
# Model - Modelling radio data communications in a mine shaft.

  command All
  [ l  1  "List the system configuration on the terminal"]
  [ r  1  "Run the model using the current data"]
  [ s  1  "Set up a new configuration"]
  [ m  1  "Modify a system characteristic"]
  [ q  1  "Quit  from the program"]
  [ Si 1  "Change the signal characteristics"]
  [ Sh 1  "Change the shaft characteristics"]
  [ Re 1  "Change the receiver characteristics"]
  [ Tr 1  "Change the transmitter characteristics"]
    ;
```

```
iterations I4
>=1 <=100
?"The number of reflections up and down the shaft for the pulse"
=1
 ;
Terminal_Type  A4
[ "4105"  4  "Tektronix 4105 colour terminal " ]
[ "4014"  4  "Tektronix 4014" ]
[ "4113"  4  "Tektronix 4113 colour terminal " ]
="4105"
 ;
Baud_Rate  I3
>=30 <=960
?"Terminal transmission speed in chars per second."
=960
;
Window_type  A1
[ "D" 1  "Default window using limits of the data" ]
[ "S" 1  "A smaller window set by the user using the cursor"]
="S"
  ;
Graph_Type  A2
[ "FR" 2  "Plot received pulse in frequency domain" ]
[ "FT" 2  "Plot transmitted or reflected pulse in frequency domain"]
[ "PR" 2  "Plot receiver reflection coefficient vs frequency" ]
[ "PS" 2  "Plot transmitter reflection coefficient vs frequency"]
[ "TR" 2  "Plot receiver coefficient of transmission vs frequency"]
[ "T"  1  "Plot pulses in time domain" ]
[ "I"  1  "Plot imaginary FFT components in time domain"]
[ "N"  1  "No plot continue processing" ]
  ;
```

```
#file receiver.s
#receiver - The details of the receiver


    R_C_M_Ind  F7.3
    >=.10  <=100.0
    ?"How much mutual inductance does the receiver coupler have?"
    "µH"
    =2.08
     ;
    Headframe_Resistance  F7.2
    >=0.0  <=1000.0
    ?"The headframe will have some resistance to ground how much ?"
    "ohms"
    =10.0
    ;
    Headframe_Inductance  F7.2
    >=0.0 <=1000.0
    ?"The headframe structure is likely to exhibit some inductance in "
    ?"The termination impedance it presents to the transmission line."
    ?"How much?"
    "µH"
    =250.0
    ;
    Filter_cutoff_Frequency  F8.2
    >=10.0 <=300.0
    ?"The output of the demodulator is put through a Low Pass Filter."
    ?"What frequency does this filter start to take effect ie., -3 dB?"
    "kHz"
    =20.0
    ;
```

```
Filter_Order  F8.2
>=1.0 <=6.0
?"The filter is a Butterworth design what order is it ie., how "
?" many stages ?  For each order, the filter will reduce high "
?"frequencies by 6 dB per octave."
=3.0
;
Cable_Factor F7.2
>=1.0 <=30.0
?"The input receiver voltage will be lower than the coupler "
?"output voltage due to the losses in the cable interconnecting"
?"the two.  What is the ratio of the coupler to receiver voltage ?"
=15.0
;

{
Receiver    "r.dat"
   !Type
  R_C_M_Ind
  Headframe_Resistance
  Headframe_Inductance
  Filter_Cutoff_Frequency
  Filter_Order
  Cable_Factor
}
```

```
#file shaft.s
#Shaft - Details about the shaft and the location of the transmitter.

     Shaft_Radius    F6.3
     >=1.0  <=10.0
     ?"The shaft is presumed to be of circular cross-section."
     ?"What is the effective radius?"
     "metres"
     =4.0
       ;
     Rope_radius   F6.3
     >=0.5    <=10.0
     ?"What is the radius of the wire rope supporting the skip ?"
     "cm"
     =2.4
       ;
     Rope_Offset  F6.3
     >=0.001 <=10.0
     ?"The rope may be offset from the shaft axis, if so how much?"
     ?"Must be less than the shaft radius."
     "metres"
     =0.001
     ;
     Rope_Conductivity F9.2
     >=0.1 <=100.0
     ?"What is the conductivity of the wire rope material ?"
     ?"For steel σw = 0.1 microsiemens per metre for copper "
     ?"σw = 10.0 microsiemens per metre."
     "μS/m"
     =0.1
     ;
```

```
Rock_Conductivity   F7.1
>=5   <=10000.0
?"What is the resistivity of the surrounding rock in"
?"ohms per meter?"
"Ω/m"
=100.0
  ;
Skip_Position   F8.2
>=0.0   <=10000.0
?"The transmitter is mounted on the skip. How far down the shaft"
?"do you wish to model the transmission from ?"
"metres"
=500.0
  ;

 {
   Shaft   "sh.dat"
    !Type
    Shaft_Radius
    Rope_Radius
    Rope_Conductivity
    Rope_Offset
    Rock_Conductivity
    Skip_Position
 }
```

```
#file signal.s
#Signal _ The details about the signal

    Frequency  F7.2
    >=10.0   <=2000.0
    ?"What is the radios link's carrier frequency in kHz?"
    "kHz"
    =321.0
      ;
    Length   F8.3
    >=10.0    <=2500.0
    ?"What is the symbol duration in microseconds ?"
    "μs"
    =55.5
      ;
    Start_Time    F8.2
    >=-1500.0   <=1500.0
    ?"The time at which transmission of the symbols start."
    "μs"
    =0.0
      ;
    Number_Of_Pulses  I4
    >=1 <=10
    ?"You can send a stream of pulses to the receiver and look"
    ?"at the demodulated output to determine the effects of ISI"
    =1
    ;
    Type    A5
    ?"A unique character string identifying"
    ?"this particular subsystem."
      ;
```

```
    {
      Signal   "si.dat"
        !Type
        Frequency
        Length
        Number_Of_Pulses
        Start_Time
    }


#file transmit.s
#Transmit - The details of the transmitter


      Skip_Capacitance    F8.2
      >=10.0   <=1000.0
      ?"The capacitance between the skip and the shaft."
      "pF"
      =68.0
       ;
      Skip_Resistance  F10.2
      >=1.5 <=1000.0
      ?"There could be some leakage resistance, due to moisture and"
      ?"dirt, between the skip and "the shaft if so how much ?"
      "kΩ"
      =1000.0
      ;
```

```
Transmitter_Output    F8.2
>=10.0   <=1000.0
?"The peak to peak transmitter output voltage measured across"
?"the transmitter signal coupler"
"volts"
=700.0
 ;
T_C_M_Ind  F7.2
>=0.5 <=20.0
?"How much mutual inductance does the transmitter coupler have?"
"μH"
=3.72
;
T_C_S_Ind  F7.2
>=0.5 <=6.0
?"How much mutual inductance does the transmitter coupler have?"
"mH"
=1.0
;

{
 Transmitter   "t.dat"
   !Type
   Skip_Capacitance
   Skip_resistance
   Transmitter_Output
   T_C_M_Ind
   T_C_S_Ind
}
```

When the model is started these schema files are read and the default values are stored in the fields. The user can by entering the command:

a) M - modify a field value with the data base carrying out range checking and validation.

b) S, si, sh, re or tr - change all the fields belonging to that relation and have them stored in a disc file.

When the parameter values have been recalled or set up as required the user can then run the program by selecting the 'r' command.

A2.2.2 MODEL EXECUTION

The model uses a number of arrays, during execution, for data storage they are:

a) TPulse - Complex(4096) - Used for storing the transmitted and reflected pulse. Also used by the FFT as the input/output array.

b) DPulse - Complex(4096) - Used for storing the demodulated received pulse.

c) Rpulse - Complex(4096) - Used for storing the cumulative received pulse.

d) Factor - Complex(4096) - Stores the factor ΓZ for each frequency bin. Where Γ is the propagation coefficient and Z is the shaft vehicle position.

e) Pr - Complex(4096) - Stores the reflection coefficients for the receiver for each frequency bin.

f) Pt - Complex(4096) - As above except for the transmitter end.

There are four stages to the execution section namely:

a) Set up.

b) Transmitter signal generation.

c) Propagation through the shaft.

d) Received signal demodulation.

The set up stage carries out three functions. Firstly, where appropriate, unit multiplication factors are applied to parameters. For example, the user enters the Headframe inductance in units of microhenries, but before running the model it is converted to Henries. Secondly, the propagation coefficient must be evaluated for each frequency bin and stored in the Factor array. Thirdly, the same must be done for the reflection coefficients ρ_r and ρ_t.

The transmitter signal generation is carried out by evaluating the following algorithm:

```
time = 0
for( n = 1; n <= Number_of_Samples; n = n + 1){
    if( n <= Number_of_Samples / 2 )              ! +ve time
        time = (n - 1) / Sample_Frequency
    else                                          ! -ve time
        time = ( n - Number_of_Samples - 1) /  Sample_Frequency
    if(time >= Start & time < Start + Pulse_Length x No_of_Pulses){
```

$$\mathrm{TPulse(time)} = \frac{M_t}{L_t\,|Z_t + Z_o|} \cdot \mathrm{Window(time)} \cdot \mathrm{Vmax} \cdot \mathrm{Sin}(\ \omega(\mathrm{time} - \mathrm{start}) + \Delta\mathrm{Phase(Pulse\_No)})$$

```
    }
    else
        TPulse(time) = 0
}
```

After executing the above algorithm the TPulse array contains the the time domain representation of the current i_t.

Modelling the shaft propagation and the reception of the current is achieved in four steps:

a) Shaft propagation - By multiplying each element of the TPulse array by the value $e^{-Factor(n)}$ where n is the corresponding element number of the Factor array.

b) Receiver reception and reflection - By summing to each RPulse(n) an amount equal to $[1 - Pr(n)] \cdot TPulse(n)$ for each n. Multiplying each TPulse(n) by -Pr(n).

c) Shaft propagation - As in (a). The second shaft propagation is for the return reflection from the receiver to the transmitter.

d) Transmitter reflection - By multiplying each TPulse(n) by -Pt(n).

Steps (a) to (d) are in a loop executed m times, where m is the number of iterations specified by the user. After the loop has completed the RPulse array is transferred to the TPulse array. An inverse DFT is then performed to give the received signal in the time domain.

The received signal is demodulated by applying the following algorithm:

```
for( n = 1; n <= Number_of_Samples; n = n + 1) {
    m = n - 1 - Sample_Frequency × Pulse_Length    ! go back 1 pulse
    DPulse(n) = TPulse(n) × TPulse(m) × Normalisation_Factor
}
```

The Normalisation_Factor is used to model, in a crude way, the receiver's AGC and to ensure that the plotted pulse shapes have the same height.

The result of the algorithm is converted to the frequency domain so that the demodulation filter can be applied. The filter is modelled as having a Butterworth response of order b, specified by the user. After the filter has been applied the result is converted back to the time domain ready for graphing. Demodulating the received signal in this way produces the Bit n value, see section 4.1.2.

A2.2.3 GRAPHICAL DISPLAYS

Graphical displays of the results are available at the following points in the program execution:

a) After transmitter signal generation - Graphical displays in both the time and frequency domains are available.

b) After demodulation of the transmitted signal - That is before the signal is propagated up the shaft. This allows determination of the standing wave and propagation effects on the pulse shape by comparing (b) with (d). Time and frequency displays are available both before and after demodulation filtering.

c) Received signal prior to demodulation - Time and frequency displays.

d) After demodulation of received signal - Time and frequency before and after demodulation filtering.

The graphical displays are generated on a Tektronix 4105 colour terminal using software, developed by the author, which emulates the Plot 10 package. The software allows the plotting of X - Y graphs using both linear and logarithmic axes. A windowing facility is used to allow the user to zoom in on an area of interest. Hard copy plots can be produced from a Tektronix 4695 ink jet plotter.

APPENDIX 3

APPENDIX 3

SYSTEM ENCLOSURES, CIRCUIT BOARDS AND DIAGRAMS

In this appendix details of the enclosures, circuit boards and a full set of circuit diagrams are provided.

A3.1 ENCLOSURES

The requirements for enclosures for the transmitter and receiver were quite different. The receiver required an enclosure of a convenient size and weight that could house the circuitry. The transmitter required one that would protect the circuitry from vibration and water and provide a convenient method for attaching the transmitter to the skip.

A polycarbonate enclosure with a transparent lid is used for the receiver. The two wire wrap boards are fixed at right angles to each other. One vertical and the other horizontal. The enclosure is quite large to fit all the circuitry in while enabling easy access. Figure 68 shows the layout of the circuit boards in the enclosure.

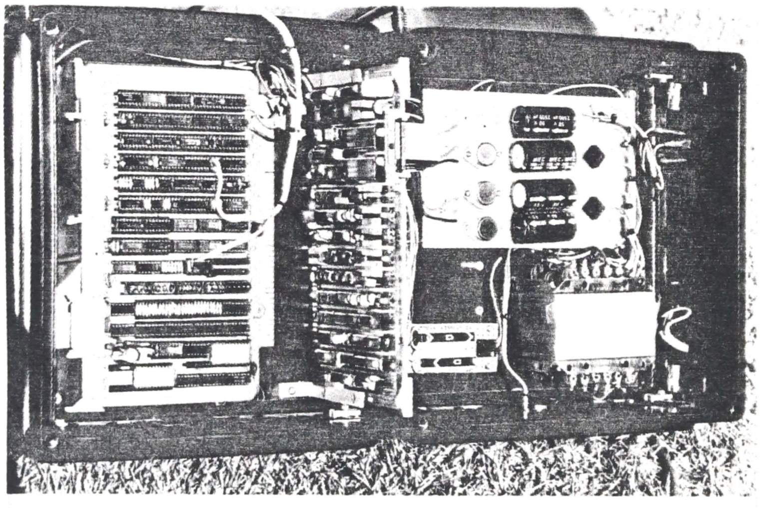

Figure 68

The Complete Receiver Set

The transmitter enclosure is a metal box which fits closely in the bin used to mount the transmitter on the skip. Two angle iron fittings are bolted onto the bin to keep the transmitter in place see Figure 69.

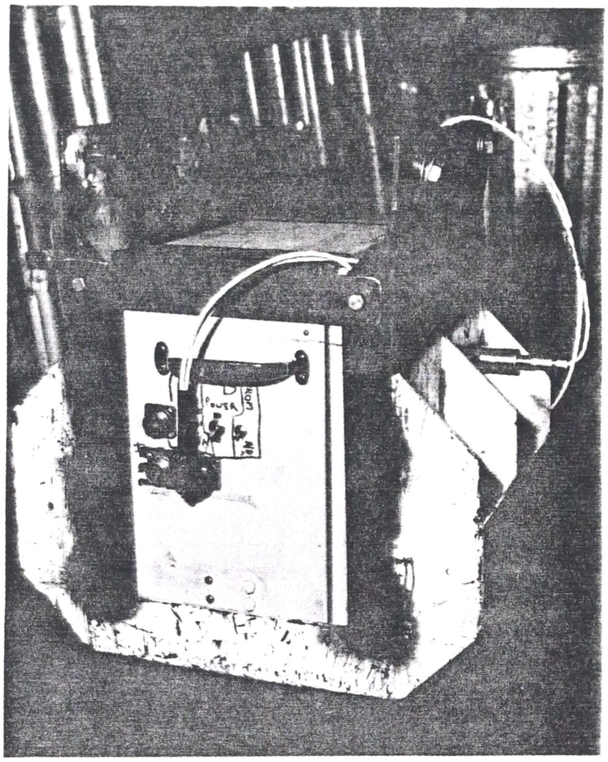

Figure 69

The Transmitter Mounted in the Metal Bin

The three cannon sockets on the transmitter enclosure are for:

Top	-	Signal coupler
Left	-	Recharging Socket
Right	-	Transducers

A3.2 CIRCUIT BOARDS

For both the transmitter and receiver there are two main and one minor board. For the transmitter they are:

a) The analog board was constructed as a printed circuit board, this made modifications very difficult. The experiences with it were convincing enough to ensure PCBs would not be used again in the development of the system. It contains all the circuitry from sheets 2 and 3 of the circuit diagrams. That is, input amplifiers, ADC, the serial to parallel converter and the DC to DC converter.

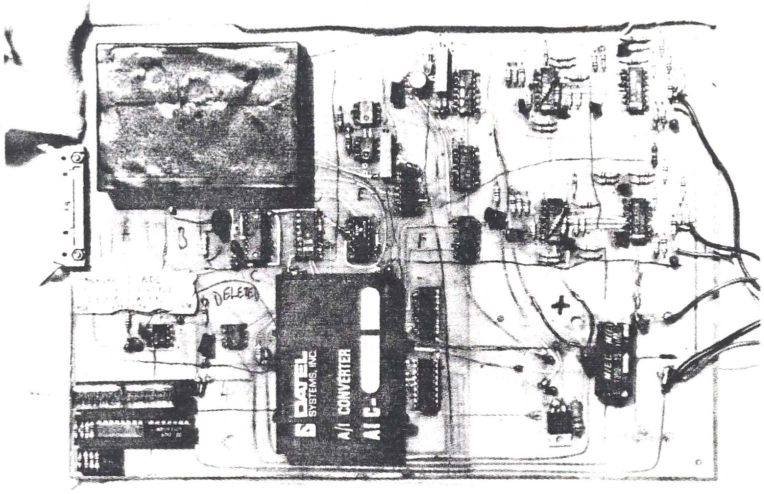

Figure 70

Analog Transmitter Board

b) The Digital board, a wire wrap board contains the remaining transmitter circuitry except the final power amplifier. That is the circuitry shown on sheets 4, 5, and 6.

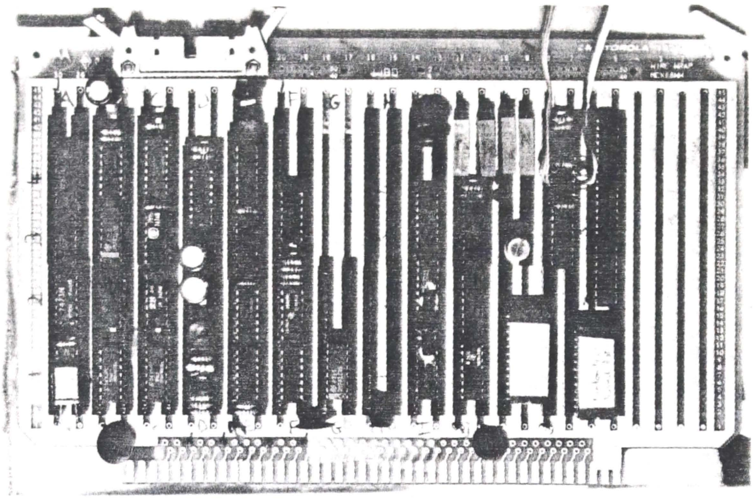

Figure 71

Digital Transmitter Board

c) The Amplifier board, a vero board, contains the power amplifier feeding the signal coupler. This board is mounted on the side of the transmitter box using the power transistors heat sink. See sheet 8 of the circuit diagrams.

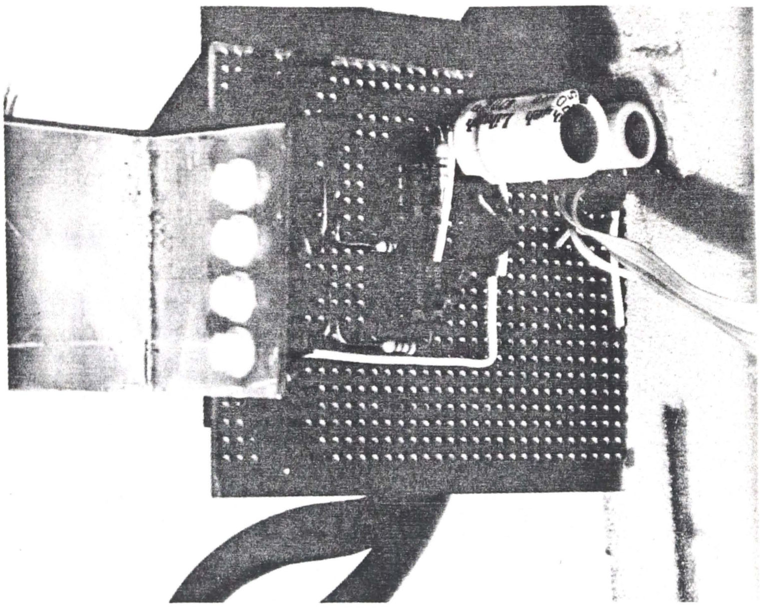

Figure 72

Power Amplifier for the Transmitter

The boards for the receiver are:

a) The Analog board, a wire wrap board containing all the circuitry from the front-end amplifier up to the serial to parallel converter ie., Sheets 2, 3, 4, 5 and 10 of the receiver circuit diagrams.

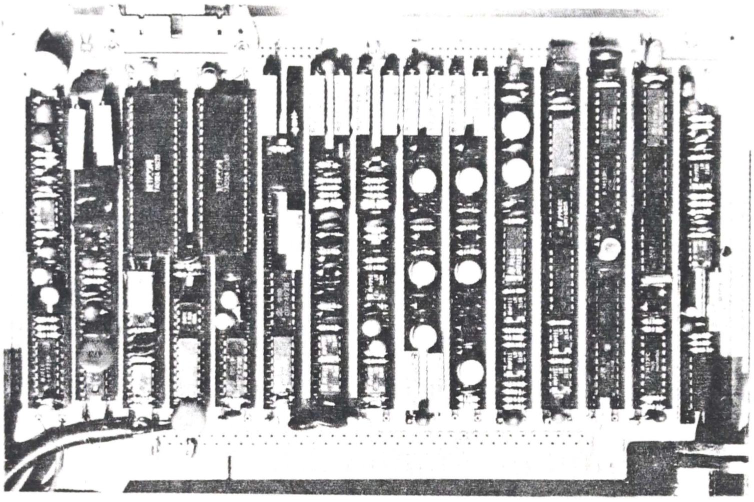

Figure 73

Analog Receiver Board

b) Digital receiver board, a wire wrap board containing the remainder of the receiver circuitry, as detailed on sheets 6, 7, 8, 9 and 10 of the receiver circuit diagrams.

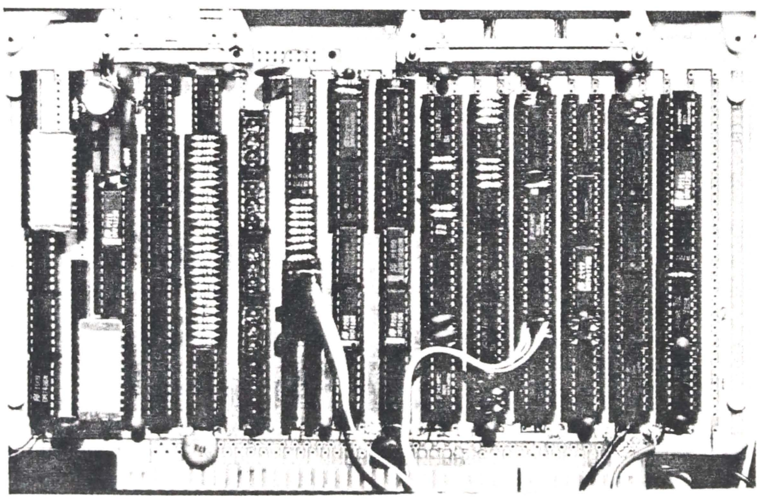

Figure 74

The Digital Receiver Board

c) The receiver power supply, a PCB board contains the ± 5 V and ± 15 V supplies for the receiver. See sheet 7 of the receiver circuit diagrams.

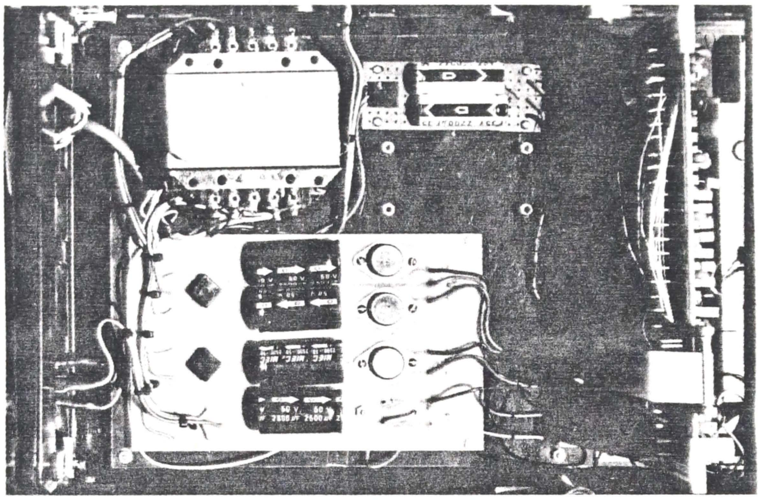

Figure 75

The Receiver Power Supply

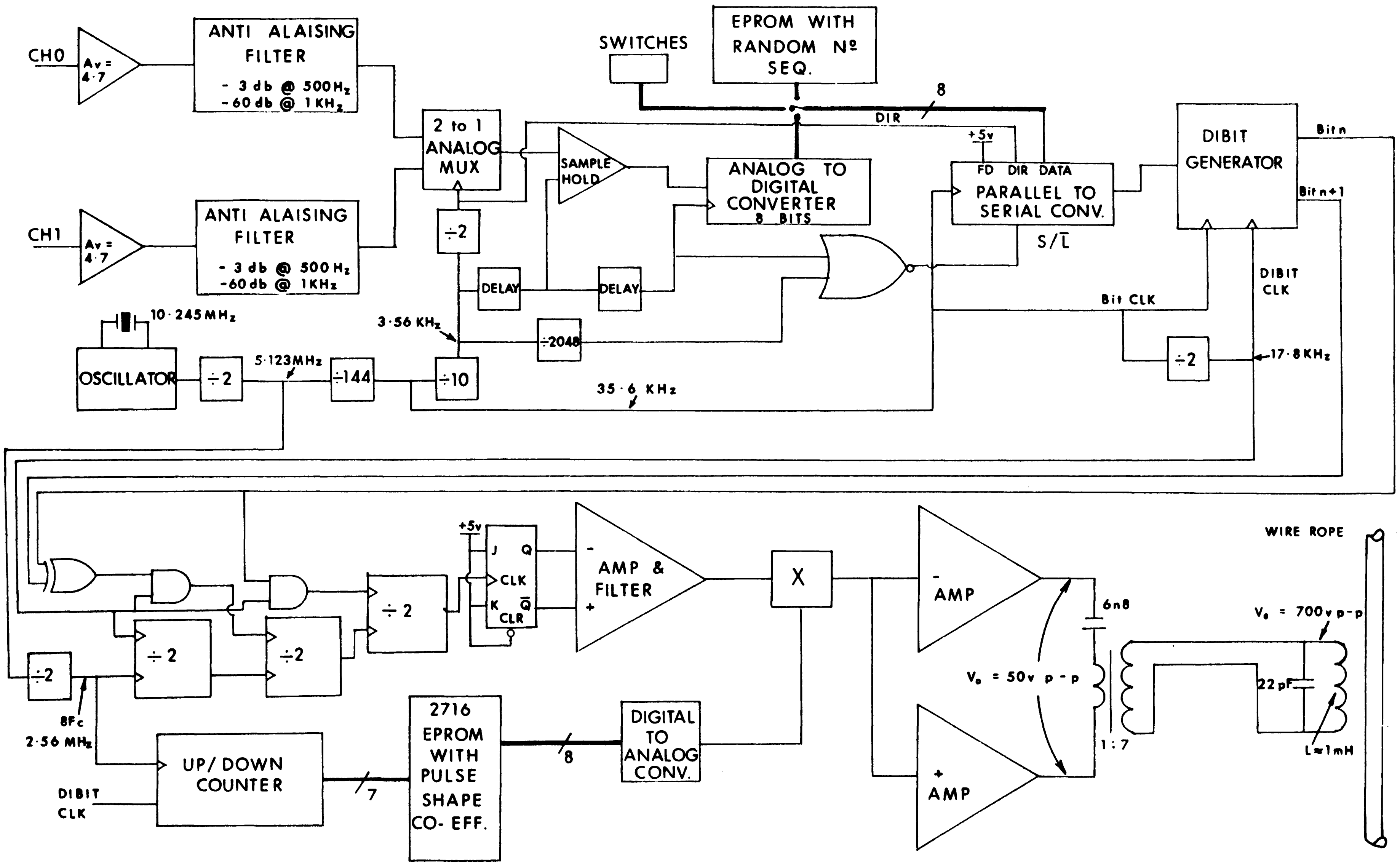

Transmitter Circuit Diagrams: Sheet 1 of 6 Block Diagram

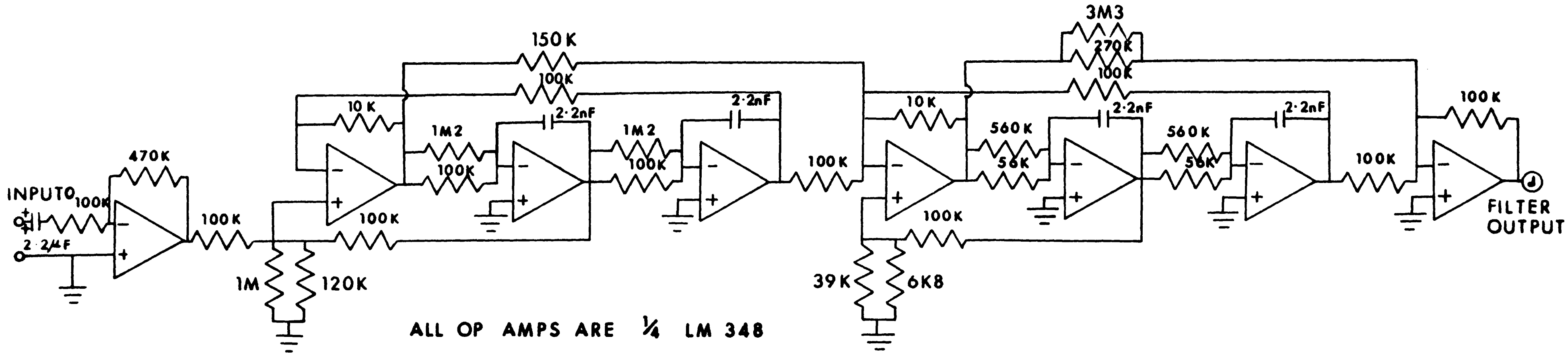

ANTI ALIASING FILTERS

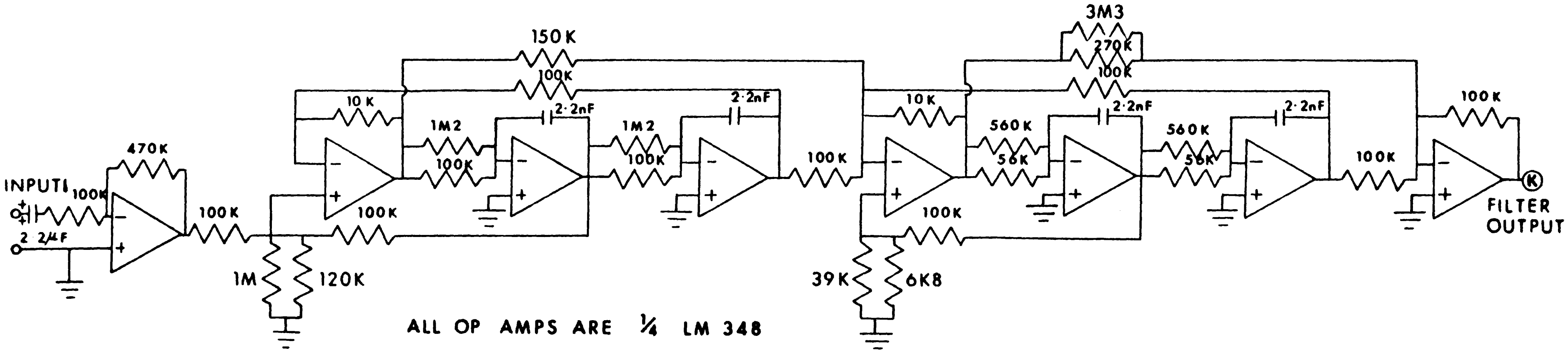

Transmitter Circuit Diagrams: Sheet 2 of 6

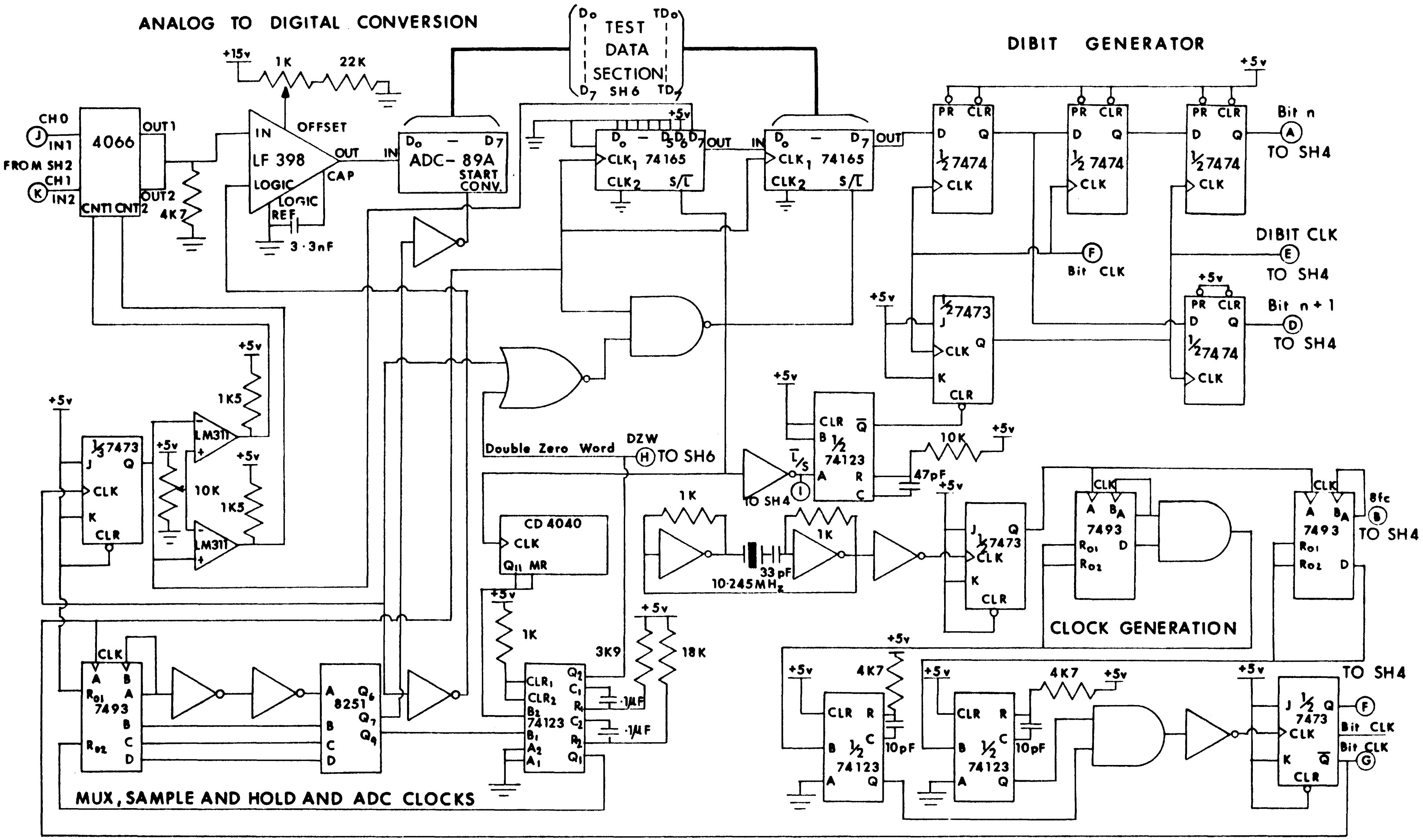

Transmitter Circuit Diagrams: Sheet 3 of 6

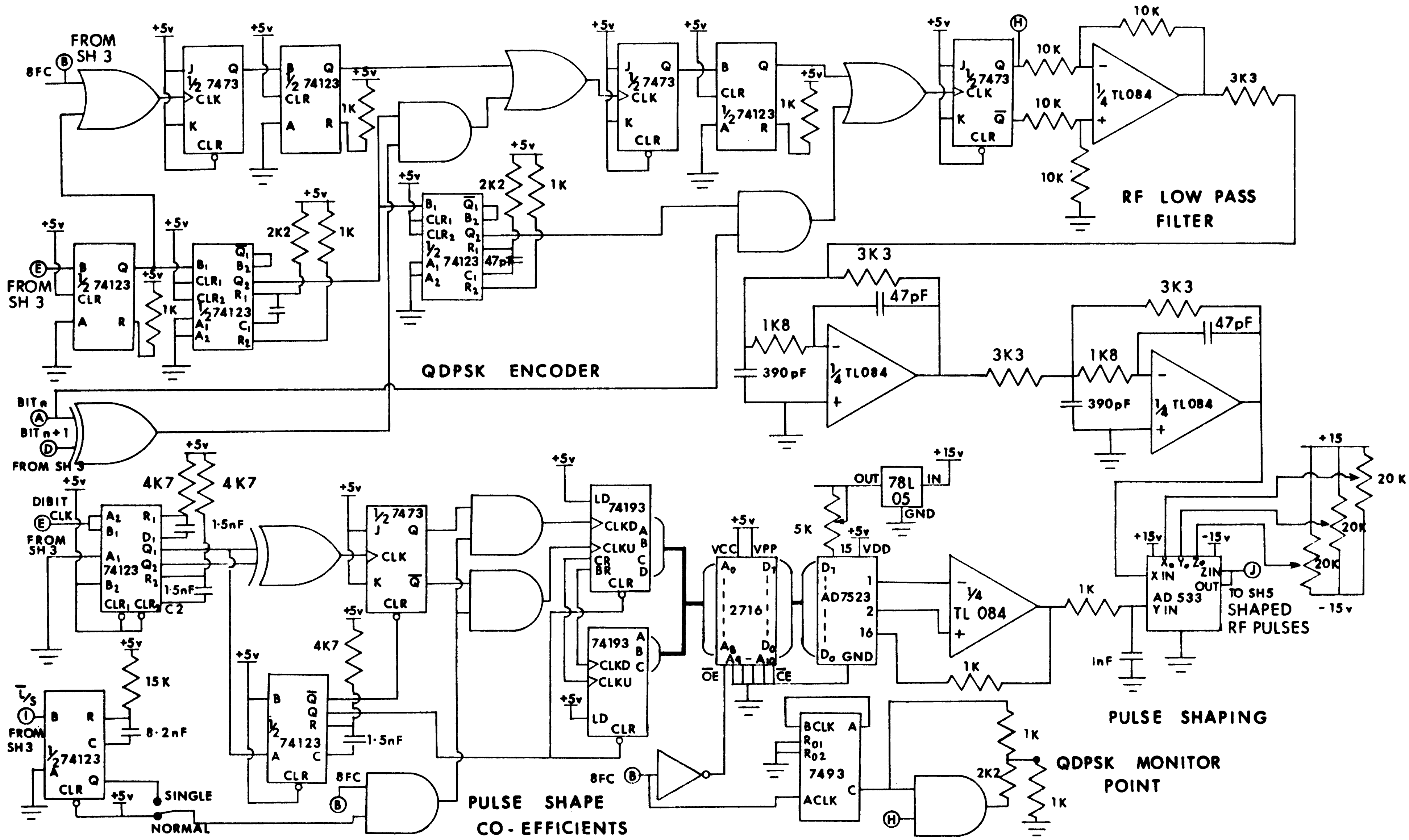

Transmitter Circuit Diagrams: Sheet 4 of 6

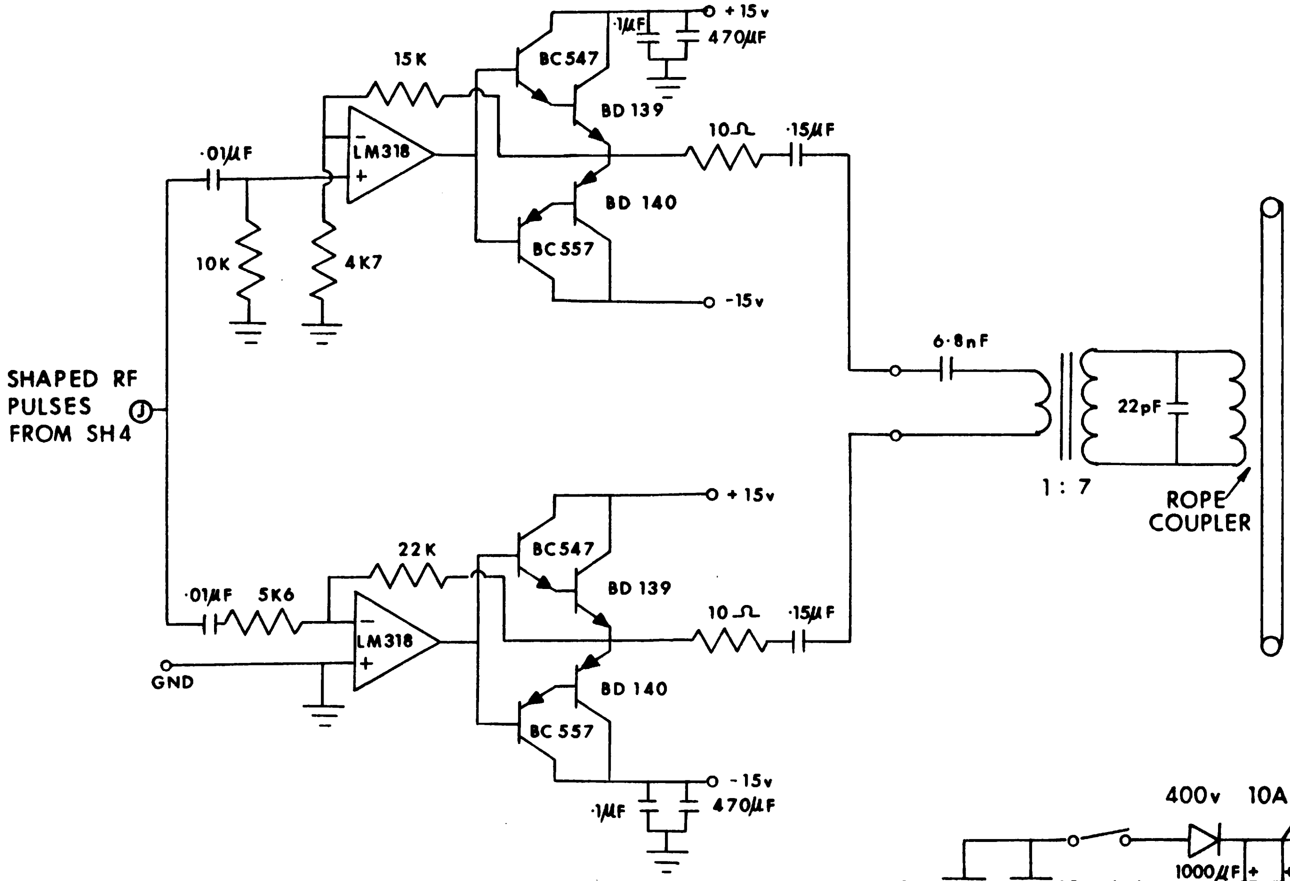

TRANSMITTER AMPLIFIER

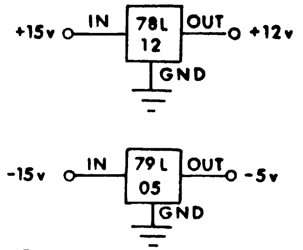

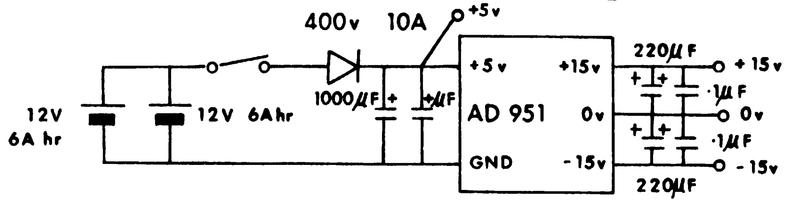

TRANSMITTER POWER SUPPLY

Transmitter Circuit Diagrams: Sheet 5 of 6

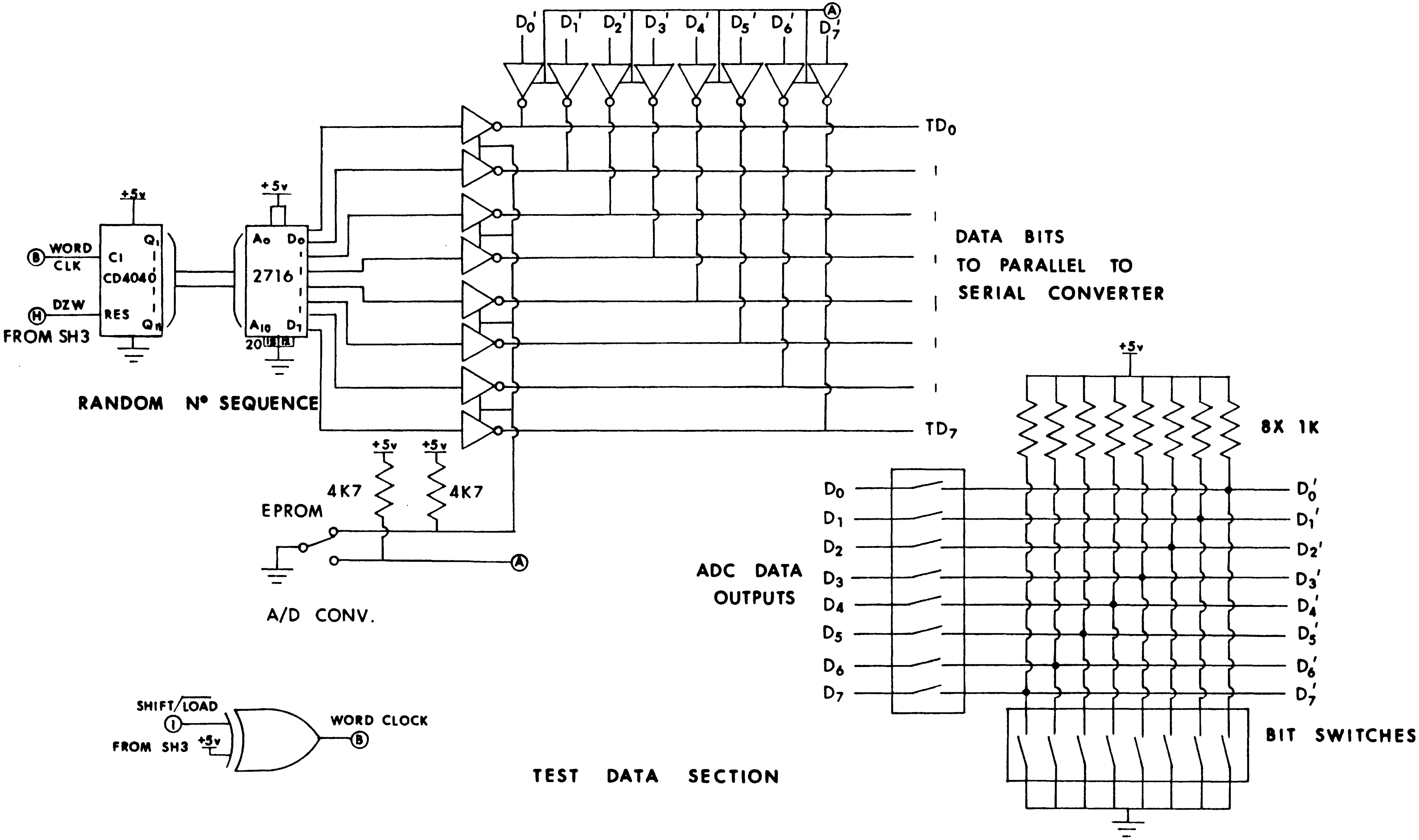

Transmitter Circuit Diagrams: Sheet 6 of 6

TABLE 14

26 Way Connector For Transmitter Boards

PIN NO.	DESCRIPTION	PIN NO.	DESCRIPTION
1	+ 5V	14	Bit 1 to Board 2
2	GND	15	Bit 2 from Board 2
3	Bit Clock (35.52kHz)	16	Bit 2 to Board 2
4	Serial Data (inverted)	17	Bit 3 from Board 2
5	+ 15V	18	Bit 3 to Board 2
6	- 15V	19	Bit 4 from Board 2
7	Double Zero Word Clock	20	Bit 4 to Board 2
8	Shift/Load	21	Bit 5 from Board 2
9	+ 5V	22	Bit 5 to Board 2
10	GND	23	Bit 6 from Board 2
11	Bit 0 (MSB) returned from Board 2	24	Bit 6 to Board 2
12	Bit 0 (MSB) to Board 2	25	Bit 7 from Board 2
13	Bit 1 returned	26	Bit 7 to Board 2

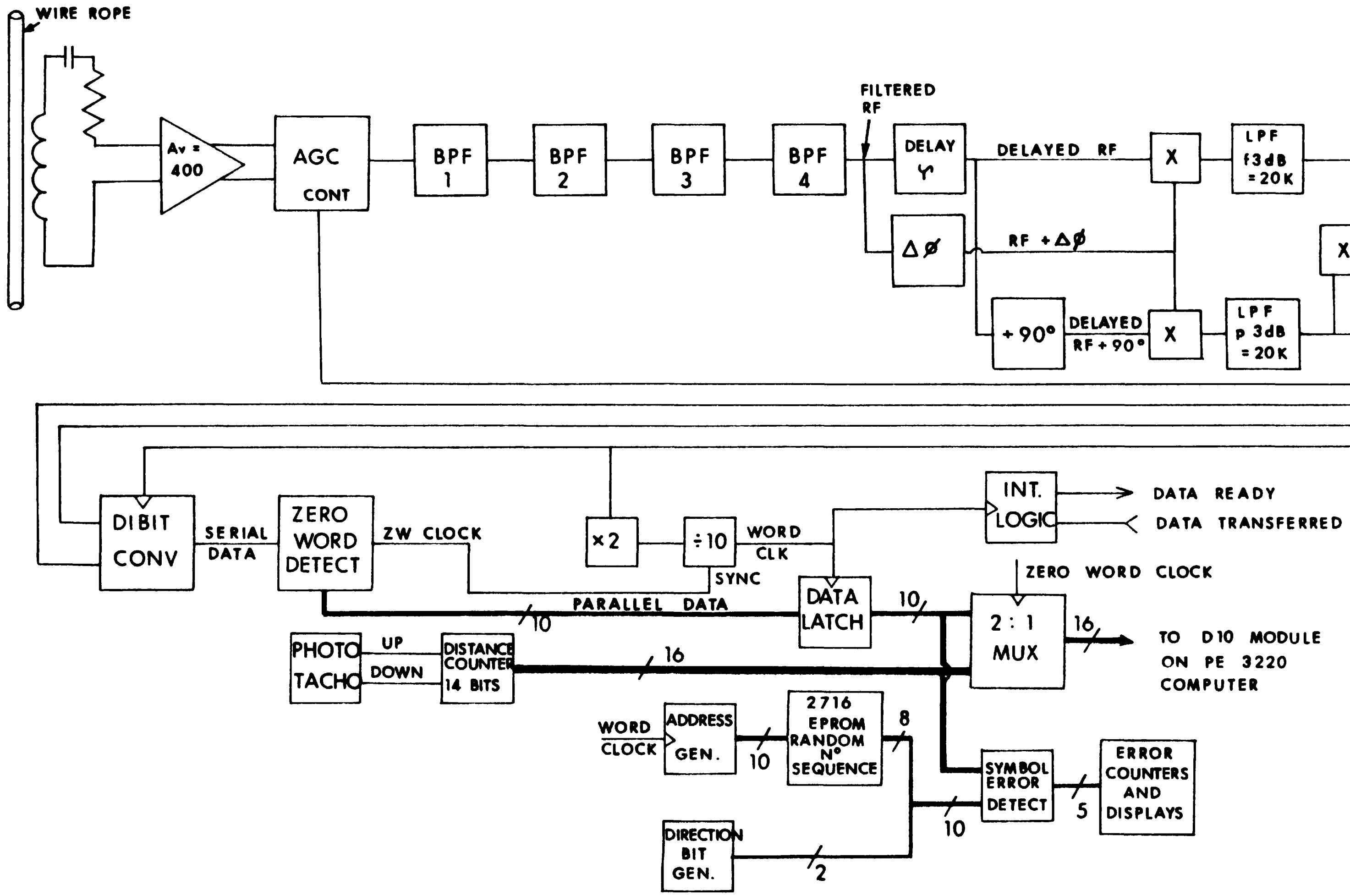

Receiver Circuit Diagrams: Sheet 1 of 7

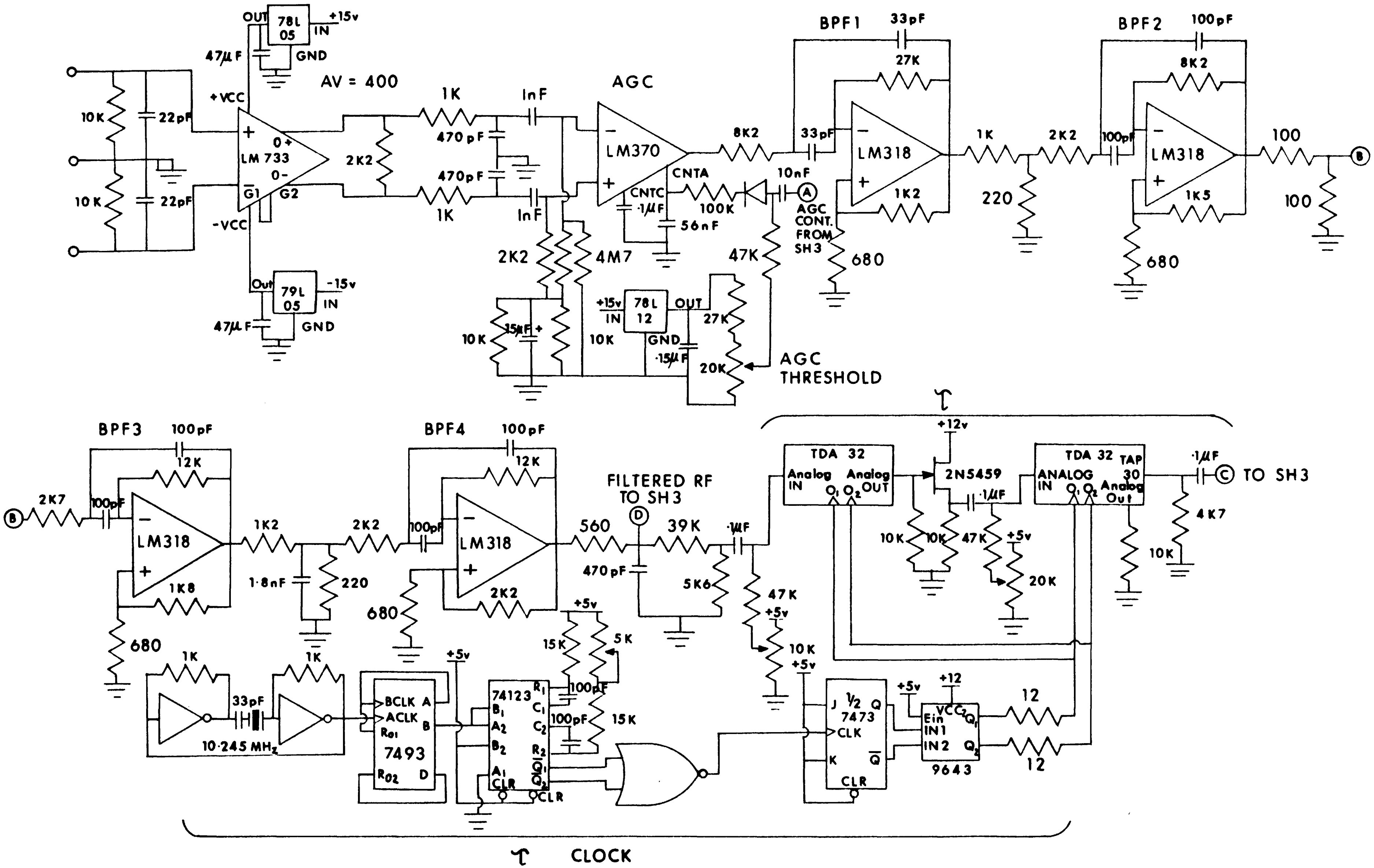

Receiver Circuit Diagrams: Sheet 2 of 7

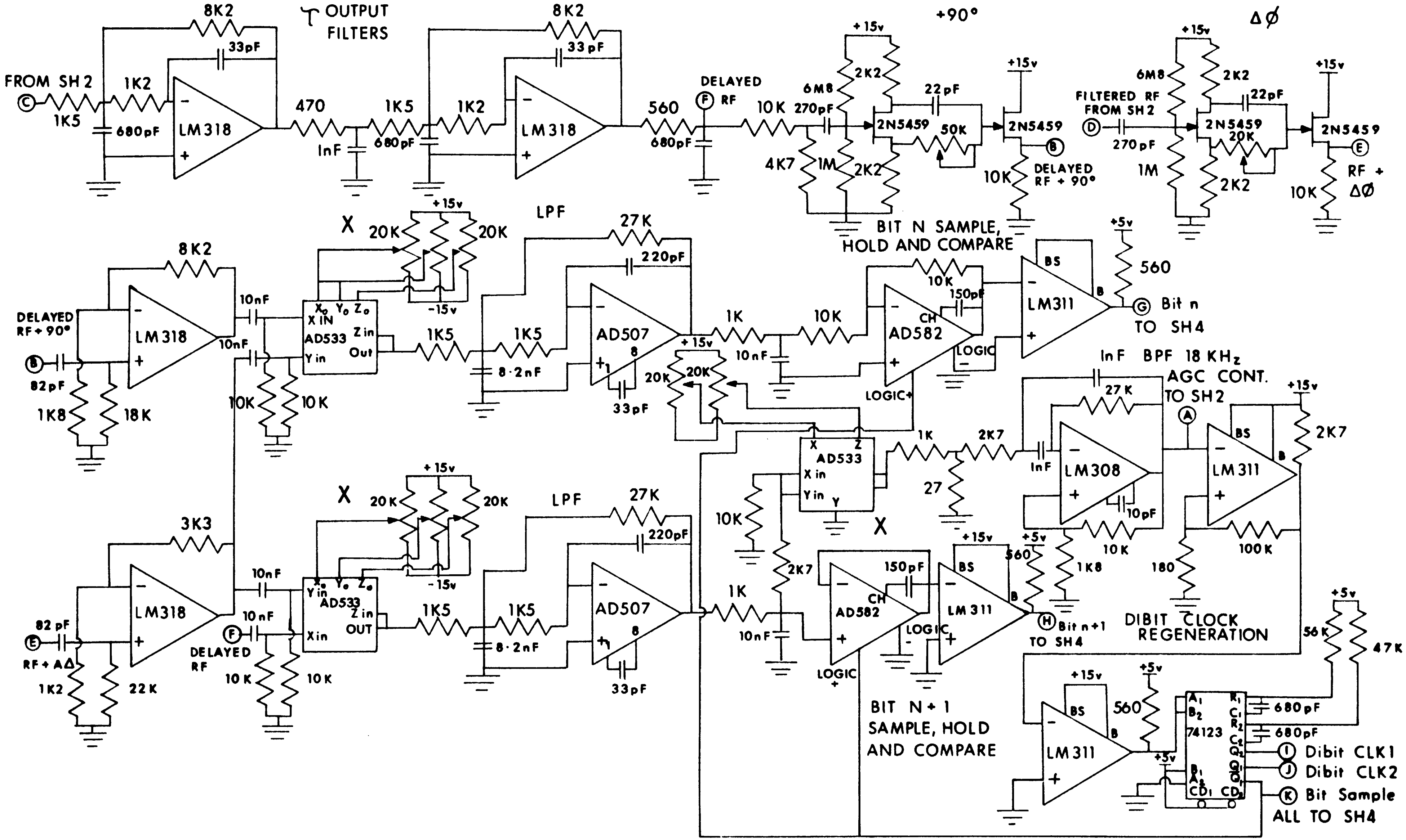

Receiver Circuit Diagrams: Sheet 3 of 7

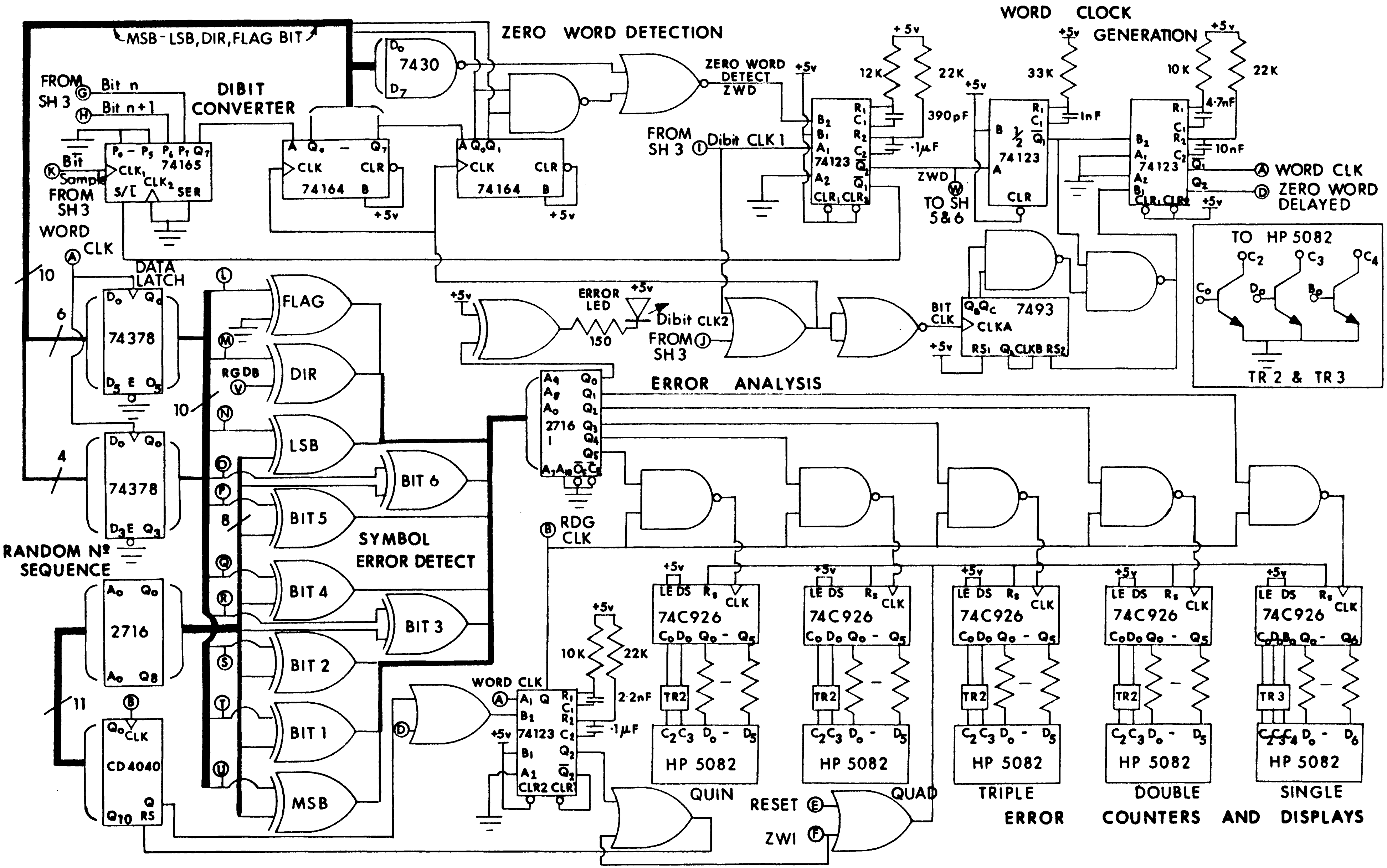

Receiver Circuit Diagrams: Sheet 4 of 7

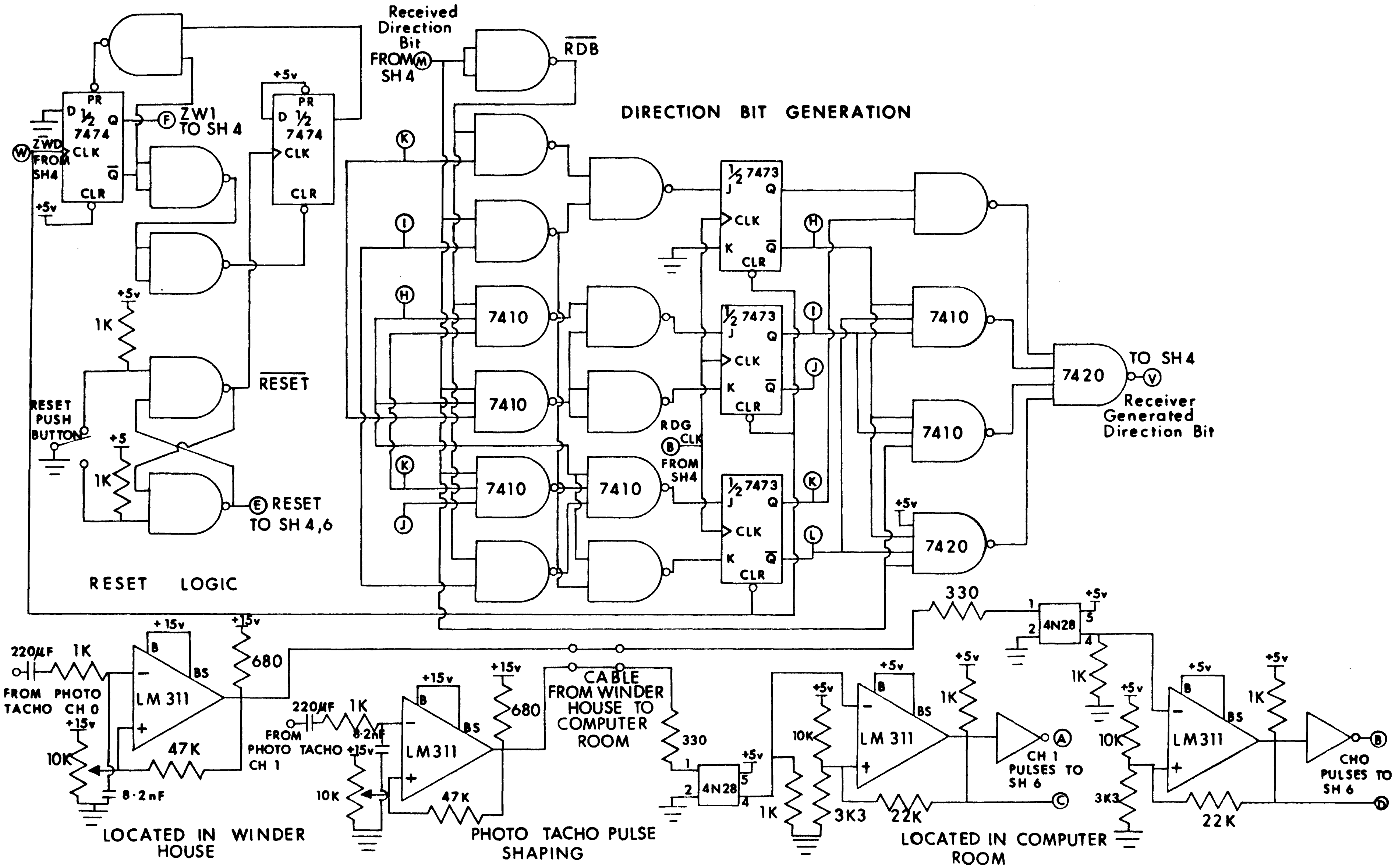

Receiver Circuit Diagrams: Sheet 5 of 7

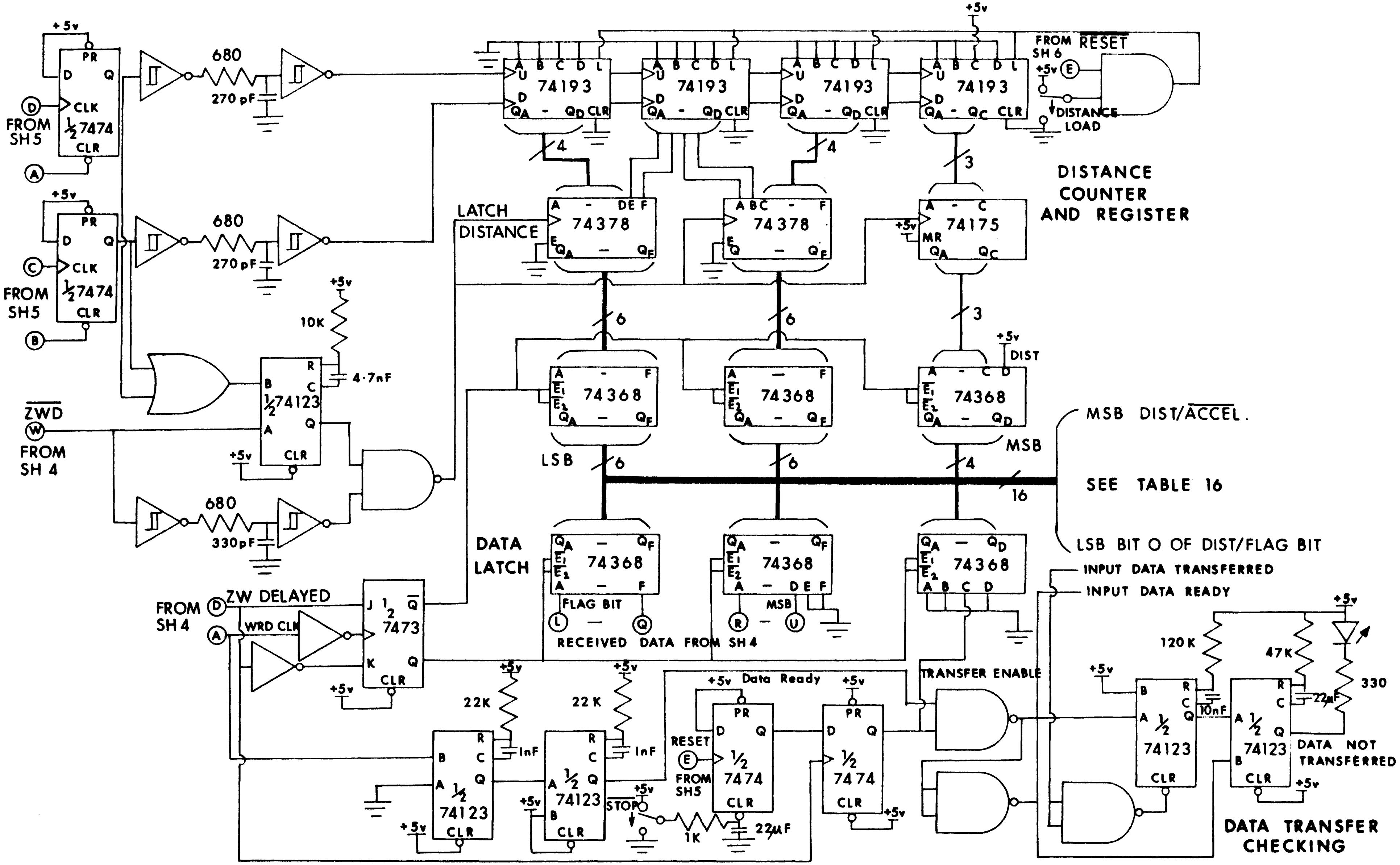

Receiver Circuit Diagrams: Sheet 6 of 7

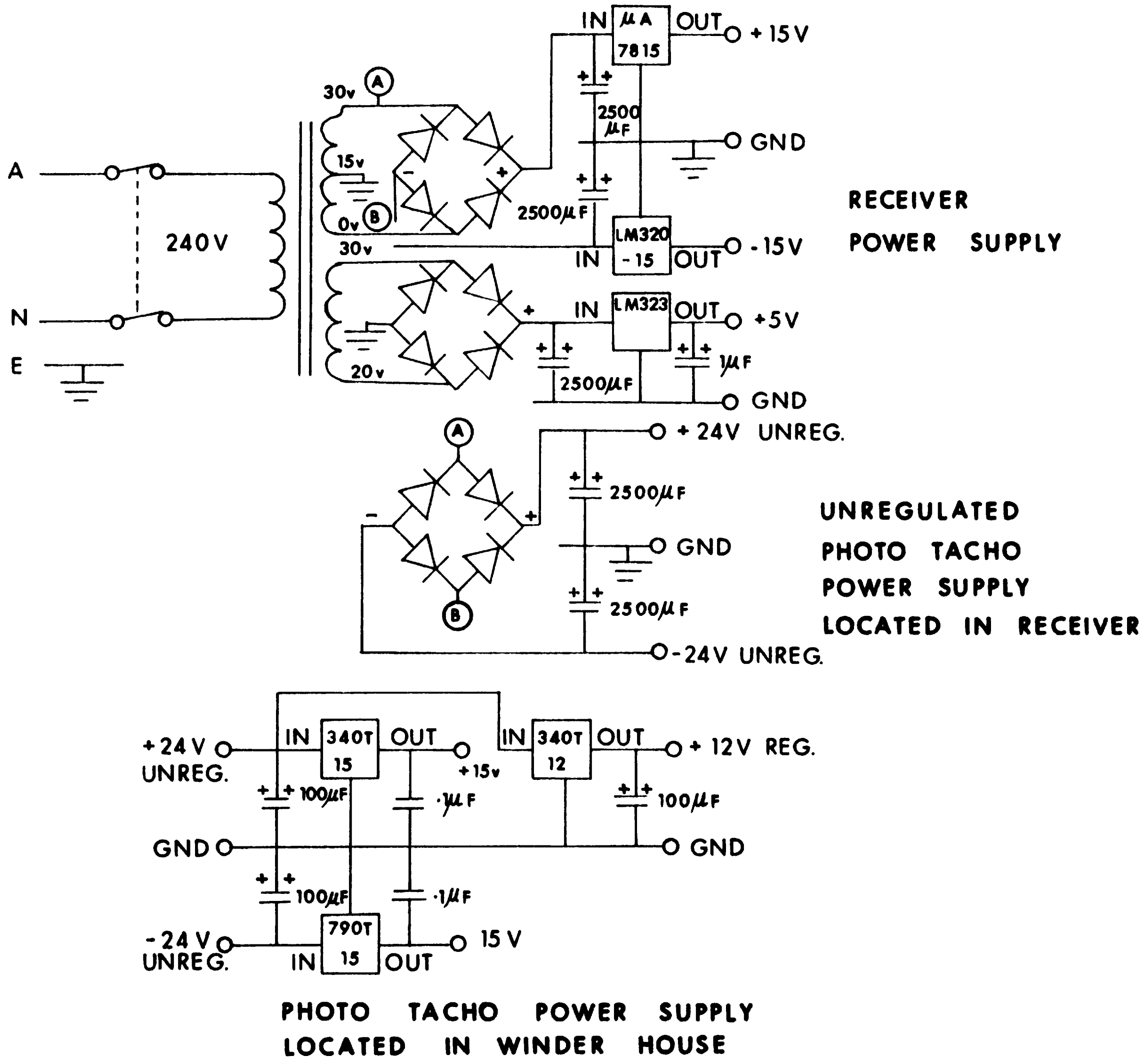

Receiver Circuit Diagrams: Sheet 7 of 7

TABLE 15

26 Way Connector For Receiver Boards

PIN NO.	DESCRIPTION	PIN NO.	DESCRIPTION
1	+ 5V	14	Bit 2
2	GND	15	Bit 1
3	GND	16	MSB Bit 0
4	GND	17	Zero Word Delayed
5	+ 15V	18	Word Clock
6	- 15V	19	Word Clock
7	Flag Bit	20	Zero Word Detect
8	Direction Bit	21	NC
9	LSB Bit 7	22	NC
10	Bit 6	23	NC
11	Bit 5	24	NC
12	Bit 4	25	NC
13	Bit 3	26	NC

TABLE 16

50 Way Connector Between Receiver And P.E. Computer

PIN NO.	DESCRIPTION	PIN NO.	DESCRIPTION
1	Distance/Acceleration	26	GND
2	GND	27	Bit 2 of Dist./Bit 0 of Accel.
3	MSB of Distance/Transfer Bit	28	GND
4	GND	29	Bit 1 of Dist./Dir Bit Accel.
5	Bit 13 of Distance/Low	30	GND
6	GND	31	Bit 0 of Dist./Flag Bit Accel.
7	Bit 12 of Distance/Low	32	GND
8	GND	33	Input Data Transferred
9	Bit 11 of Distance/Low	34	GND
10	GND	35	Input Data Ready
11	Bit 10 of Distance/Low	36	GND
12	GND	37	+ 5V
13	Bit 9 of Dist./MSB of Accel.	38	+ 5V
14	GND	39	+ 5V
15	Bit 8 of Dist./Bit 6 of Accel.	40	+ 5V
16	GND	41	NC
17	Bit 7 of Dist./Bit 5 of Accel.	42	"
18	GND	43	"
19	Bit 6 of Dist./Bit 4 of Accel.	44	"
20	GND	45	"
21	Bit 5 of Dist./Bit 3 of Accel.	46	"
22	GND	47	"
23	Bit 4 of Dist./Bit 2 of Accel.	48	"
24	GND	49	"
25	Bit 3 of Dist./Bit 1 of Accel.	50	NC

APPENDIX 4

APPENDIX 4

DATA SHEETS

These data sheets are included for the sake of completeness and to allow full analysis of the circuit diagrams. Only data sheets for unusual components used in the system are included.

Accelerometer —industrial

CV 100 SERIES

(MODEL 1501)

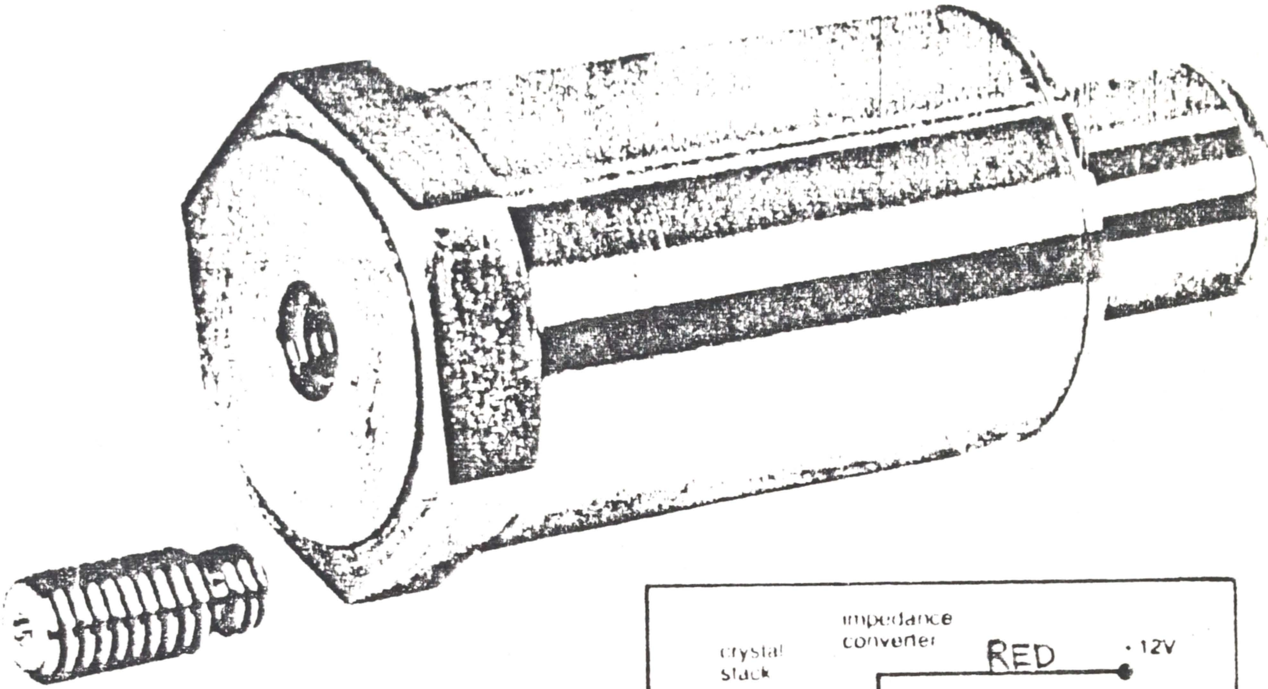

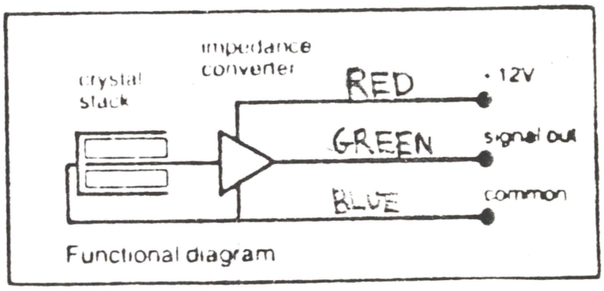

Functional diagram

GENERAL DESCRIPTION

The CV100 Series of Accelerometers has been designed for general industrial use. They are particularly suitable for permanent monitoring on machine bearings.

The crystal stack of the accelerometer is in a double sandwich form and is of the compression type. The crystal stack and its connections are collectively isolated from the stainless steel case. Built into the accelerometer casing is an impedance converter which provides a calibrated output at a level of 100mV-g. The electronic circuitry is encapsulated in an epoxy resin and is capable of withstanding a shock of 1000g-pk. The output is via a Fischer quick release connecter which can if required be supplied with waterproof, heat shrink sleeving.

SPECIFICATION CV 100

FREQUENCY RANGE	5Hz - 7KHz ± 3dB.
VOLTAGE SENSITIVITY	100 mV-pk/g-pk ±4%
DYNAMIC RANGE	Without ZENER BARRIERS .001 - 50 g-pk With ZENER BARRIERS .001 - 30 g-pk
SHOCK LIMIT	10 millisecs half sine 1000 g-pk
AMPLITUDE LINEARITY	.001 - 50 g-pk <± 1%
TRANSVERSE SENSITIVITY	<5%
TEMPERATURE RESPONSE	-25°C to 150°C
ACOUSTIC NOISE RESPONSE	50Hz - 50KHz 140dB less than 0.05g RMS equivalent signal.
MAGNETIC FIELD RESPONSE	Less than .001 g RMS/100 gauss 50-60Hz
OUTPUT	±5 volts (50 g-pk) without ZENER BARRIERS ±3 volts (30 g-pk) with ZENER BARRIERS +5 volts DC off-set Floating. Insulation resistance >50 Megohms to accelerometer case.
HUMIDITY EFFECTS	Cases are sealed Vacuum or 15Kg/Cm2

Note: When fitted in installations where steam, water, oil etc. are present, the output connector is fitted with a heat shrink sleeve to prevent ingress into the connector assembly. Disconnection of the cable assembly takes place at a junction box fitted in a relatively clear, dry position.

POWER SUPPLY	+12v DC
LOAD	Minimum Resistance 10K Ohms Maximum Capacitance 0.5 uf
CONNECTIONS DIMENSIONS & WEIGHTS	Refer to drawings

ORDERING INFORMATION

MODELS ~~CV 100A~~ 1501 Integral 6mm Stud

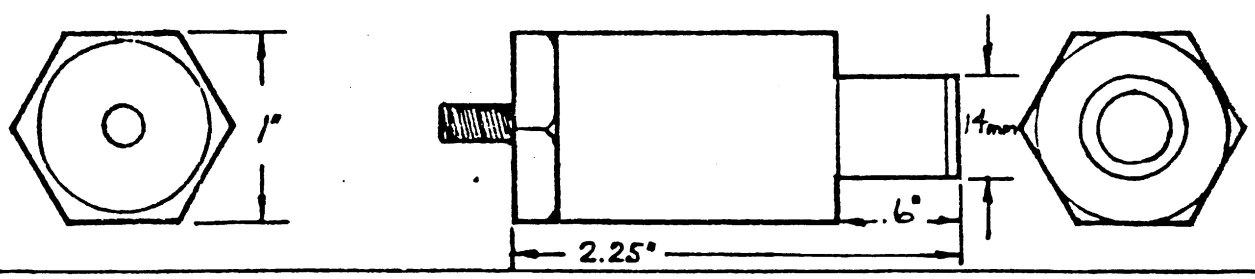

ENVIRONMENTAL EQUIPMENTS LIMITED

Eastheath Avenue
Wokingham
Berkshire, England

Tel: Wokingham 784922 (0734)
Cable: ENVIRON Wokingham
Telex: 847151 Environ Wkgham

DATEL SYSTEMS, INC.

LOW COST, 8 BIT ANALOG TO DIGITAL CONVERTER

MODEL ADC-89A

FEATURES

- Counter Type
- No Adjustments
- Unipolar or Bipolar
- Binary or BCD Coding
- Up to 10,000 Conv./Sec.
- Low Cost

GENERAL DESCRIPTION

Model ADC-89A is a low cost, 8 bit A/D converter using the counter method of conversion. The converter operates by using a digital counter to step the output of the D/A converter until it is equal to the input voltage. At this time the conversion is complete and the 8 bit parallel output data is valid. The simplified operation, small size, and low cost of this converter make it an ideal choice for OEM applications where 8 bit resolution with moderate speed are required.

The ADC-89A is available with either binary or BCD output coding. The binary version operates in both unipolar and bipolar modes with a full scale conversion time of 200 µsec. maximum (5kHz word rate). The BCD version operates in unipolar mode only with a 100 µsec. full scale conversion time (10kHz rate). The conversion time is proportional to the input analog voltage and is, therefore, faster for smaller inputs. No external adjustments are required and 8 bit accuracy with monotonic operation is achieved over the full 0°C to 70°C operating temperature range. The input voltage ranges are 0V to +10V unipolar and -5V to +5V bipolar; unipolar or bipolar operation is determined by the external connection of pin 2.

Outputs include 8 parallel lines of data, end of conversion (status) pulse, and a clock output for external synchronizing and counting applications. Other specifications include full scale temperature coefficient of 50ppm/°C maximum and long term stability of .05% per year. Power requirement is ±15VDC and +5VDC.

The ADC-89A is an improved version of Datel's former model ADC-89. The new model is identical in specifications and pin positions to the previous model except for a small change in input impedance, an added Clock Out pin, and an increase in +5V power supply current.

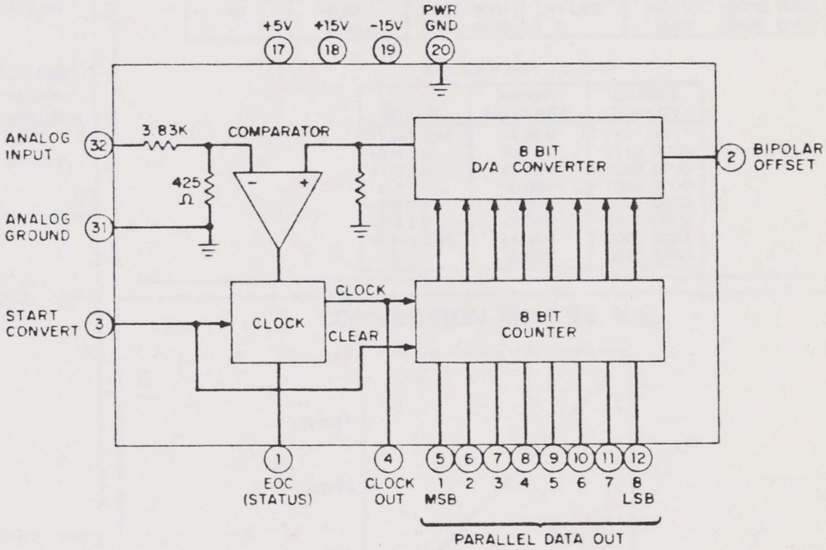

MECHANICAL DIMENSIONS INCHES (MM)

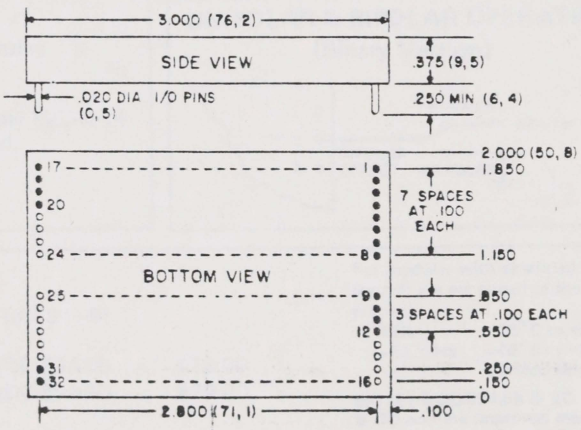

NOTES:
1. OPEN DOTS DESIGNATE OMITTED PINS
2. 0.100 INCH = 2.5mm

INPUT/OUTPUT CONNECTIONS

PIN	FUNCTION
1	E.O.C. (STATUS)
2	BIPOLAR OFFSET
3	START CONVERT
4	CLOCK OUT
5	BIT 1 OUT (MSB)
6	BIT 2 OUT
7	BIT 3 OUT
8	BIT 4 OUT
9	BIT 5 OUT
10	BIT 6 OUT
11	BIT 7 OUT
12	BIT 8 OUT (LSB)
17	+5V POWER IN
18	+15V POWER IN
19	-15V POWER IN
20	POWER GROUND
31	ANALOG GROUND
32	ANALOG IN

SPECIFICATIONS, ADC-89A
(Typical at 25°C, ±15V & +5V supplies unless otherwise indicated)

INPUTS

Analog Input Range	0V to +10V FS or ± 5V FS
Input Impedance	4.25K ohms, ± 15 ohms
Input Overvoltage, no damage	± 20V
Start Conversion	2V min. to 5.5V max. positive pulse with duration of 150 nsec. min. Rise and fall times <500 nsec. Logic "1" resets converter. Logic "0" initiates conversion. Loading: 4 TTL loads

OUTPUTS

Parallel Output Data	8 parallel lines of data held until next conversion command. Vout ("0") ≤ +0.8V. Vout ("1") ≥ +2.4V. Each output capable of driving up to 6 TTL loads.
Coding, Unipolar Operation	Straight Binary, positive true. Two Digit BCD, positive true
Bipolar Operation	Offset Binary, positive true (BCD version does not operate in bipolar mode).
End of Conversion (E.O.C.)	Conversion Status signal. Vout ("0") ≤+0.8V indicates conversion completed. Vout ("1") ≥ +2.4V during reset and conversion period. Loading: 8 TTL loads.
Clock Output	Internal clock pulse train of 320 nsec. 0 to +5V pulses gated on during conversion time. Each negative transition occuring after the rise of the EOE indicates one count (255 FS. binary, 99 FS BCD). Loading: 8 TTL loads.

PERFORMANCE

Resolution	8 Bits (1 part in 256) for Binary. 2 Digits (1 part in 100) for BCD.
Accuracy at 25°C	± 0.2% of FS ± 1/2 LSB
Linearity	± 1/2 LSB
Temp. Coeff. of Gain	± 50ppm/°C max.
Temp. Coeff. of Offset, Unipolar	± 50 μV/°C max.
Bipolar	± 50ppm of FS/°C max.
Long Term Stability	± .05%/year
Power Supply Rejection	± .07% of FS/% supply
Conversion Time	200 μsec. max. (Binary) 100 μsec. max. (BCD)

POWER REQUIREMENT	+15VDC ± 0.25V @ 25mA max. -15VDC ± 0.25V @ 15mA max. + 5VDC ± 0.25V @ 90mA max.

PHYSICAL-ENVIRONMENTAL

Operating Temp. Range	0°C to 70°C
Storage Temp. Range	-55°C to +85°C
Relative Humidity	Up to 100% non-condensing
Case Size	2 x 3 x 0.375 inches (50,8 x 76,2 x 9,5mm)
Case Material	Black diallyl phthalate per MIL-M-14
Pins	.020" round, gold plated, .250" long min.
Weight	3 oz. max. (85g.)

TIMING DIAGRAM FOR ADC-89A8B Output: 1000 0000

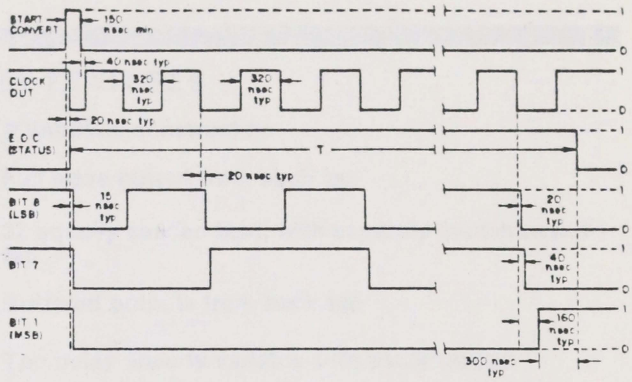

NOTE: If V_{IN} is less than -FS or greater than +FS, the output code will be 0000 0000

T = 200 μsec max. for binary coding
T = 100 μsec. max. for BCD coding

OUTPUT CODING

UNIPOLAR (0 TO +10V)

SCALE	INPUT VOLTAGE	STRAIGHT BINARY
+FS-1 LSB	+9.96V	1111 1111
+7/8 FS	+8.75V	1110 0000
+3/4 FS	+7.50V	1100 0000
+1/2 FS	+5.00V	1000 0000
+1/4 FS	+2.50V	0100 0000
+1 LSB	+0.04V	0000 0001
0	0.00V	0000 0000

SCALE	INPUT VOLTAGE	2 DIGIT BCD
+FS-LSD	+9.9V	1001 1001
+.87 FS	+8.7V	1000 0111
+3/4 FS	+7.5V	0111 0101
+1/2 FS	+5.0V	0101 0000
+1/4 FS	+2.5V	0010 0101
+1 LSD	+0.1V	0000 0001
0	0.0V	0000 0000

BIPOLAR (-5V TO +5V)

SCALE	INPUT VOLTAGE	OFFSET BINARY
+FS-1 LSB	+4.96V	1111 1111
+3/4 FS	+3.75V	1110 0000
+1/2 FS	+2.50V	1100 0000
0	0.00V	1000 0000
-1/2 FS	-2.50V	0100 0000
-3/4 FS	-3.75V	0010 0000
-FS+1 LSB	-4.96V	0000 0001
-FS	-5.00V	0000 0000

CONVERSION TIME VS. V_{IN}

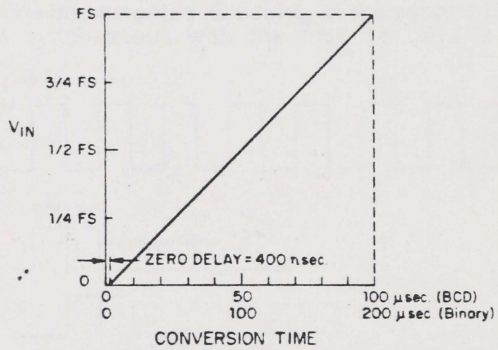

UNIPOLAR & BIPOLAR OPERATION
(Binary Version)

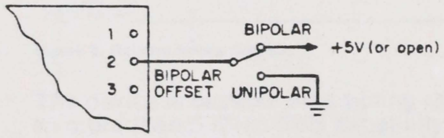

For bipolar operation Pin 2 is connected to the +5V supply or left open. This turns on the internal offset current. For unipolar operation Pin 2 is connected to ground, turning off the internal offset current. The BCD output model (ADC-89A8D) has no internal connection to Pin 2 and therefore Pin 2 need not be connected externally.

ORDERING INFORMATION

ADC-89A

NO. OF BITS & CODING
8B = 8 BINARY BITS
8D = 2 DIGIT BCD

PRICES (1-9)

ADC-89A8B	\$79.00
ADC-89A8D	\$79.00

For modules with extended temperature range operation the following suffixes are added to the model number. Consult factory for pricing.

-EX	-25°C to +85°C operation
-EXX-HS	-55°C to +85°C operation with hermetically sealed semiconductor components.

NOTE: ADC-89A8B & 8D replace former Datel models ADC-89 8B & 8D and are improved models of these units respectively. The only difference from the previous models is the additional output Clock Out (pin 4), the change in input impedance from 5K ohms to 4.25K ohms, and the change in 5V supply current from 75 mA typical to 90 mA maximum.

THE ADC-89A8B & ADC-89A8D ARE COVERED UNDER GSA CONTRACT

DATEL SYSTEMS, INC. 11 CABOT BOULEVARD, MANSFIELD, MA 02048 / TEL. (617)828-8000 / (617)339-9341 / TWX 710-346-1953 / TLX 951340
Santa Ana, (714)835-2751, (L.A.) (213)933-7256 • Sunnyvale, CA (408)733-2424 • Gaithersburg, MD (301)840-9490 • Houston, (713)932-1130 • Dallas, TX (214)241-0651
OVERSEAS: DATEL (UK) LTD—TEL: ANDOVER (0264)51055 • DATEL SYSTEMS SARL 620-06-74 • DATELEK SYSTEMS GmbH (089)77-60-95

EG&G RETICON TAD-32 TAPPED ANALOG DELAY

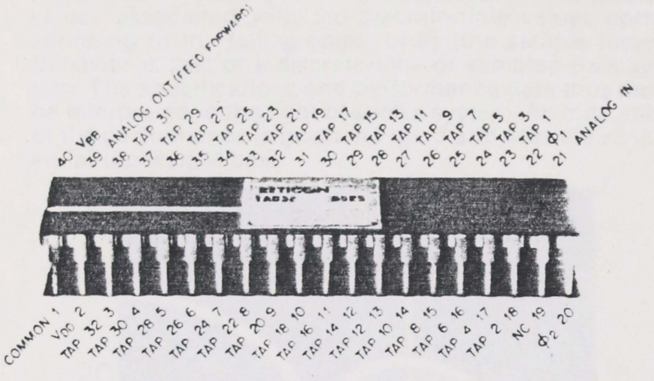

The Reticon TAD-32 is a tapped analog delay line fabricated with the most advanced n-channel silicon-gate integrated-circuit technology. It consists of a charge-transfer device with 32 taps equally spaced one sample-time apart along the device. It is designed specifically for use in the realization of transversal filters, but it likewise is applicable to recursive or other filter types. Typical applications include: low pass filters, band pass filters, matched filters, phase equalizers, phase shifters, tone generators, function generators, correlators, and simple tapped delays.

KEY FEATURES

- Monolithic construction
- Full wave output from each tap
- 32 equally spaced taps, with separate feed-forward tap
- Buffered outputs from each tap
- Tap delay linearly variable with clock period
- Sampling rates to 5 MHz
- 40 db passband-to-stopband ratio (as a filter)
- 60 db dynamic range
- Simple I/O and clock circuit
- Low power dissipation
- 40-pin dual-in-line package

GENERAL DESCRIPTION

TAD-32 is a 32-stage charge-transfer device which permits the storage of analog signals with recovery of the signals at multiple separate outputs at successive delay times later. The taps on each stage are brought to the outside through buffer amplifiers. Each buffer amplifier output appears as a source follower, thus permitting variable loading of the taps in order to create various tap-weight functions. The taps are spaced one sample time apart along the delay. An additional special feed-forward output tap is provided so that multiple devices may be cascaded without causing discontinuity in the spacing of the taps from one device to the next. With this arrangement, timing integrity is maintained. The ability to cascade devices permits the user to build processors (such as transversal filters) with more than 32 taps.

DEVICE OPERATION

The equivalent circuit is shown in Fig. 1. Samples are set up on the initial storage node during the time period when the $Ø_1$ clock waveform is at its high (positive) level. When $Ø_1$ drops, the sample value is frozen and the simultaneous rise of $Ø_2$ permits exchange of charge with the tap-1 node; similarly for other nodes. The sample values thus first appear at the various tap outputs when $Ø_2$ rises. When $Ø_2$ falls and $Ø_1$ rises, the charge state is transferred to the second node for each tap. The paralleling of the buffer outputs thus maintains the output value at the tap for both halves of the clock period. The resulting output is a full-wave (or full-period) output. Further, there is one sample time delay between the samples as they appear at successive output taps. The last node supplies a feed-forward tap at the proper time to provide the set-up signal for another, series-connected TAD-32, so that multiple-section processors with more than 32 taps can be implemented. Clocking of the second device must be synchronous with the first, i.e., $Ø_{1A} = Ø_{1B}$.

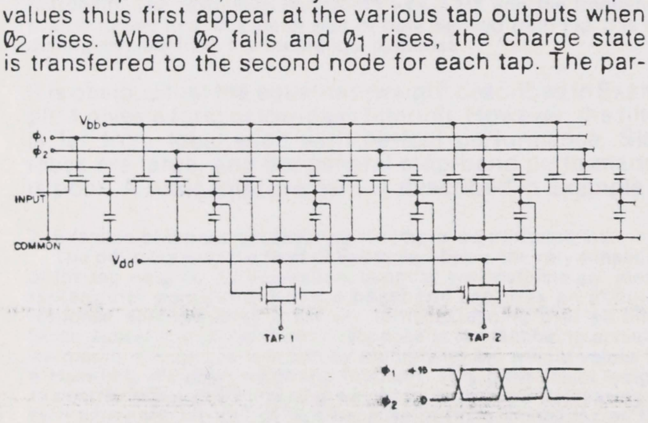

Figure 1. A tapped analog delay line made using metal-oxide-silicon integrated circuit technology.

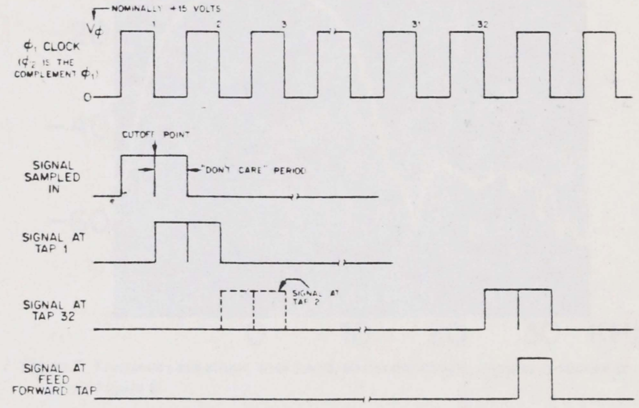

Figure 2. Relative timing diagram.

The device is capable of sampling rates from below 1KHz to more than 5 MHz. This capability permits the translation of a given filter characteristic over a range of more than three orders of magnitude in frequency simply by varying the clock rate. A two-phase complementary square-wave clock with amplitude in the range of 12 to 15 volts is required to drive the device. The clock phases are positive square waves, as shown in the inset of Fig. 1 and in more detail in Fig. 2. The clocks drive the nodes positive, thus providing a positive output with reference to ground at each tap. The output from each tap is a full-wave or boxcar output, as discussed above; no additional filtering is necessary before summing with the desired weights. The summing amplifiers can combine the summing and filtering functions.

EG&G RETICON • 345 POTRERO AVENUE • SUNNYVALE, CALIFORNIA 94086
TELEPHONE: (408) 738-4266 • TWX 910-339-9343

FUNCTIONAL PERFORMANCE

The TAD-32 functions as a discrete-time processor. Time is quantized, but signal amplitudes retain the analog values associated with the discrete-time values corresponding to the falling edges of $\emptyset_1$ (the sample times). Behavior is that of a discrete-time or sampled-data system. The specifications and performance data thus must be interpreted in the light of such a system. An indication of the performance is given in Figs. 3 and 4 for the simple equal-tap-weight case.

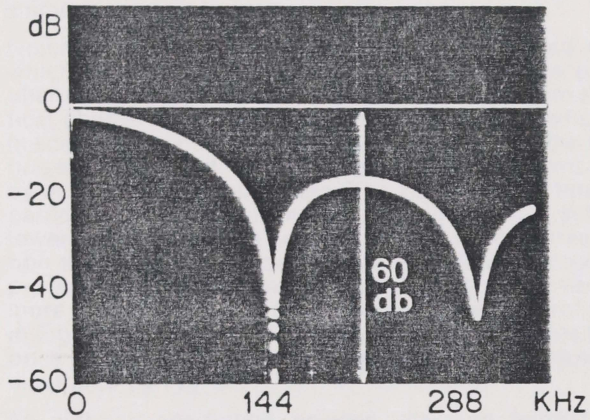

Figure 3. Frequency spectrum for equal-weight FIR filter; 3 MHz clock frequency, 3 Hz resolution bandwidth, 360 KHz scan. (Note the 60-db dynamic range as shown by the null depth.)

1. Example of Performance

The simplest form of a low-pass filter has all taps weighted equally and summed. For this equal-weight transversal filter, the frequency response is as shown in Fig. 3 above. The impulse response, which bears a unique relationship to the frequency response, is shown in Fig. 4. Filter design may be based on a desired frequency response, but generally proceeds by first finding the impulse response corresponding to the frequency response.

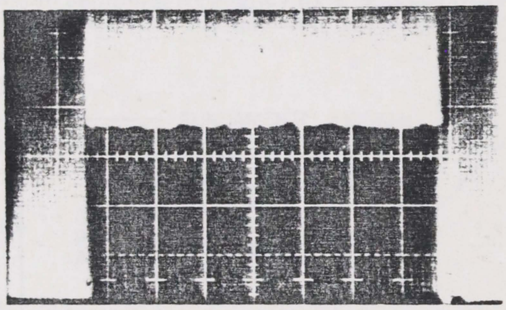

Figure 4. Oscillogram of equal-weight impulse response.

For the case of Fig. 4, a single (unit-weight) sample is provided as input. This sample then appears once at each tap output, then moves to the next, and finally out of the system. Thus, the summed tap outputs is a string of 32 successive unit-amplitude segments as in Fig. 4. The frequency response for this case is ideally $\sin(32 \pi f_S/f_C)/\sin(\pi f_S/f_C)$, where f_S is the signal frequency and f_C the sample frequency. The spectrum of Fig. 3 shows this pattern with a 60-db null depth. The resolution bandwidth was 3 Hz and the frequency scan 0 to 360 KHz. A careful plot of data derived from Fig. 3 is indistinguishable from the theoretical response.

It is obvious that the equal-tap-weight described in Example 1 gives a form of low-pass filtering. However, the filter is far from ideal even with perfect performance. Side lobes are large, and the general stop-band performance is poor. A basic improvement is described in Example 2.

2. Example of tap-weight tailoring for improved performance

The difficulty with the filter of Example 1 lies in the very simplicity of the tap weights. As illustration, suppose we postulate an "ideal" rectangular passband. Such a passband requires an impulse response approximating a sin x/x form, extending over all time. Since, however, such an "ideal" response is impractical to achieve, we modify the sin x/x function by multiplying tap weight values by a Hamming window[1] weighting function. This gives major weight to central taps and diminishing weight to outer taps, decreasing to zero where we run out of taps because of finite limitations on the possible number. Such a weighting, for 16 taps between zero crossings of the weighted sin x/x function, is shown in Fig. 5 as a calculat-

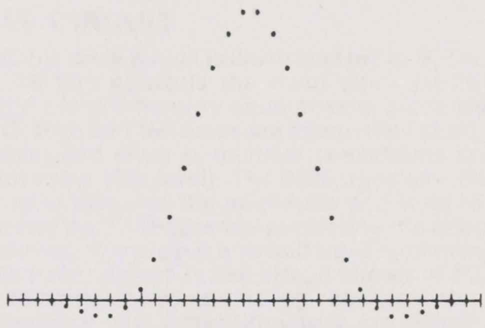

Figure 5. Oscilloscope overlay for Hamming-windowed sin x/x impulse response, 16 taps between zero crossings.,

ed oscilloscope overlay. An actual measured impulse response corresponding to this weighting is shown in Fig. 6, and the frequency response, measured with a spectrum analyzer of 1 KHz resolution

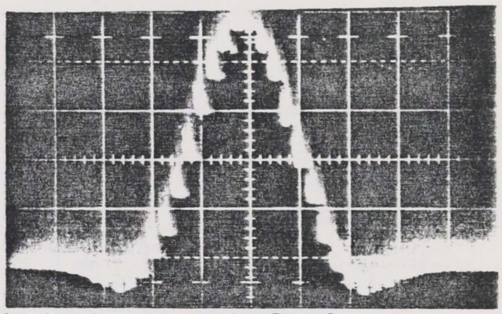

Figure 6. Actual impulse response matching Figure 5.

bandwidth, is shown in Fig. 7. Further details of the measurements and design procedure may be found in Refs. 1 and 2. For Figs. 6 and 7, tap weights were initially selected to 1%, then the major taps slightly altered by simply adjusting the tap weights until the actual output best approximates the desired pattern overlaid on the face of the oscilloscope (see Fig. 5).

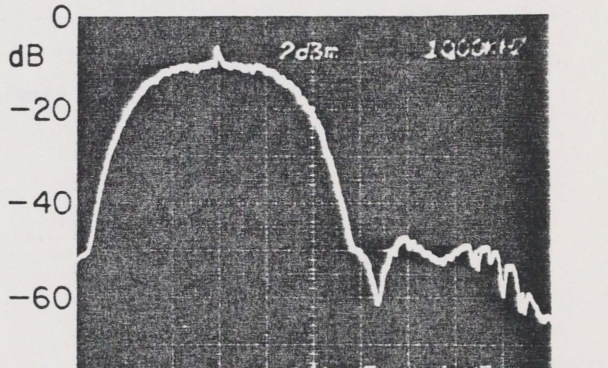

Figure 7. Frequency spectrum, wide band, corresponding to impulse response of Figure 6.

DYNAMIC RANGE

The usable dynamic range normally exceeds 60 db, as shown in Figs. 3 and 8. The data were taken on a spectrum analyzer, which provided the required filtering against clock noise, while retaining any spurious or harmonic responses, as well as showing the noise floor. In any normal application, adequate input and output filtering are an integral part of the design. The input filter is required to prevent aliasing responses, the output filter to separate base-band components from the clock-frequency components (and harmonics). The latter also serves to smooth the full-period boxcar variation of the individual or summed outputs so as to recover the base-band components. The dynamic-range measurements of Fig. 8 are applicable to the low-pass filters of the examples.

LINEARITY, DISTORTION, AND NOISE

These attributes of the device give supplemental measures of its performance. For small signals, the relationship between input and output is highly linear. As the signal amplitude increases, slight departure from linearity occurs. Ultimately, an overload limit is reached where a rapid onset of clipping distortion accompanies any further signal increase. The rapid rise of distortion with excessively high signal level is indicated by the data of Fig. 8. The linearity and distortion data are obtained from single-tap measurements.

Noise is of two general types: (a) clock-related noise which can largely be eliminated by appropriate output filtering, and (b) random noise, which arises from statistical charge variations, resistance in transfer paths, and miscellaneous other sources. Without filtering, the clock noise is dominant, but this noise is largely removable by appropriate output filters. The residue after filtering, particularly that within the desired signal band, sets the lower signal limit. On a broadband oscilloscope presentation the tangential noise is more than 40 db below a 4V p-p reference signal. In a 3 KHz filter band, the noise is more than 60 db below the reference signal, as indicated in Fig. 8. This figure shows various measurements taken on a single-tap basis; multiple-tap performance is illustrated by Fig. 3.

As with all solid-state devices, elevated temperature increases background current and hence increases noise. It also modifies slightly the desired bias point, particularly at low clock frequencies where delay is maximum. But because there are only 64 charge transfers per device, the effects are minimal. Performance at very low clocking frequencies is most affected by elevated temperature because of the increased discharging effect of the leakage (background) current. Increasing the temperature increases the leakage and thus increases the minimum sampling frequency by a factor of two for every 7°C increase above normal room temperature.

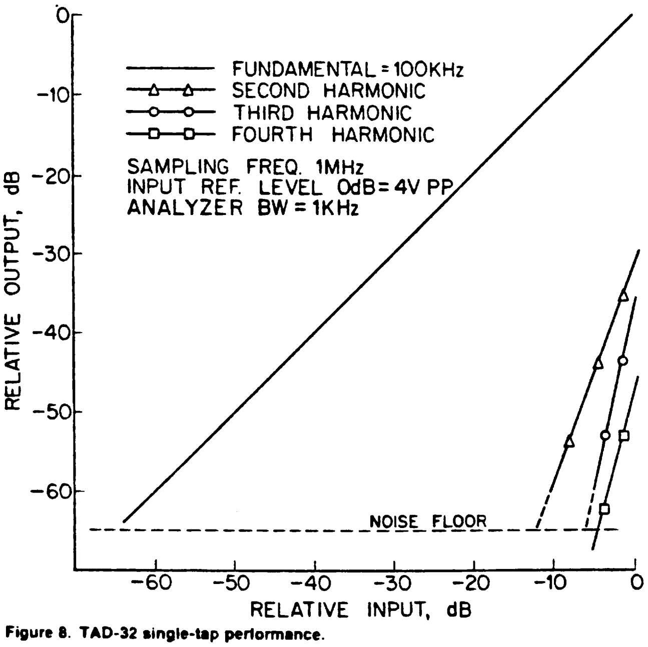

Figure 8. TAD-32 single-tap performance.

FREQUENCY RESPONSE

It should be remembered that the TAD-32 is a sampled-data system. Input signals may be successfully sampled at rates up to 5 MHz. Low-frequency signals are sampled many times per cycle and reproduced at the output without loss. High frequency signals when sampled and reestablished are subject to a $\sin(\pi f_S/f_C)/(\pi f_S/f_C)$ roll off, characteristic of sampled data systems. The device itself introduces negligible attenuation.

DRIVE CIRCUIT

A suitable drive circuit is illustrated in Fig. 9. The Schottky TTL flip-flop converts the input clock (at $2f_c$) into the desired complementary square-wave clock signals at Q and $\overline{Q}$. Rise and fall times are adequately short (less than 20 nsec) and skew is minimal (waveforms cross at the approximate 50% level). The 0026 translator (National or Motorola) converts the amplitude and level to those required by the TAD-32 while preserving the integrity of the waveforms. The output bias and signal summing arrangements have evolved to the circuit shown in Fig. 9 as the best compromise to conflicting requirements. For equal tap weights, the potentiometers are offset by equal amounts (i.e., resistor values to the + line are all equal, as are the complementary values to the - line; a centered potentiometer gives zero tap weight); for other filter arrangements, the ratio of the resistances determines the tap weight. The TC-32A Evaluation Circuit Card incorporates the test circuit shown in Figure 9.

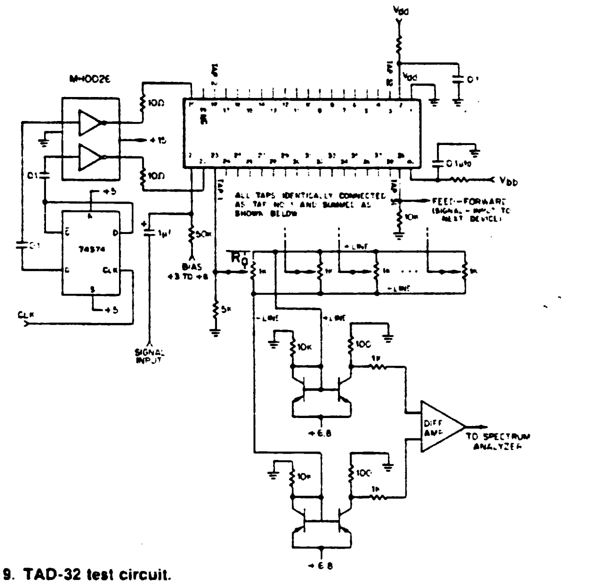

Figure 9. TAD-32 test circuit.

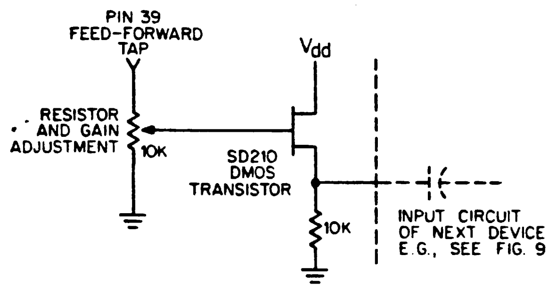

Figure 10. Suggested interface for serial operation. Clocks are synchronous.

To obtain a greater number of taps, devices may be cascaded using synchronous clocks. The feed-forward output of the first device becomes the input to the second device. Figure 9 shows the required arrangements and d-c load on the feed-forward tap — pin 39 — (the latter is needed only when cascading multiple devices). The circuit of Fig. 10 permits an adjustment of gain to unity, and the SD210 source follower provides the requisite buffer to give good high-frequency performance when driving a capacitive load. A bipolar transistor in place of the SD210 is less suitable because of its larger effective input capacitance.

In normal operation, V_{dd} operates at the same level as the clock; V_{bb} is preferably adjusted to a slightly lower potential, in the region of zero to one volt *lower* than the maximum voltage of the clock. Since, with the 0026, the maximum clock voltage is approximately one diode drop below V_{dd}, an adjustment of V_{bb} approximately one to one and one-half volts below V_{dd} is typical.

Although the clock drive circuit shown is preferred, a CMOS D-type flip-flop, such as the type 4013 (B version preferred), will directly provide complementary clock waveforms which are adequate for many applications.

Note that there are conflicting requirements in the tap output circuit. For linearity and minimization of tap-to-tap crosstalk, it is desirable that the taps see a relatively low a-c impedance; further, d-c coupling is desirable to avoid coupling difficulties at low scan rates. On the other hand, it is desirable that the d-c current level be much less than would flow into a low-resistance path to ground. Further, individual differences in source-follower thresholds, etc. give rise to a tap-to-tap variation which requires relatively low gain until the differential combination has been accomplished. The circuit of Fig. 9 compromises effectively among the above factors. Weighting is adjustable over the range $-1 \leq W \leq +1$ for each tap by adjustment of the ratio of resistances connecting the + line and − line, respectively. Designated as R_a the resistance between the potentiometer slider (Fig. 9) and the positive bus, where $0 \leq R_a \leq 1000$ ohms. Then $R_a = 500$ ohms gives the central or zero-weight value, $R_a = 0$ gives the maximum positive weight, and $R_a = 1000$ ohms gives the maximum negative weight. The tap weight is then given by $W = (500 - R_a)/500$, or the resistance value by $R_a = 500\,(1-W)$ ohms where W is the tap weight and is $-1 \leq W \leq +1$. Note that resistance values other than 1000 ohms are possible; higher values lead to excessive crosstalk and lower values lead to excessive d-c balance sensitivity.

It is important that an active tap see a low a-c impedance; a potential variation at the tap couples a small charge variation into the next earlier and next later charge packet. In a filter application such crosstalk merely requires slight adjustment of the tap weights, but it is better to avoid the coupling by means of low impedance load. For the same reason, unused taps should either be left floating or, preferably, connected to V_{dd}. They should *not* be loaded or connected to common, both to avoid crosstalk and to avoid dissipation.

TC-32A EVALUATION CIRCUIT CARD

The TC-32A Evaluation Circuit Card incorporates the basic circuit shown in Fig. 9 and is available from RETICON. It provides the required peripheral circuitry including bias, signal buffering, and clock and start waveforms. External interface with timing logic, etc. is at TTL level to assist in functional use of the TAD-32. The board may be incorporated into systems, if desired, and is particularly useful during evaluation and initial system design. A descriptive data sheet is available for the TC−32A. The board is available in three versions, designated by dash numbers (-01), (-02), and (-03).

The (-01) version is standard and has fixed resistors of 800 ohms and 200 ohms in place of the potentiometers of Fig. 9: all weights are of the same polarity.

The (-02) version is the most versatile, with adjustable tap-weight potentiometers as shown in Fig. 9.

The (-03) version is supplied without weighting resistors, so that any customer-desired weighting arrangement may be implemented.

REFERENCES

1. G.P. Weckler: "A Tapped Analog Delay for Sampled Data Signal Processing" (Reticon Technical Note No. 105)
2. R.R. Buss and S.C. Tanaka: "Implementation of Discrete-Time Analog Filter and Processing Systems" (Reticon Technical Note No. 111)
3. U. Strasilla, G.P. Weckler: "Charge Transfer Devices for Sampled-Data Processing" (Reticon Technical Note No. 114)

SPECIFICATIONS (25° C)

Absolute Maximum Rating	Min.	Max.	Units
Voltage on any terminal with respect to common	-0.4	+20	Volts
Storage temperature	-55	+125	°C
Temperature under bias	-55	+85	°C

Drive	Min.	Typical	Max.	Units
Clock frequency	0.001		5*	MHz
Clock amplitude, V_ϕ (Figs. 1, 2)	10	15	16	Volts
Clock line capacitance (each)		50		pf
V_{bb} (optimum)		V_ϕ-1	V_ϕ	Volts
V_{dd}	V_ϕ	+15	16	Volts
DC power dissipation**		200	700	mwatts

*Performance degraded above 2 MHz clock rate.

**DC power dissipation is strongly dependent on the number of taps used and on tap load currents. When all 32 taps are used with 10 K ohm loads, typical dissipation is 200 mwatts.

***Optimum bias is dependent on clock and supply voltages.

WARNING: Damage to the device may result if the input terminal is a.c. coupled. When the power is removed from the device while signal is applied to input terminal, the substrate may become biased in the forward direction causing the input gate protection to "short circuit".

Input/Output	Typical	Max.	Units
Input capacitance @ +4 V Bias	8		pf
Output capacitance of each tap @ +5 V Bias	3		pf
Output transconductance (at +5 V level, 10 K Ω d-c load)	1.1		ma/v
Input Bias***	3		Volts
Input signal (p-p)		4	Volts
Tap d-c level	+5		Volts
Unused taps	Connect to V_{dd}		

Performance Characteristics	Typical	Max.	Units
A. Single-tap response:			
Dynamic range (See Figs. 3 and 8)	60		db
Linearity (See Fig. 8)			
Harmonic intercepts (See Fig. 8)			
B. 32-tap summed response:			
Dynamic range (See Fig. 3)	60		db
Input sensitivity, S/N ~1	4		mV p-p

PERKIN-ELMER

Interdata

MINI INPUT/OUTPUT SYSTEM

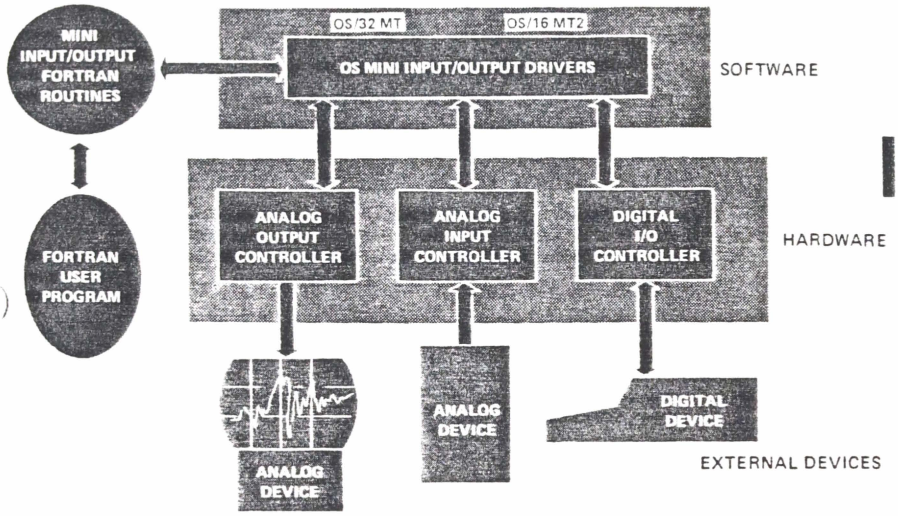

MINI INPUT/OUTPUT FUNCTIONAL CHARACTERISTICS

Mini Input/Output System

PRODUCT DESCRIPTION

The Interdata Mini Input/Output System provides low-cost, highly flexible real-time A/D, D/A, and digital I/O interfacing capability for the entire range of Interdata processors.

The independent Mini Input/Output subsystems are:

- Analog Input Subsystem — 10 or 12-bit analog-to-digital converter subsystem with up to 16 differential or 32 single-ended channels.
- Analog Output Subsystem — 12-bit digital-to-analog converter system with 4 channels or 2 channels with oscilloscope control channels.
- Digital I/O Subsystem — 16-bit digital input/output subsystem for parallel transfers to and from any Interdata central processing unit.

All subsystems are fully supported under OS/16 MT2 and OS/32 MT, the Interdata 16 and 32-bit operating systems.

I/O handlers are provided for the ISA real-time extensions of FORTRAN which allow operation through the use of single Read/Write calls. Each subsystem is compactly packaged on a single 15-by-15 inch or 7-by-15 inch printed circuit board that occupies a single or half slot in any Interdata processor or expension chassis.

The Mini Input/Output system is ideal for data collection and reduction, data logging, and industrial testing.

SUBSYSTEM FEATURES

- 10 or 12-Bit Analog Input Subsystem
- 12-Bit Analog Output Subsystem
- 16-Bit Digital Input/Output Subsystem
- Compact Packaging — One Board, Single or Half Slot
- Fully Software Supported — OS16MT2 and OS/32MT, ISA FORTRAN Extensions.

Digital Input/Output Subsystem

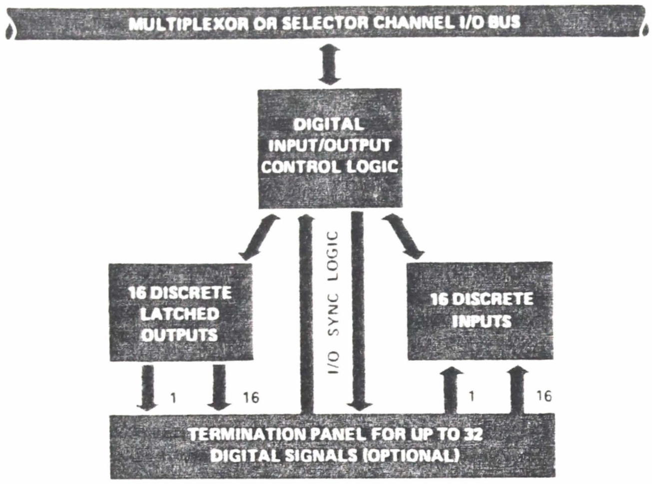

DIGITAL INPUT/OUTPUT SUBSYSTEM DESCRIPTION

The Digital Input/Output Subsystem is a highly flexible, low-cost product for parallel transfer of 16-bit digital data to and from the CPU. The input and output data paths contain individual synchronization logic to enable the user to synchronize the data transfers with external hardware. Both input and output data paths contain universal signal conditioning logic which allows the data paths to be compatible with a wide variety of I/O signal levels.

The Digital I/O subsystem is packaged on a single 7-by-15 inch printed circuit board that occupies one half slot in any Interdata CPU or expansion chassis. All I/O connections are made via connectors mounted on the front edge of the Digital I/O printed circuit board. The signals within each connector are arranged in a manner that allows total I/O diagnostic testing by simply jumping inputs to outputs.

Digital output circuits provide compatibility with TTL logic and are open collector switches capable of switching 100 milliamps at 50 volts. The circuit also provides an output signal with the high output voltage level controlled by external voltage. Output synchronization logic is available to sync output data transfers with external devices.

A digital input circuit may be used as a TTL input, contact sense input, or voltage sense input. Input synchronization lines are also available to sync input data transfers with external devices.

FEATURES

16-Bits of Digital Output

- Universal Signal Conditioning
- TTL Compatible
- Relay/Lamp Driver
- Voltage Source
- Output Synchronization Logic

16-Bits of Digital Input

- Universal Signal Conditioning
- TTL Inputs
- Contact Inputs
- Voltage Inputs
- Input Synchronization Logic

DIGITAL INPUT/OUTPUT SYSTEM SPECIFICATIONS

Inputs:	16 Data Input Lines 2 Input Control Lines
Input Logic:	
TTL Inputs –	Logic Level or +5 volt current source Logic 1 equals 1 volt at 0.7 milliamps Logic 0 equals 4 volts at −130 microamps or 30K ohms leakage to ground
Contact Sense Inputs –	+25 volts current source Logic 1 equals 1 volt at 5 milliamps for Closed Contact Logic 0 (leakage ⩾ 1K ohm) for Open Contract
Voltage Sense Inputs –	Logic 1 ⩽ 0.9 volts at 40 microamps Logic 0 equals 4 to 50 volts at 150 microamps to 2.25 milliamps
Outputs:	16 Data Output Lines 2 Output Control Lines
Output Logic:	
TTL Outputs –	Logic 1 equals current sinking of 100 milliamps at ⩽ 0.4 volts Logic 0 ⩾ 2.4 volts at 0.4 milliamps
Relay/Lamp Driver Outputs –	Logic 1 equals current sinking of 100 milliamps at ⩽ 0.4 volts Logic 0 ⩾ 12.5 volts at 2.4 milliamps Logic 0 ⩽ 100 microamps with 50 volt source and no pull up resistor
Environmental	
Temperature:	0 to 50°C – Operating −40° to 85°C – Storage
Humidity:	0 to 90% – Non Condensing
Dimensions:	7 in. x 15 in. (17.7 cm x 38.1 cm) printed circuit board
Weight:	1 lb. (.4 Kg)
Power Requirements:	1 amp at 5 Volts